A FUNDAMENTAL STUDY ON THE STRUCTURAL INTEGRITY OF MAGNESIUM ALLOYS JOINED BY FRICTION STIR WELDING

by

HARISH MANGEBETTU RAO

J. BRIAN JORDON, COMMITTEE CHAIR
MARK E. BARKEY
YUEBIN GUO
HARSHA BADARINARAYAN
MARK L WEAVER

A DISSERTATION

Submitted in partial fulfillment of the requirements
for the degree of Doctor of Philosophy in the
Department of Mechanical Engineering
in the Graduate School of
The University of Alabama

TUSCALOOSA, ALABAMA

2014

ABSTRACT

The goal of this research is to study the factors that influence the physical and mechanical properties of lap-shear joints produced using friction stir welding. This study focuses on understanding the effect of tool geometry and weld process parameters including the tool rotation rate, tool plunge depth and dwell time on the mechanical performance of similar magnesium alloy and dissimilar magnesium-to-aluminum alloy weld joints. A variety of experimental activities were conducted including tensile and fatigue testing, fracture surface and failure analysis, microstructure characterization, hardness measurements and chemical composition analysis. Investigation of the friction stir spot welded magnesium-to-magnesium alloys revealed, welds produced in a manner that had a large effective sheet thickness and smaller interfacial hook height exhibited superior weld strength. Furthermore, in fatigue testing of friction stir spot welded magnesium-to-magnesium alloy, lap-shear welds produced using a triangular tool pin profile exhibited better fatigue life properties compared to lap-shear welds produced using a cylindrical tool pin profile. The welds produced using a triangular tool exhibited superior structural-integrity.

In friction stir spot welding of dissimilar magnesium-to-aluminum alloy, the formation of intermetallic compounds in the stir zone of the weld had a dominant effect on the structural-integrity of the weld. Lap-shear dissimilar welds with good material mixture and discontinues intermetallic compounds in the stir zone exhibited superior weld strength compared to lap-shear dissimilar welds with continuous formation of intermetallic compounds in the stir zone. The weld structural geometry like the interfacial hook, hook orientation and bond width also played a major role in influencing the weld strength of the dissimilar lap-shear friction stir spot welds. Fatigue test

data of the friction stir linear welds of aluminum-to-magnesium alloys exhibited a scatter in fatigue life. The lap-shear dissimilar friction stir linear welds failed in three different modes; top sheet failure, bottom sheet failure and interfacial failure along the weld nugget. Investigation of the lap-shear welds revealed the presence of weld voids or channel defects which reduced the fatigue life of the welds. Presence of a thin layer of intermetallic compound along the faying surface accelerated the failure due to fretting.

DEDICATION

To my Amma, Appa and my Guru's

"You have the right to perform your duties,

but you're not entitled to the fruits of the duties.

Do not let the fruit be the purpose of your duties,

and therefore you won't be attached to not doing your duties."

- Śrīmad Bhagavad-Gītā

Chp: 2, V: 47

LIST OF ABBREVIATIONS AND SYMBOLS

FSW	Friction Stir Welding
RSW	Resistance Spot Welding
FSSW	Friction Stir Spot Welding
FSLW	Friction Stir Linear Welding
SZ	Stir Zone
TMAZ	Thermo-mechanically Affected Zone
HAZ	Heat Affected Zone
BM	Base Metal
DC	Dominant Crack
SC	Secondary Crack
PH	Primary Hook
SC	Secondary Hook
D	Tool Shoulder Plunge Depth
T	Effective Sheet Thickness
W	Weld Bond Width
D1	Distance Between Tip of Primary Hook on Either Side of the Weld
D2	Distance Between Tip of Secondary Hook on Either Side of the Weld
H	Hook Height in Spot Welds
H1	Effective Sheet Thickness on Retreating Side in Linear Welds
H2	Effective Sheet Thickness on Advancing Side in Linear Welds
BW	Bond Width in Linear Welds
RS	Retreating Side Hook
AS	Advancing Side Hook
W1	Weld Number 1
W2	Weld Number 2
IMCs	Inter Metallic Compounds

ACKNOWLEDGMENTS

With a strong belief in teamwork, I will be honest to say, this work would not have been possible without the strong support and guidance from the entire team of my committee members, colleagues, family and friends. First and foremost I would like to thank my committee chair and my advisor, Dr. J. Brian Jordon for all the help and guidance he has given me from day one of my graduate studies. I am fortunate to have an advisor who has given me the freedom to explore the subject on my own and at the same time has advised and guided when I went wrong. He has taught me to question not just "why and how?" but "why not ?" His patience to sit with me to explain the ideas and concepts of this research in the initial years has allowed me to accomplish my professional goals in my graduate school career.

My co-advisor, Dr. Mark E. Barkey has always been kind enough to listen and guide me when needed. He has always been there to help me in the materials testing lab and give inputs on testing methodology and analyzing the test results. His courses have been of great help to understand the concept and the science behind the failure of materials.

I would also like to thank Dr. Yubein Guo for insightful comments and constructive criticism through different stages of my research. I am grateful to him to have taught me to understand my research in production and manufacturing point of view. I would like to extend my gratitude to Dr. Mark L. Weaver for allowing me to work in his lab to prepare the samples for microstructure analysis. His courses have helped me in better understanding the microstructure of materials and its influence on mechanical properties.

I am grateful to Dr. Harsha Badarinarayan, project manager at Hitachi America, Ltd., MI, for providing me with welded samples throughout this research work. I am thankful to him for giving me an opportunity to work as an intern at Hitachi America, Ltd. This internship has helped me immensely to gain hands-on experience and knowledge of friction stir welding and process development techniques. I am also indebted to Dr. Wei Yuan, researcher at Hitachi America, Ltd., who has been very helpful during my entire work period. His insights on concepts of writing the scientific reports have helped me immensely to understand and write journal articles. I appreciate his efforts and patience to discuss with me the various concepts of friction stir welding throughout my internship at Hitachi America, Ltd.,

I would also like to acknowledge all my teachers who have taught me through years and who took special interest in my career and pushed me hard and made me believe in myself: Faculty and staff members of Nitte Meenakshi Institute of Technology, Bangalore, India; The late Dr. CRL Murthy who introduced me to field of research and seeded my interest in materials science at Indian Institute of Science, India; Dr. Mahesh Hosur who guided me through my masters and provided me with an opportunity to work under his supervision at Tuskegee University, Alabama; Dr. Sheik Jeelani, VP Research of Tuskegee University for all his guidance and support during my stay at Tuskegee University.

It would be incomplete if I do not acknowledge my colleagues, Andrew Brammer, Rogie I. Rodriguez, Joao Moraes, and Robert McCullough for all their help during this research at The University of Alabama. I would also like to thank Dr. K Clark Midkiff, Dept. Head and the staff at the Dept. of Mechanical Engineering at The University Alabama including Ms. Lynn Hamric, Ms. Lisa Hinton and Ms. Betsy Singleton for all their help during my stay at the university. I would

like to acknowledge Mr. Johnny Goodwin, at the Central Analytical Facility of The University of Alabama for training me to use the scanning electron microscopy

I would like to thank my close friends Prateek Hejmady, Kautalya Mishra, Bharath N Gowda, Harsha Banavara, Dr. Santosh Kulkarni, Dr. Pratap Simha, Dr. Vijay Sheshadri, Abhilash Kittanna, Sabarish Raghupathy, Sashi Kiran, Sujith Shetty, Shiba Shetty, Subhodh Shetty, Ravindra Poojary, Vikram Bhat, Vishnu Prasad, Santosh Kumar, Sandeep Shetty, Sandeep Ayappa, Uday Amin who have been with me in the toughest of the times and encouraged me and have given their shoulder to walk the last mile. My friends in Tuscaloosa Avinash Reddy, Dr. Neha Pachauri, Ishan Jaithwa, Dr. Priyank Upadhyay, Abhishek Kumar, Shoieb Shaik, Shoiab Belim and Haroon Sheik. My close friends in Farmington Hills, MI who supported me through my internship days, Narayan Namboodri, Padmini Venkatesh, Konda Reddy and Nikhil Seera.

Most importantly, none of this would have been possible without the love, patience and support of my family. My sincere thanks to my parents Kusuma Rao and Ramachandra Rao and my sister Shruthi Rao and brother-in-law Deepak Muralidhar for all their love and unconditional support throughout my studies. Also my thanks to my extended family in US who stood by me in the toughest times and supported and encouraged me, my cousins Anil S Rao and his family and Dr. Indira Vysa Rao and her family. Last but not the least, thanks to the Almighty who gave me the strength, health, courage and opportunity to pursue this study.

CONTENTS

LIST OF TABLES

LIST OF FIGURES

CHAPTER 1

INTRODUCTION

1.1. Motivation

With an increase in the use of automobiles around the globe, much effort has been put forth to reduce the greenhouse gases and pollution by making automobiles more fuel efficient and environmentally friendly. Current research has attempted to resolve this problem by exploring alternate fuel and power train options, and aerodynamic improvements. A potentially more cost effective approach in achieving this goal is by reducing the overall weight of the automobile [1–5]. As such, manufacturers are exploring the possibility of replacing significant portions of traditional steel based alloys of the automobile with lightweight aluminum and magnesium alloys.

Magnesium alloys in general have received a considerable attention in the past decade due to its superior physical and mechanical properties. Magnesium alloys have low density, and good strength-to-weight ratio [3,6,7]. In addition, magnesium alloys have high specific strength and relatively good energy absorbing characteristics, and are readily available [6,8]. However, magnesium alloys have some disadvantages compared to aluminum and steel based alloys. The major setback for magnesium alloys is that most alloys have high chemical reactivity and limited corrosion resistance. However, recent studies have shown that the corrosion resistance of the

magnesium alloys improved when they were coated with Al-alloyed metallic coating [9]. The corrosion resistance of high-purity magnesium alloy is found to be better than A380 aluminum alloys in atmospheric and saline environments. However, galvanic corrosion has remained a concern for design and assembly. To address this, the use of a compatible isolation metal like aluminum shims or washers [7] have shown to reduce galvanic corrosion. Some of the newly developed magnesium alloys including AZ91E, WE43B and AZ31 have displayed superior corrosion resistance compared to previous magnesium alloys and are feasible in automobile applications. The other major drawback to magnesium alloys is the limitation of cold formability. In fact, the application of commonly used magnesium alloys, such as AZ31 and AZ61, have been limited by their poor formability at room temperature [10–12]. To address this issue, the addition of rare-earth elements together with zinc has been shown to improve the formability of magnesium alloys at room temperature which is attributed to the weakening of the strong basal texture commonly observed on wrought magnesium alloys [13–15].

While recently developed magnesium alloys with good corrosion resistance and good formability at room temperature have enabled the potential use of these lightweight alloys in automobiles, joining methods still remain as a significant issue preventing widespread implementation. Resistance welding, which is a common welding technique in the automotive industry, has proved problematic on joining aluminum and magnesium alloys primarily due to the low melting point and high heat dissipation capacities of the alloys [2,16–19]. The magnitude of this problem is compounded further because the average mid-sized automobile contains thousands of spot welds. Consequently, the higher welding currents require larger capacity equipment, which in turns leads to higher capital investments. In addition, the durability of the copper electrodes

used in resistance spot welding is limited to approximately 400-900 individual welds. In the context of the automobile assembly-line, few alternatives to resistant spot welding exist that do not require major capital investments. As such, an attractive alternative method to join magnesium alloys effectively is by using solid state welding techniques like friction stir welding (FSW).

Solid state welding is a process in which the material to be joined is not melted, but rather is plastically deformed. In most cases there is no filler material to be used and the process is much more economical and environmentally friendly compared to traditional welding techniques. Friction stir welding (FSW) was developed by The Welding Institute, UK in 1991, as a novel method to join aluminum alloys [20]. Several techniques of FSW are targeted for the automotive industry: friction stir linear welding (FSLW); and friction stir spot welding (FSSW). For any of these methods to be successfully implemented in industry, a thorough understanding of the factors influencing the structural-integrity needs to be established. The structural-integrity of the FSW joints are highly influenced by the micro and macro features of the weld and these features are dependent on weld processes such as the weld tool geometry, weld tool rotation rate, tool shoulder plunge depth and dwell time. Only a handful of studies have been conducted on the influence of tool geometry and process parameters on mechanical performance, including fatigue, of friction stir welded joints of Mg and Al alloys [18,19,21-37]. Furthermore, even fewer studies have focused on the joining of magnesium alloys [28,35–37]. This lack of understanding is further compounded when joining magnesium to aluminum alloys. While, literature exist only on the feasibility and factors governing the dissimilar FSSW [38] and FSLW of Al and Mg alloys [25,37,39–49], there are no studies on structural-integrity of the dissimilar welded joints. In real-world applications, welded joints are subjected to fatigue loading conditions and hence it's

imperative to study and understand the fatigue behavior and structural-integrity of the FSW and FSSW joints.

1.2. Research Objectives

The research objective of this research is to understand the effect of tool geometry and weld process parameters on the mechanical behavior of friction stir welding of magnesium alloys. This research objective focuses on both similar (magnesium-to-magnesium) and dissimilar (magnesium-to-aluminum) welding. The basic research approaches of this study are as follows:

- Determine the feasibility and characterize the coupling effects between welding parameters and static strength of rare earth added FSSW magnesium alloy joints
- Determine and characterize the coupling effects between welding parameters and fatigue behavior of similar FSSW magnesium alloys joints.
- Determine and characterize the coupling effects between welding parameters and static strength and fatigue behavior of dissimilar FSSW and FSLW magnesium-to-aluminum alloys joints.

1.3. Technical Background

1.3.1. Overview of Friction Stir Linear Welding (FSLW)

Friction stir linear welding (FSLW) is a solid state thermo-mechanical welding process in which a rotating cylindrical weld tool comprising a tool shoulder and probe pin moves along the welding region of the work piece to be joined. Initially the probe pin is plunged into the weld region of the work-piece, which in turn, generates a small amount of frictional heat. Upon further

plunging the weld tool, additional frictional heat is generated as the rotating tool shoulder comes in contact with the top surface of the work-piece. This heat is sufficient enough to soften the material around the probe pin and under the tool shoulder. The combined action of the probe pin and tool shoulder results in severe plastic deformation and flow of the plasticized metal occurs as the tool moves along the weld region. Material gets transported from the front of the tool to the trailing edge where the downward force of the tool forges the work-piece [50–58]. Schematic representations of the FSLW in butt weld conditions are shown in Fig. 1-1 [56].

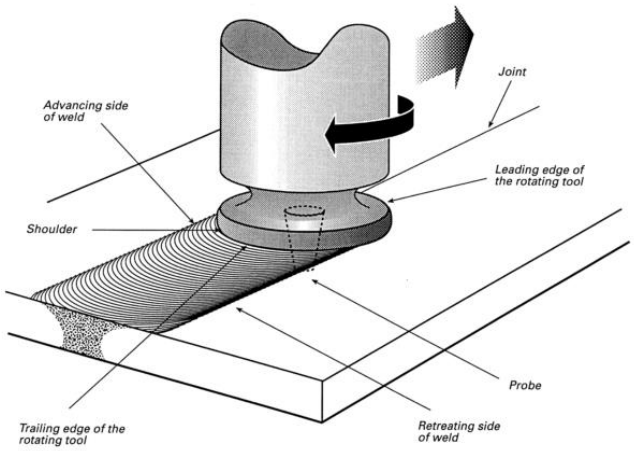

Figure 0-1 : Schematic of the friction stir linear welding (FSLW) process.

FSLW welds can also be made in lap-shear, T-joint and other weld configurations. The weld that is formed is generally free of defects that are observed in fusion welding process. The process is also free of fumes and does not consume any filler materials and distortion is typically lower compared to fusion welding [56]. During the FSLW process, the material is removed from the rotating side of the tool which is in the traversing direction of the tool. This side of the weld is called the advancing side. The extracted material is retrieved back into weld zone at the other end of the rotating tool, which is opposite to the traverse direction and is called the retreating side. See

section 1.4 for more details regarding the geometrical and microstructural features of FSW, including the advancing and retreating side. Generally speaking, the strength of the FSLW joints is affected by the geometric features of the weld including the hooking or cold lap feature along with the microstructure of the weld zone. Along with the microstructure features of the weld, these geometrical features influence the weld strength. These parameters include; the tool geometry, weld tool rotation rate, weld tool plunge depth and weld tool traverse speed. A significant amount of studies have shown the strong dependence of the FSLW strength on the weld process parameters [53,59–67].

1.3.2. Overview of Friction Stir Spot Welding (FSSW)

Friction stir spot welding (FSSW) is a variant of the FSLW used for spot welding sheet metals in mostly lap-shear weld configuration. A schematic illustration of the FSSW process is shown in Fig. 1-2 [27].

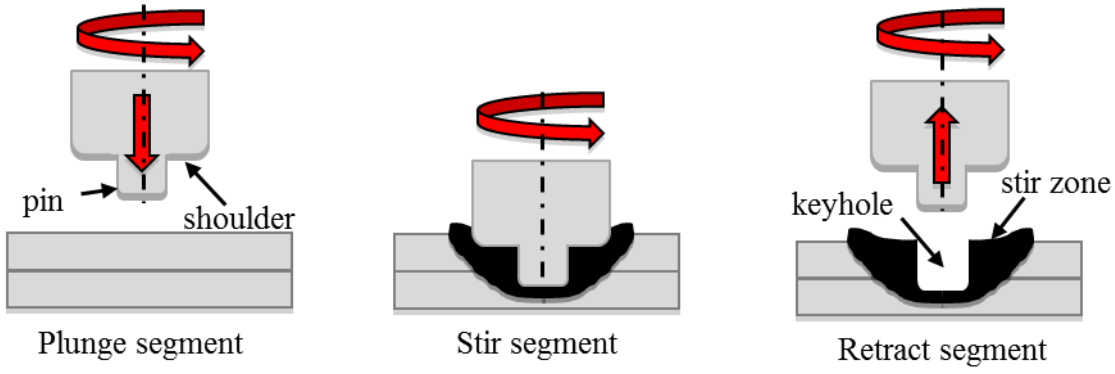

Figure 1-2: Schematic of friction stir spot welding (FSSW) process.

As in FSLW, the rotating cylindrical weld tool consists of a tool shoulder and probe pin. The probe pin penetrates the upper sheet completely and then passes into the bottom sheet to various depths

according to the process condition. The downward force and rotational speed of the tool generates frictional heat at the tool-material interface. This frictional heat is sufficient enough to plastically deform metal adjacent to the tool and a solid-state bond is formed at the interface of the two sheets to be joined [18,19,22,25,27,30,41,42,50–52,54,55,68–73]. The amount frictional heat generated and plastic deformation depends on the downward force, dwell time of the tool and plunge depth of the tool. The FSSW is characterized by a key hole that is left behind after the extraction of the tool at the end of the weld process [19,69]. Unique to the FSSW process is the formation of partially bonded 'hooks' at the interface of the two sheets. During FSSW, trapped oxide films present between the overlapping sheets are often displaced in an upward direction toward the top sheet into a ''hook-like'' shape. This hooking is largely due to the plastic flow of the material resulting from the downward plunge of the pin into the bottom sheet. The interfacial hooks have shown to significantly influence the weld strength of the FSSW [21,22,27,28,68]. See section 1.4 for more details regarding the geometrical and microstructural features of FSSW, including the interfacial hook.

As with any new joining technique, for successfully implementing and using FSSW, it is important to understand the mechanisms behind the formation of the weld bond, the failure mechanisms and weld strength of the spot welds. Various studies have shown that the FSSW strength depends on the weld geometry which is largely influenced by the weld tool geometry and the weld process condition. The geometric feature of the FSSW including the weld bond width, the interfacial "hook" height, the effective sheet thickness, and the microstructure in the weld zone have all been found to be dependent on welding parameters. In terms of static strength, the weld process parameters that are found be influential are: the tool rotation rate; tool geometry; tool

plunge depth; tool plunged speed; and dwell time. The interdependence and influence of weld process parameters on the weld geometry, the microstructure and the weld strength has been studied and reported widely [21,22,26,27,32,36,37,39,68,70,74–76].

1.4. Factors influencing the strength of FSW

1.4.1. Geometrical Features and Microstructure

As stated earlier, the strength of the FSSW is influenced by the microstructure and the geometrical features of the weld nugget. The geometrical features mentioned earlier including the hook height, weld bond width, and effective sheet thickness have been found to be dominant features [18,19,21,22,26,28,58,68]. The cross section view of a FSSW and FSLW lap-shear specimen indicating various geometrical features in the weld nugget are shown Fig. 1-3(a) and Fig. 1-3(c). A schematic indicating nomenclature used to indicate various geometrical features of FSSW are shown in Fig. 1-3(b). The nomenclatures are: the effective top sheet thickness (T), weld bond width (W) and interfacial hook height (H). For FSLW, the interfacial hooks are much more pronounced than the hooks in FSSW. The interfacial hooks on retreating side of the weld and interfacial hook on the advancing side of the weld are designated as H1 and H2 and the bond width which is distance between the two hooks is designated as BW as illustrated in Fig. 1-3(d). Yin et al. [76] reported that the static strength of the FSSW AZ31 magnesium alloys increased for welds with a smaller hook height. It was suggested that if FSSW were produced with a smaller hook height and in a manner where the hook region is curved outwards from the tool axis and with a large bond width, the static strength of the weld would increase considerably. Sometimes the weld process condition is such that the weld bond width increases at a cost of reducing the effective sheet thickness.

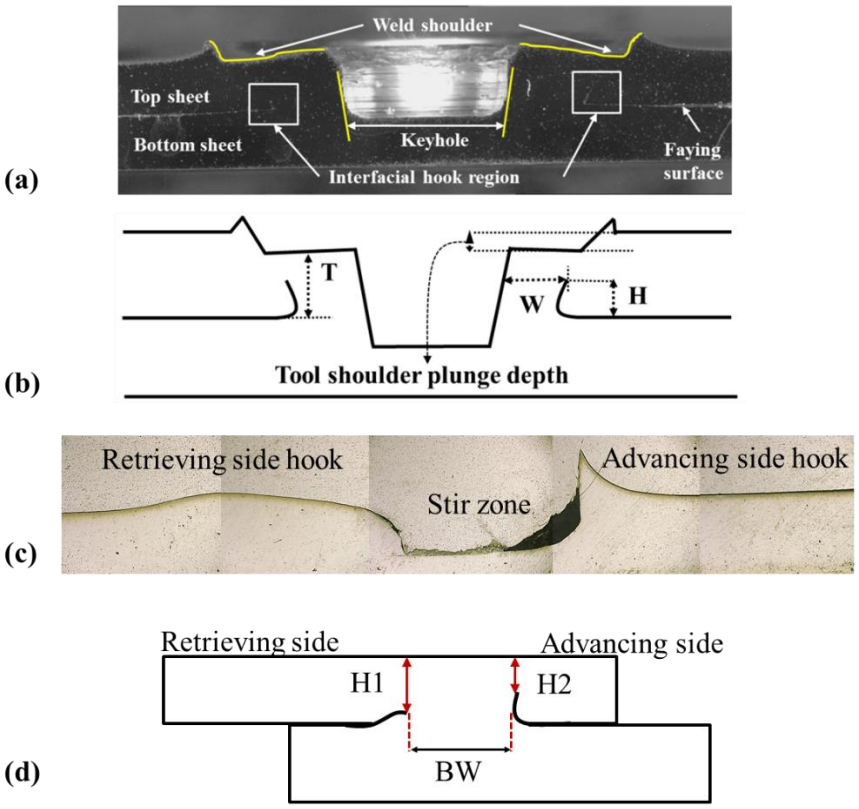

Figure 1-3: (a) Cross section view of the FSSW in lap-shear configuration. (b) Schematic of the cross section of FSSW with nomenclatures indicating various geometrical features. (c) Cross section view of the FSLW in lap-shear configuration (d) Schematic of the cross section of FSSW with nomenclatures indicating various geometrical features of the weld.

This in most cases results in a reduced strength of the FSSW as the fracture typically propagates through the hook [68]. With the increase in the distance between the tip of the hook to the top sheet increase (effective sheet thickness) the static strength of the FSSW Al-5754 alloy joint was observed to increase [21,22,76]. The strength of the FSSW was observed to be influenced by the size and orientation of the hook region [33]. Fracture was observed from the hook to the top sheet and along the circumference of the weld nugget [28,30]. In general, fracture was observed to originate from the tip of the hook for welds in static loading. For smaller effective sheet

thickness, the crack grew into the top sheet and the samples failed by nugget pullout and when the weld bond width was smaller, the samples failed by interfacial shear overload [18,24,77]. This illustrates the importance of the hook in determining the strength of the FSSW.

Very limited work has been reported on FSLW of magnesium alloys in lap-shear configuration [53]. Unlike in FSSW, the interfacial hooks of the FSLW are more prominent and pronounced. The interfacial hooks consists of retreating side hook or sometimes referred to as cold lap feature and the advancing side hook. The faying surface on the advancing of the weld tool where the material is removed tends to form into a hook shape and hence referred to as the advancing side hook. The faying surface on the retreating side of the weld tool lifts up and penetrates into the nugget forming the cold lap feature or the retreating side hook [60]. Studies have indicated the failure of FSLW lap-shear joints occurred through these hooks and hence play a dominant effect on the weld strength [53,60,78]. Due to the characteristic profile of the hooks, the friction stir linear lap-shear welds can be loaded in two different loading configuration (a) retreating side loading and (b) advancing side loading. The laps-hear strength of FSLW loaded in retreating side exhibited superior weld strength compared to welds loaded in advancing side [67]. With the increase in effective sheet thickness on the retreating side of the weld, the lap-shear strength increased considerably [53,60,78].

Studies have reported on the influence of the microstructure on the failure mode and strength of the FSW [18,25,41,59,61,63,64,66,72,79,80]. Generally the welded materials exhibit three different microstructural zones besides the base metal microstructure. The stir zone (SZ) close to the key-hole periphery, the thermomechanically affected zone (TMAZ), and the heat affected zone (HAZ). The stir zone in FSW is characterized by equiaxed grain structure, whereas

this part of the weld nugget is in constant contact with the probe pin and undergoes severe plastic deformation under high temperatures [71]. The SZ is generally observed to have the highest hardness compared to other microstructural zones in the FSSW. The TMAZ which is adjacent to the SZ, and for most part is located in the area under the tool shoulder, is exposed to large heat and mechanical deformation and as a result is characterized by large recrystallized grains. The HAZ is the zone between the base material and the TMAZ and is characterized by partially recrystallized grains [18,37,72]. Figure 1-4 shows an example of representative microstructure zones in FSSW in magnesium alloy.

1.4.2. Effect of tool geometry

In friction stir welding, the weld tool plays a crucial role in material mixture and in formation of the weld bond. Considerable work has been done on identifying the influence of the tool geometry on the weld strength [21,22,28,68].

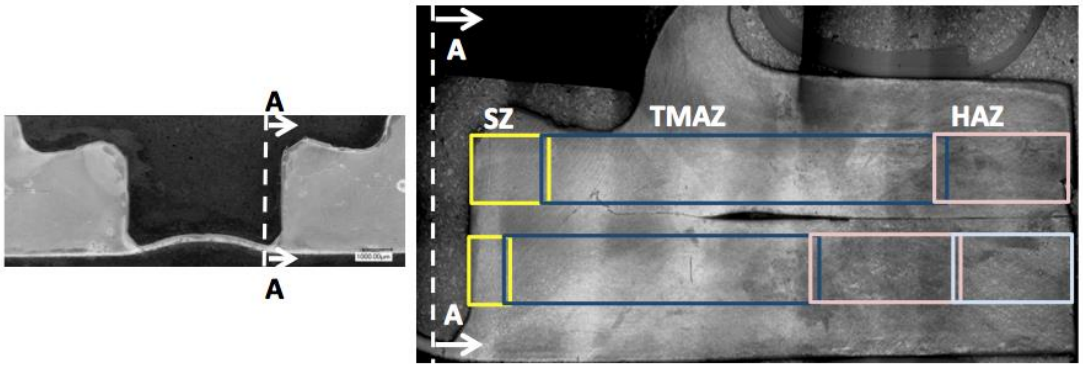

Figure 1-4: Representative cross-sectional view of the microstructure zones of AZ31 magnesium alloy joined by friction stir spot welding.

Tool geometry such as tool shoulder diameter, probe pin length, shape and surface morphology have been found to highly influence the frictional heat generated and material flow during the

welding [21,22,24,26,52,75,76]. A schematic example of different FSSW weld tools consisting of a probe pin and a tool shoulder are shown in Fig. 1-5 (a) - triangular probe pin and Fig. 1-5 (b) - a cylindrical probe pin.

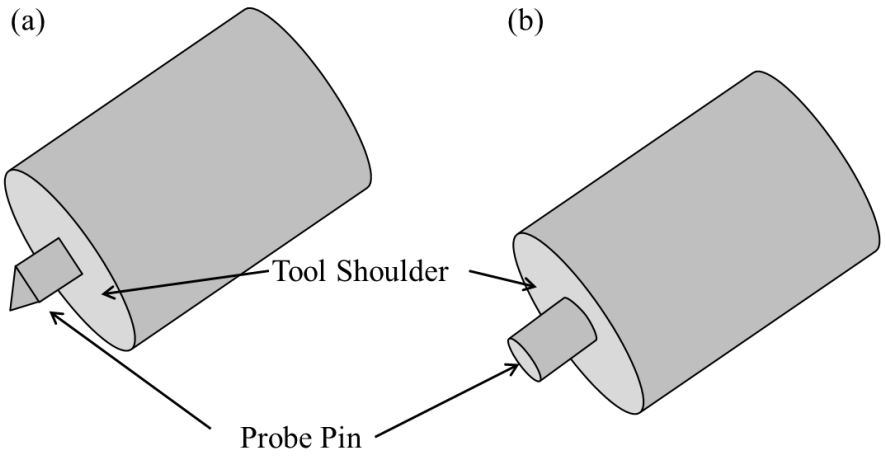

Figure 1-5: Schematic of a representative FSSW tool (a) with triangular probe pin (b) cylindrical probe pin.

During the FSW, the tool shoulder and pin play different roles. The tool shoulder comes in contact with the upper sheet only later in the process when the plunge depth is increased. The role of the tool shoulder begins to play a dominant role when the material is extruded from the bottom sheet and pushed upwards and trapped between the tool shoulder and the upper sheet surface [73]. Hence the design of the tool shoulder is of crucial importance for optimum weld strength. Badarinarayan et al. [21] studied the effect of tool shoulder profile on the static strength of the FSSW 5754 aluminum alloy sheets. It was reported that the FSSW with a concave tool shoulder yielded a better static strength compared to the FSSW with convex and flat tool shoulder profile. Elsewhere similar observations were made of FSW produced using the concave tool shoulder [22,26,53,63]. The higher static strength of the FSSW using concave tool shoulder has been

attributed to the weld geometry that shows a higher effective sheet thickness. During the fatigue testing of the FSSW aluminum alloy, the failure modes varied for welds made with flat shoulder and concave shoulder. Lin et al. [33] studied fatigue failures in friction spot welded aluminum 6111-T4 sheets processed using different geometrical tools. For spot welds created using a flat tool shoulder, cracks initiated from several locations compared to a singular mode of failure using a concave tool shoulder. The amount of material deformation during the welding process due to the shape of the tool shoulder was identified as the likely reason for the difference in failure modes of the flat and concave tool.

The other important feature of the tooling is the probe pin. The probe pin influences the material flow and the material mixture during the FSW [21,22,53,62–64,68,75,76]. An increase in static strength of the FSSW Al alloys was reported when the cylindrical probe pin was replaced with a triangular probe pin. The increase in static strength was attributed to a more favorable geometrical feature of the weld created by the triangular probe pin. In fact, the triangular probe pin produced hooks which were shorter and contained a smaller stir zone, while the cylindrical pins produced a larger stir zone and with hooks much larger which terminated close to the key-hole surface [21,22]. The effect of probe pin surface morphology on FSSW strength has also been documented [22,75,76]. An increase in static strength was observed in FSSW AZ31 magnesium alloys that were produced with a triangular probe pin having a three- flat threaded surface [76]. The welds produced using three-flat threaded tool produced a larger weld bond width, smaller hook height, thereby increasing the load baring capacity of the welded joint. FSSW made with cylindrical probe pin and threaded surface resulted in lower static strength compared to welds produced with triangular probe pin and unthreaded [21].

The length of the probe pin has also been shown to influence the weld geometry and strength of the FSSW. Tozaki et al. [24] reported in FSSW Al 6061 alloys, the welds made with longer probe pin length had superior static strength compared to welds made with shorter probe pin length. With the shorter probe pin, the tool plunge depth needs to be increased in order to maintain good material mixture. Doing so, however, decreased the effective sheet thickness and thereby causing failure at much lower loads. In FSLW of magnesium alloys, lap-shear welds produced using a triangular pin suppressed the hook and thereby increasing the effective sheet thickness resulting in higher lap-shear strength [63]. A longer probe pin length increased the failure loads in dissimilar magnesium to steel joints [64]. Chowdhury et al. [62] reported the ultimate tensile strength and yield strength of the FSLW magnesium alloy produced with tool pin profile having left-hand threaded profile due to downward material flow.

1.4.3. Effect of Tool Rotation Rate

Tool rotation rate and dwell period essentially determine the heat generated and material plasticization around the pin, and in turn influence the weld geometry and the mechanical properties of the FSSWed joint [22]. In FSSW of lap-shear joints produced at varying tool rotation rates, the lap-shear strength of the welds gradually increased with increase in tool rotation rate and reached a peak value. Further increase in the tool rotation rate resulted in a decline of the lap-shear strength in these welds [18,19,69,75–77]. Thus, it appears that there is an optimal process window for achieving peak lap-shear strength. As stated before, the tool rotation rate influences the amount of frictional heat generated. At low tool rotation rates, lesser amount of frictional heat is generated which results in insufficient plastic deformation of the material. On the other end, significantly higher tool rotational rates produce high frictional heat which resulted in the formation of large

grains in the weld zone and introduced higher residual stresses resulting in lower weld strength [75]. The increase in tool rotation rate typically leads to increase in grain size due to the higher heat input and thereby reducing the strength of the FSW joints. The increasing tool rotation can also affect the size of the weld nugget. These two changes typically resulted in reduced tensile strength in FSSW Al alloys [18]. In general, the SZ in the weld nugget is characterized by fine recrystallized grains which inhibit the crack growth and propagation.

The increase in tool rotation beyond a certain rate has shown to reduce the size of the SZ and as well increase the average grain size in the SZ [61,65,66,79,81] and hence, leading to easy shear fracture of the weld nugget [19,77,82]. The high friction heat generated with increased tool rotation rate resulted in tool slippage at the contact interface between the periphery of the rotating tool probe pin and adjacent material in the SZ. This phenomenon is due to the spontaneous melting of the second phase particles which is immediately followed by solidification of liquid droplets that increases the material viscosity, heating rate and temperature [41,83,84]. In addition to affecting the grain structure, the tool rotation rate has a signification impact on the size and shape of the interfacial hook. Yin et al. [76] noted that the static strength of the FSSW joints in Mg AZ31 increased with an increase in tool rotation rate up to a certain point and then decreased on further increase in tool rotation rate. This reduction in static strength was attributed to the height increase of the interfacial hooks as the tool rotation rate increased. A schematic of typical hook geometry formed in the FSSW joint under various tool rotation rates for multiple tool designs are shown in Fig. 1-6 [76].

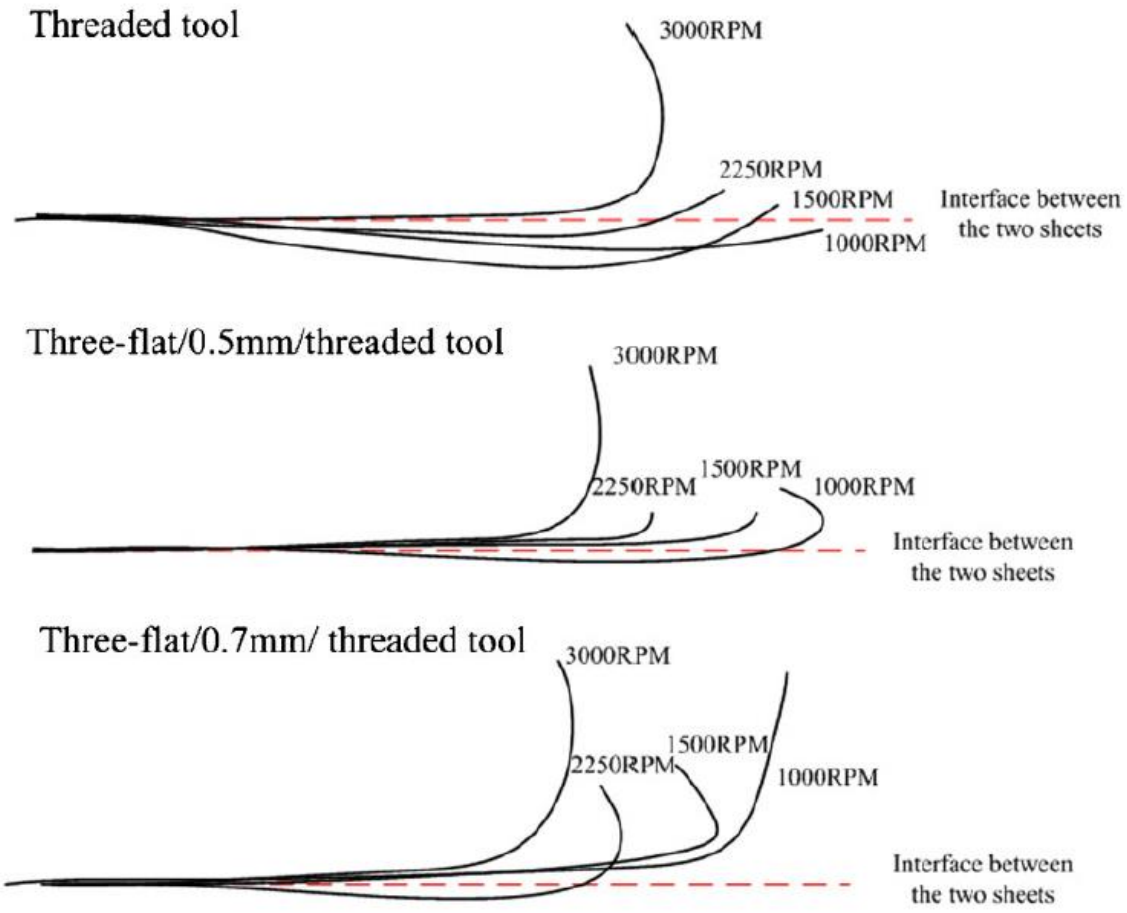

Figure 1-6: Hook formation in FSSW under varying tool rotation rate.

It is noted that if the ratio of the effective sheet thickness to the weld bond width is maintained to smaller value, the static strength of the FSSW joints increases significantly. In lap-shear fatigue testing of magnesium alloys, fatigue cracks were found to initiate from these interfacial hooks [28]. The coupons were observed to fail once the crack grew from the tip of the hook towards the nearest free surface. Hence, the geometry of the interfacial hook was found to be significant in determining the failure characteristics of the welded coupons [37,68]. However, beyond the work of Mallick and Agarwal [35], Jordon et al. [28] and Chowdhury et al. [37] the fundamental understanding of fatigue mechanisms in FSSW lap-joints is primarily restricted to

aluminum alloys. Tran et al. [85] observed that under low-cycle fatigue loading, fatigue cracks propagated through the interfacial hooks into the top sheet and then through the nugget. Likewise, under high-cycle fatigue loading, the cracks propagated through the hook into the upper sheet and lower sheet thickness

1.4.4. Effect of Dwell Time

Regarding dwell time, in FSSW AM60 magnesium alloy, the size of the SZ increased with increase in dwell time. The size was relatively larger for the tool made with triangular tool and least for cylindrical tool [70]. Tozaki et al. [77] observed that the static strength of the FSSW aluminum alloys increased with increased dwell time under very low tool rotation rate. The downside of lower tool rotation resulted in less frictional heat required for the plastic deformation which was countered by increased dwell time. With the gradual increase in tool rotation rate, the effective sheet thickness of the FSSW join decreased with increase in dwell time and resulted in lower weld strength. The grain size in the SZ of the FSSW 7075 aluminum alloy increased when the dwell time increased from 1 sec to 4 sec while the tool rotation rate was kept constant [79]. In addition, Zhang et al. [18] reported the weld bond width of the FSSW Al 5052 alloys decreased with increase in dwell time for tool rotation rate of 1541 rpm. This resulted in reduced FSSW strength. The static strength of the FSSW Mg AZ31 alloys was particularly low for welds made without the application of the dwell time since weld bond width formed were extremely small [68]. In FLSW, dwell time has no significant impact on the geometrical or microstructural features of the weld. Rather, the tool traverse rate does play a significant role. A very low tool traverse speed produces high frictional heat and results in unfavorable microstructure properties. While high tool traverse speed produces very low frictional heat resulting in insufficient material mixture

[37,63,65,66]. Hence the tool traverse speed should be chosen in a manner the frictional heat produced compensates with the tool rotation rate. A high tool rotation rate and high tool traverse speed or low tool rotation and low tool traverse speed.

1.4.5. Effect of Shoulder Plunge Depth

Strong weld bonds are typically produced when there is sufficient material mixture. For good material mixture, the material from the bottom sheet needs to be extruded and mixed with the top sheet material. This is possible only when the tool shoulder penetrates into the top sheet. Badarinarayan et al. [21] reported that for FSSW made using the cylindrical probe pin tool, the hook geometry was greatly influenced by the tool plunge depth. At lower plunge depths the height of the hook increased with increasing the plunge depth. The hook geometry takes its shape only when the probe pin penetrates past the interface of the two sheets. Beyond this point the material from the bottom sheet gets extruded. On further increasing the tool plunge depth, the tool shoulder comes in contact of the top sheet surface. This results in more frictional heat and material plasticization and formation of good weld bond by pushing the hook more outwards from the tool rotation axis [68]. But beyond a certain depth, the material extracted from below the probe pin surface is expelled outside the tool shoulder and forms flash. This decreases the effective sheet thickness and the tip of the hook terminates very close to the top surface of the weld resulting in lower FSW strength. Yin et al. [76] suggested the weld strength increased with increase in weld bond width and smaller ratio of the effective sheet thickness to hook height. While increasing the tool shoulder plunge depth, the weld bond width increased as more material is displaced upwards, hence forming a weld bond. But for most cases, increasing the bond width resulted in shorter effective sheet thickness, which leads to lower strengths. As in case of tool rotation rate and tool

dwell time, there is an optimal process window such that the static strength of the FSW joints increased to a certain should plunge depth and then decreased upon further plunging the tool [19,23,26,76].

1.5. Overview of Friction Stir Welding of Dissimilar Materials

To integrate the optimum physical, mechanical and chemical properties of magnesium alloys with existing components, it is paramount to be able to join magnesium and aluminum alloys. However, the challenge of joining the dissimilar alloys lies in the formation of the brittle intermetallics compounds (IMC) in the weld zone. Research studies until now have reported on the formation of IMCs and its influence on the tensile strength of the FSW [25,37,38,42,46–48]. Peak temperature ranging to 450^{o}C is easily attained in the stir zone during the FSW of magnesium to aluminum. This temperature is well below the melting point of both aluminum and magnesium, but high enough to form liquid films. On cooling of this liquid film, the IMCs ($Al_{12}Mg_{17}$, $Al_{3}Mg_{2}$) were produced at the weld interface due constitutional liquation [37,42,46–48]. These IMCs are brittle, fragile and much harder compared to the base material and act as points for easy fracture. Several studies have reported the effect of IMCs on the weld strength in FSW joints. In certain FSW joints of magnesium to aluminum, the weld strength was affected by the dimension and distribution of the IMCs. The lap-shear strength of FSSWed aluminum-to-magnesium reduced in welds that had continues formation of IMCs in the stir zone [25]. In FSLW of aluminum to magnesium, the lap-shear strength of the welds were much lower for welds with thicker layer of IMCs compared to welds with thinner layer of IMCs [47].

The material position in FSLW of aluminum-to-magnesium in butt weld configuration has been shown to affect the weld strength. This was mainly due to the frictional heat that's produced while the tool removes the material from the advancing side of the weld. Placing magnesium on the advancing side of the weld was shown to improve the weld strength compared to placing aluminum on the advancing side of the weld [43]. As in FSW of similar materials, the welding process condition such as the tool rotation rate, dwell time affected the weld strength of the dissimilar joints. Increase in friction heat due to higher tool rotation rate and dwell time favored the formation of IMCs and resulted in lower lap-shear strength in FSSWed aluminum-to-magnesium [45]. At very low tool rotation rate, defects such as voids were observed in the weld due to insufficient material mixture. And as the tool rotation increased, defect free welds were produced [39]. This suggests that the weld process condition is different for different combination of materials. Offsetting the weld tool center into magnesium in friction stir butt welding resulted in welds with good lap-shear strength compared to welds produced when the weld tool was offset into aluminum [43]. Most of the literature on FSW of dissimilar magnesium-to-aluminum is mainly on butt welded configuration [40,44,45,47–49,86]. Limited attention has been given to FSW of dissimilar materials in lap-shear configuration [43,87,88], although lap-shear welding configuration is the most commonly used weld configuration for the automotive industry.

1.6. Preface to chapters

This research study can be broadly classified into two parts. Part I discusses friction stir spot welding of similar magnesium-to-magnesium alloys. In part II, friction stir spot welding and friction stir linear welding of dissimilar magnesium-to-aluminum alloys is discussed.

Part I of the study will mainly discuss the process-structure-property relations in FSSWed magnesium-to-magnesium alloys. In particular, a feasibility study to investigate the use of FSSW as a viable technique to join rare earth added magnesium ZEK100 alloy is presented in Chapter two. The influence of welding process conditions such as the tool rotation rate, tool plunge depth is analyzed in depth and presented. How does the structural-integrity of the FSSWed magnesium ZEK100 alloy compare that to FSSWed non-rare earth element containing magnesium alloy will also be presented. In chapter three, the effect of structural-integrity and fatigue performance of lap-shear FSSW magnesium-to-magnesium AZ31 alloys produced using two different weld tools and two different weld process conditions will be presented. In this chapter, the influence of weld tool on macro and micro features and how these features affect the fatigue performance of the lap-shear FSSW magnesium-to-magnesium alloys is presented. The results presented in part I of this study is significant for two reasons; first, no research to-date has been performed on the feasibility of FSSW rare-earth containing magnesium ZEK100 alloy; and second, this study provides insight on factors influencing the fatigue performance and structural-integrity in magnesium-to-magnesium alloy joining via FSSW.

Part II of the study will focus on the joining of dissimilar magnesium-to-aluminum via the FSSW and FSLW. In chapter four, the feasibility of joining magnesium AM60B and aluminum 6022-T4 alloys by FSSW is presented. The effect of tool rotation rate, tool shoulder plunge depth on the formation of IMCs, and the weld macro and micro features and its influence on lap-shear strength of the FSSWed aluminum-to-magnesium alloy is examined. In chapter five, the effect of welding process conditions such as the tool rotation rate and tool traverse speed on FSLW of aluminum-to-magnesium will be discussed. In chapter six, a detailed study on how the macro

features and micro features such as the grain size and formation of IMCs effect the fatigue properties and failure modes in these FSLW dissimilar joints will be presented. Finally, in chapter seven, the main conclusions of this research and future work with regards to the FSW as a viable technique to join similar and dissimilar magnesium alloys is discussed.

1.7. Bibliography

[1] H. Friedrich, S. Schumann, J. Mater. Process. Technol. 117 (2001) 276.

[2] G.S. Cole, A.M. Sherman, Mater. Charact. (1995) 3.

[3] E. Aghion, B. Bron, D. Eliezer, J. Mater. Process. Technol. 117 (2001) 381.

[4] C. Blawert, N. Hort, K.U. Kainer, Trans. Indian Inst. Met. 57 (2006) 397.

[5] J. Davis, in:, SAE Tech. Pap. 910551, Detroit, MI, 1991.

[6] B.L. Mordike, T. Ebert, Mater. Sci. Eng. A 302 (2001) 37.

[7] A. A. Luo, J. Mater. Sci. 54 (2002) 42.

[8] M. Easton, A. Beer, M. Barnett, C. Davies, G. Dunlop, Y. Durandet, S. Blacket, T. Hilditch, P. Beggs, J. Mater. Sci. 60 (2008) 57.

[9] G. Song, Adv. Eng. Mater. 7 (2005) 563.

[10] J.C. Mariusz Boba, Michael J. Worswick, Raja Mishra, in:, 9th Int. Conf. Magnes. Alloy. Their Appl., 2012, pp. 397–402.

[11] S. Lee, Y. H. Chen, J. Y. Wang, J. Mater. Process. Technol. 124 (2002) 19.

[12] F.-K. Chen, T.-B. Huang, J. Mater. Process. Technol. 142 (2003) 643.

[13] K. Hantzsche, J. Bohlen, J. Wendt, K.U. Kainer, S.B. Yi, D. Letzig, Scr. M 63 (2010) 725.

[14] D.G.J. Griffiths, J. Robson, B. Davis, in:, 9th Int. Conf. Magnes. Alloy. Their Appl., 2012.

[15] J. Bohlen, M.R. Nürnberg, J.W. Senn, D. Letzig, S.R. Agnew, Acta Mater. 55 (2007) 2101.

[16] P. Thornton, A.R. Krause, R.G. Davies, Weld. J. 75 (1996) 101s.

[17] A. Gean, S.A. Westgate, J.C. Kucza, J.C. Ehrstrom, Weld. Journal- New York 78 (1999) 80s.

[18] Z. Zhang, X. Yang, J. Zhang, G. Zhou, X. Xu, B. Zou, Mater. Des. 32 (2011) 4461.

[19] S. Bozzi, L. Helbert-Etter, T. Baudin, V. Klosek, J.G. Kerbiguet, B. Criqui, J. Mater. Process. Technol. 210 (2010) 1429.

[20] W. Thomas, E. Nicholas, J. Needham, M.. Murch, P. Templesmith, C.. Dawes, Frcition Stir Butt Welding, G.B. Patent 9125978.8, 1991.

[21] H. Badarinarayan, Y. Shi, X. Li, K. Okamoto, Int. J. Mach. Tools Manuf. 49 (2009) 814.

[22] H. Badarinarayan, Q. Yang, S. Zhu, Int. J. Mach. Tools Manuf. 49 (2009) 142.

[23] D. Mitlin, V. Radmilovic, T. Pan, J. Chen, Z. Feng, M.L. Santella, Mater. Sci. Eng. A 441 (2006) 79.

[24] Y. Tozaki, Y. Uematsu, K. Tokaji, Int. J. Mach. Tools Manuf. 47 (2007) 2230.

[25] Y.S. Sato, a. Shiota, H. Kokawa, K. Okamoto, Q. Yang, C. Kim, Sci. Technol. Weld. Join. 15 (2010) 319.

[26] W. Yuan, R.S. Mishra, S. Webb, Y.L. Chen, B. Carlson, D.R. Herling, G.J. Grant, J. Mater. Process. Technol. 211 (2011) 972.

[27] W. Yuan, R.S. Mishra, B. Carlson, R. Verma, R.K. Mishra, Mater. Sci. Eng. A 543 (2012) 200.

[28] J.B. Jordon, M.F. Horstemeyer, S.R. Daniewicz, H. Badarinarayan, J. Grantham, J. Eng. Mater. Technol. 132 (2010) 041008.

[29] K.N. Solanki, J.B. Jordon, W. Whittington, H. Rao, C.R. Hubbard, Scr. Mater. 66 (2012) 797.

[30] D. A. Wang, C. H. Chen, J. Mater. Process. Technol. 209 (2009) 367.

[31] C. Zhou, X. Yang, G. Luan, Scr. Mater. 53 (2005) 1187.

[32] A.M.S. Malafaia, M.T. Milan, M.F. Oliveira, D. Spinelli, Procedia Eng. 2 (2010) 1815.

[33] P. Lin, J. Pan, T. Pan, Int. J. Fatigue 30 (2008) 74.

[34] V.X. Tran, J. Pan, T. Pan, Int. J. Fatigue 32 (2010) 1022.

[35] P. Mallick, L. Agarwal, Soc. Automot. Eng. Warrendale, PA (2009).

[36] S.H. Chowdhury, D.L. Chen, S.D. Bhole, X. Cao, P. Wanjara, Mater. Sci. Eng. A 562 (2013) 53.

[37] S.H. Chowdhury, D.L. Chen, S.D. Bhole, X. Cao, P. Wanjara, Mater. Sci. Eng. A 556 (2012) 500.

[38] C. Lee, D.. Choi, Y. Yeon, S.. Jung, Sci. Technol. Weld. Join. 14 (2009) 216.

[39] Y.H. Yin, N. Sun, T.H. North, S.S. Hu, Mater. Charact. 61 (2010) 1018.

[40] Y.S. Sato, S.H.C. Park, M. Michiuchi, H. Kokawa, Scr. Mater. 50 (2004) 1233.

[41] A. Gerlich, P. Su, T.H. North, Sci. Technol. Weld. Join. 10 (2005) 647.

[42] D.H. Choi, B.W. Ahn, C.Y. Lee, Y.M. Yeon, K. Song, S.B. Jung, Intermetallics 19 (2011) 125.

[43] V. Firouzdor, S. Kou, Metall. Mater. Trans. A 41 (2010) 2914.

[44] A. Kostka, R.. Coelho, J. dos Santos, A.. Pyzalla, Scr. Mater. 60 (2009) 953.

[45] Y.J. Kwon, I. Shigematsu, N. Saito, Mater. Lett. 62 (2008) 3827.

[46] Y.C. Chen, K. Nakata, Scr. Mater. 58 (2008) 433.

[47] N. Yamamoto, J. Liao, S. Watanabe, K. Nakata, Mater. Trans. 50 (2009) 2833.

[48] A.. McLean, G.L.F. Powell, I.H. Brown, V.M. Linton, Sci. Technol. Weld. Join. 8 (2003) 462.

[49] X.J. Cao, M. Jahazi, Mater. Sci. Forum 638-642 (2010) 3661.

[50] W. Woo, H. Choo, M.B. Prime, Z. Feng, B. Clausen, Acta Mater. 56 (2008) 1701.

[51] M.W. Mahoney, C.G. Rhodes, J.G. Flintoff, R.A. Spurling, W.H. Bingel, Metall. Mater. Trans. A 29 (1998) 1955.

[52] R.S. Mishra, Z.Y. Ma, Mater. Sci. Eng. R Reports 50 (2005) 1.

[53] W. Yuan, B. Carlson, R. Verma, R. Szymanski, Sci. Technol. Weld. Join. 17 (2012) 375.

[54] W. Xunhong, W. Kuaishe, Mater. Sci. Eng. A 431 (2006) 114.

[55] J.H. Ouyang, R. Kovacevic, J. Mater. Eng. Perform. 11 (2002) 51.

[56] W.M.U. Thomas, E.D. Nicholas, A. Hall, C. Cb, Mater. Des. 18 (1997) 269.

[57] R. Nandan, T. Debroy, H. Bhadeshia, Prog. Mater. Sci. 53 (2008) 980.

[58] D. Fersini, a. Pirondi, Eng. Fract. Mech. 74 (2007) 468.

[59] G. Buffa, G. Campanile, L. Fratini, a. Prisco, Mater. Sci. Eng. A 519 (2009) 19.

[60] M.K. Yadava, R.S. Mishra, Y.L. Chen, B. Carlson, G.J. Grant, Sci. Technol. Weld. Join. 15 (2010) 70.

[61] M. Sutton, B. Yang, A. Reynolds, R. Taylor, Mater. Sci. Eng. A 323 (2002) 160.

[62] S.M. Chowdhury, D.L. Chen, S.D. Bhole, X. Cao, Mater. Sci. Eng. A 527 (2010) 6064.

[63] Q. Yang, X. Li, K. Chen, Y.J. Shi, Mater. Sci. Eng. A 528 (2011) 2463.

[64] Y.C. Chen, K. Nakata, Mater. Des. 30 (2009) 3913.

[65] N. Afrin, D.L.L. Chen, X. Cao, M. Jahazi, Mater. Sci. Eng. A 472 (2008) 179.

[66] S.H. Chowdhury, D.L. Chen, S.D. Bhole, X. Cao, P. Wanjara, Metall. Mater. Trans. A 44 (2012) 41.

[67] L. Cederqvist, A.P. Reynolds, Weld. J. 80 (2001) 281.

[68] Y.H. Yin, N. Sun, T.H. North, S.S. Hu, J. Mater. Process. Technol. 210 (2010) 2062.

[69] S. Lathabai, M.J. Painter, G.M.D. Cantin, V.K. Tyagi, Scr. Mater. 55 (2006) 899.

[70] A.P. Gerlich, T.H. North, Innov. Mater. Manuf., 2010, pp. 193–217.

[71] M. Fujimoto, S. Koga, N. Abe, Y.S. Sato, H. Kokawa, Sci. Technol. Weld. Join. 13 (2008) 663.

[72] D. A. Wang, S. C. Lee, J. Mater. Process. Technol. 186 (2007) 291.

[73] A. Gerlich, P. Su, T.H. North, J. Mater. Sci. 40 (2005) 6473.

[74] Q. Yang, S. Mironov, Y.S. Sato, K. Okamoto, Mater. Sci. Eng. A 527 (2010) 4389.

[75] N. Sun, Y.H. Yin, A P. Gerlich, T.H. North, Sci. Technol. Weld. Join. 14 (2009) 747.

[76] Y.H. Yin, N. Sun, T.H. North, S.S. Hu, Sci. Technol. Weld. Join. 15 (2010) 81.

[77] Y. Tozaki, Y. Uematsu, K. Tokaji, Fatigue Fract. Eng. Mater. Struct. 30 (2007) 143.

[78] C. Y. Lee, W. B. Lee, J. W. Kim, D.-H. Choi, Y. M. Yeon, S.-B. Jung, J. Mater. Sci. 43 (2008) 3296.

[79] A. Gerlich, G. Avramovic-Cingara, T.H. North, Metall. Mater. Trans. A 37 (2006) 2773.

[80] M. Yamamoto, a. Gerlich, T.H. North, K. Shinozaki, Sci. Technol. Weld. Join. 12 (2007) 208.

[81] P. Su, a. Gerlich, T.H. North, G.J. Bendzsak, Sci. Technol. Weld. Join. 11 (2006) 163.

[82] S.G. Arul, S.F. Miller, G.H. Kruger, T.-Y. Pan, P.K. Mallick, a. J. Shih, Sci. Technol. Weld. Join. 13 (2008) 629.

[83] A. Gerlich, M. Yamamoto, T.H. North, J. Mater. Sci. 43 (2007) 2.

[84] A. Gerlich, M. Yamamoto, T.. North, Metall. Mater. Trans. A 38 (2007) 1291.

[85] V. Tran, J. Pan, T. Pan, Int. J. Fatigue 30 (2008) 2175.

[86] T. DebRoy, H.K.D.H. Bhadeshia, Sci. Technol. Weld. Join. 15 (2010) 266.

[87] V. Firouzdor, S. Kou, Metall. Mater. Trans. A 41 (2010) 3238.

[88] S. Kou, Weld. J. 88 (2009) 213.

Chapter 2

FRICTION STIR SPOT WELDING OF RARE-EARTH ADDITION ZEK100 MAGNESIUM ALLOY

Abstract

In this study, rare-earth containing ZEK100 magnesium alloy sheets were joined using friction stir spot welding. In order to determine the influence of welding parameters on lap-shear strength, overlap joints were created under various tool rotational speeds and shoulder plunge depths. Relationships between the maximum lap-joint strength and key features of the weld including effective sheet thickness, interfacial hook width, and shoulder plunge depth were established. Based on the results of this study, welds with larger effective upper sheet thickness and small interfacial hook height generally exhibited the highest lap-shear strength. In addition, experiments indicated that overlap joints welded at 1500 rpm and 0.2 mm tool shoulder plunge depth exhibited the highest lap-shear strength.

2.1. Introduction

Due to their high strength-to-weight properties, Mg alloys are receiving increased interest as automotive and aerospace industries move toward lightweight designs. However, the application of commonly used Mg alloys, such as AZ31 and AZ61, has been limited by their poor formability at room temperature [1–3]. To address this issue, the addition of rare-earth elements together with zinc has been shown to improve the formability of Mg alloys at room temperature which is attributed to the weakening of the strong basal texture commonly observed on wrought Mg alloys [4–6]. Among the rare-earth Mg alloys, ZEK100 is of high interest due to its excellent formability at room temperature [2,4,5,7]. While the joining of Mg alloy sheets using the innovative friction stir spot welding (FSSW) is well established [8–10], the feasibility of this joining technique for rare-earth containing ZEK100 Mg alloy is unknown. As is the case in any welding technique, variation in the welding conditions in FSSW has a large influence on the mechanical properties of the welded joint [9,11–14]. In fact, a significant factor contributing to lap-shear strength is the tool rotation rate, where a decrease in joint strength is typically observed as the tool rotation rate increases [11]. Moreover, interfacial hooks formed at the faying surface, which partially depend on tool rotation rate, also affect the joint strength of the FSSW coupons [8,9,12]. While studies have been conducted to examine the influence of welding condition on microstructure and mechanical properties of the FSSW in wrought Mg alloys, this is the first study to examine the influence of welding conditions on the lap-shear strength of the ZEK100 Mg alloy joined by FSSW.

2.2. Material and experiments

Rolled ZEK100 Mg alloy sheets of 1.4 mm thick were chosen for the present study. FSSW coupons were produced in lap-shear con- figuration. The individual sheet dimensions are shown in Fig. 2-1(a). As shown in Fig. 2-1(b), a cylindrical unthreaded FSSW tool made of tool steel (H13) having a shoulder diameter of 12 mm, pin length of 1.8 mm and pin diameter of 5 mm was used. As listed in Table 2-1, six sets of coupons were welded under various process conditions. For weld characterization, coupons were sectioned through the center of the weld nugget and cold mounted and then mechanically ground and polished. The final polishing sequence was accomplished by using 3 and 1 μm oil based diamond suspensions, followed by a 0.25 μm colloidal silica with ethylene glycol step. In order to characterize the microstructure of the FSSW coupons, the samples were etched using a 4.2 g picric acid, 10 ml acetic acid, 10 ml H 2 O and 70 ml ethanol. Representative features of the weld are shown in Fig. 2-1(c). Key features of the weld such as the size and shape of the interfacial hook, the bond width, effective upper sheet thickness, and microstructure were characterized using a Keyence VHX-1000 digital optical microscope. Microhardness measurements through the transverse cross section of the welded region were carried out using a Wilson hardness testing machine by applying a load of 100 gf and a dwell time of 5 s. The traverses were performed on the top sheet, beginning at the keyhole vertical wall and moving toward the base material using a 0.5 mm spacing between each indent. Lap shear tests were performed at room temperature using an electro-mechanical tensile tester in displacement control mode at a rate of 1 mm / min. Shims of 2mm in thickness were used in the grips of the test frame to prevent additional bending forces similar to [8-9]. The grip-to-grip distance employed for each coupon was 105 mm.

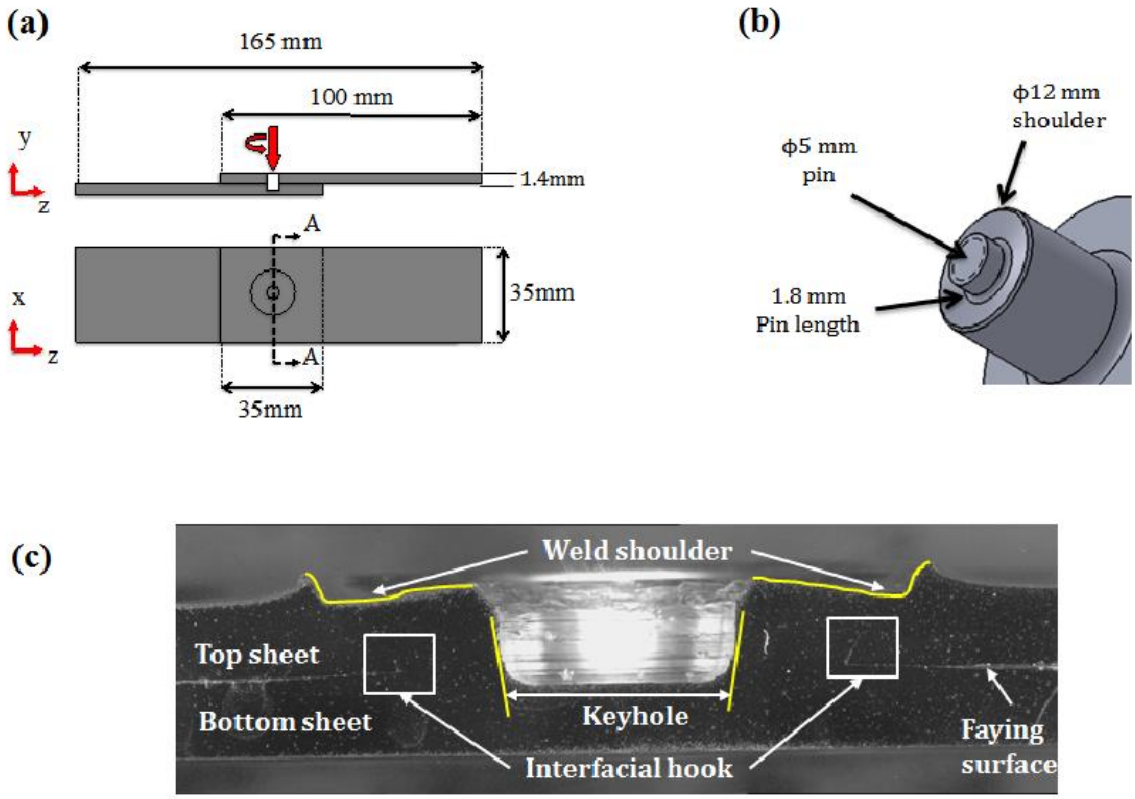

Figure 2-1: Schematic figure illustrating (a) FSSW coupons employed in this study with dimensions and (b) Geometry of the FSSW tool in this study to produce weld joints (c) Cross section view of the weld nugget indicating various weld features.

Table 2-1: FSSW process parameters adopt in this current study.

Welding Parameters	Process #1	Process #2
Tool rotation (RPM)	1500	2250
Plunge Depth (mm)	0/0.2/0.6	0/0.2/0.6
Dwell Time (sec)	2.5	2.5

2.3. Results and discussion

Optical microscopy of the FSSW joint revealed a hook-like formation near the keyhole periphery and the faying surfaces. This hooking is a result of oxide films trapped between the faying surfaces that are displaced upward due to the plastic flow of the material resulting from the downward plunge of the tool pin during the welding process. The mechanism of hook formation and influence of tool geometry, tool rotation rate and plunge depth have been well documented in other studies of FSSW [8, 9, 12, 13, 15]. In fact, parameters such as the tool rotation rate and tool shoulder plunge depth determine the frictional heat and the material plasticization around the pin, which in turn influence the weld geometry and the mechanical properties of the FSSW [16]. Fig. 2-1(c) shows representative cross section of the weld with different weld features. Key geometrical features of the weld such as the tool shoulder plunge depth (D), effective top sheet thickness (T) and hook width (W) were measured as a function of lap-shear strength.

Figure 2-2(a) shows the lap-shear strength against the tool shoulder plunge depth (D). The FSSW coupons joined at a high tool rotation rate (2250 rpm) and large tool shoulder plunge depth (0.6 mm) failed at much lower loads compared to coupons joined at lower tool rotation speed and lower tool shoulder plunge depths. In fact, coupons fabricated at 1500 rpm and 0.2 mm tool shoulder plunge depth exhibited the highest lap-shear failure load of ~3.2 kN. As shown in Fig. 2-2(a), an increase in lap-shear strength was observed as the plunge depth increased from 0.0 to 0.2 mm followed by a decrease at a shoulder plunge depth of 0.6 mm. This decrease in lap-shear strength is attributed to the reduced effective upper sheet thickness (T) which is defined as the distance from the tip of the hook to the nearest free surface. Furthermore, tool rotation rate was

observed to influence the lap-shear strength performance revealing higher lap-shear strengths for coupons welded at 1500 rpm.

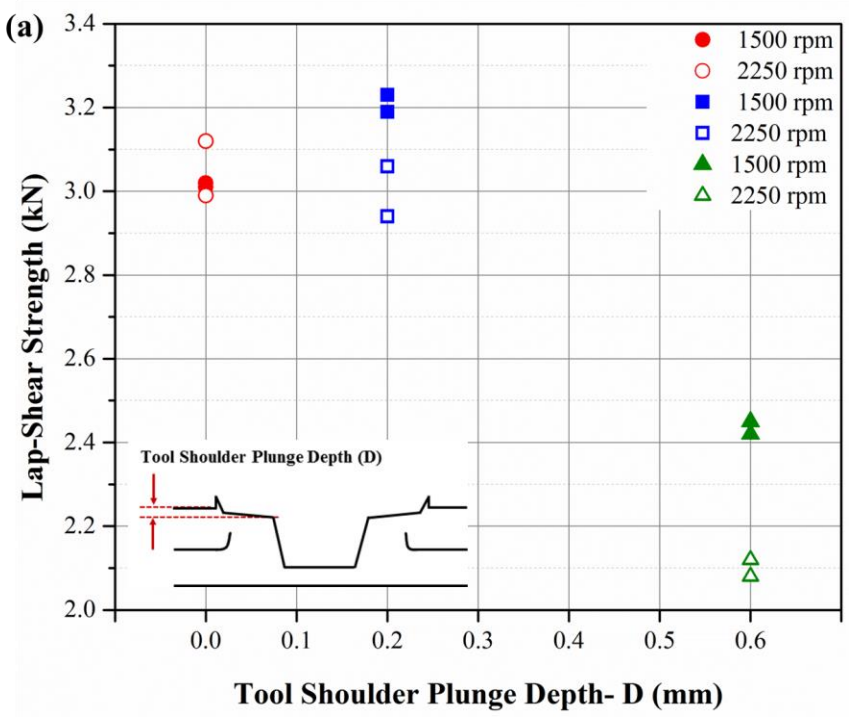

Figure 2-2 (a): Lap-shear strength as a function of tool shoulder plunge depth-D.

Figure 2-2(b) compares the lap-shear strength of individual coupons against the effective upper sheet thickness (T). For the same tool shoulder plunge depth, a larger effective sheet thickness was observed for welds produced at 1500 rpm when compared to welds produced at 2250 rpm. With the increase in tool shoulder plunge depth more material is removed from the top sheet and as a result, the distance from the hook tip to nearest free surface is reduced. Similar results were reported in other studies conducted on FSSW of lightweight alloys [9, 13, 16]. Also, the interfacial hook height was observed to in- crease with increased tool shoulder plunge depth and tool rotation speed. An inverse relation exists between the hook height and effective sheet

thickness. As the hook height increased, the effective sheet thickness decreased. For brevity's sake, only the plot comparing the effective sheet thickness against lap-shear strength is presented in this study. The height of the interfacial hooks are highly influenced by welding conditions including shoulder plunge depth, tool rotation speed, and tooling design [8, 9, 12, 13, 16].

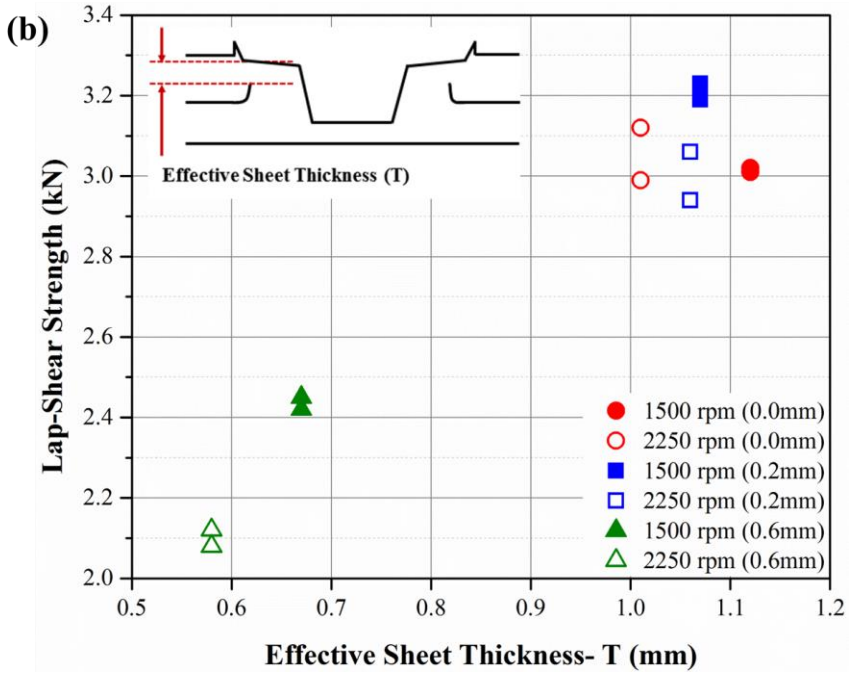

Figure 2-2 (b): Lap-shear strength as a function of effective sheet thickness-T.

The results of this study suggest that the height of the interfacial hooks and effective sheet thickness (T) are highly influenced by welding process parameters mainly due to the tool shoulder plunge depth and the tool rotation rate. Previous studies of FSSW report similar observations on the influence of the weld process parameters on the geometrical features of the weld [8, 9, 12, 13, 17]. The results in Fig. 2-2(b) show that the effective sheet thickness (T) decreased with an increase in tool shoulder plunge depth (D). Similar observations were made in a study of FSSW aluminum alloys using a cylindrical tool pin [17]. Additionally, Yin et al. [12, 18] proposed that for an

acceptable weld joint strength in FSSW magnesium alloys, a large bond width with a smaller hook height-to-sheet thickness ratio should be maintained. In the current study, the welds produced at 1500 rpm and 0.2 mm plunge depth had the smaller hook height-to-sheet thickness ratio and a relatively large hook width (W).

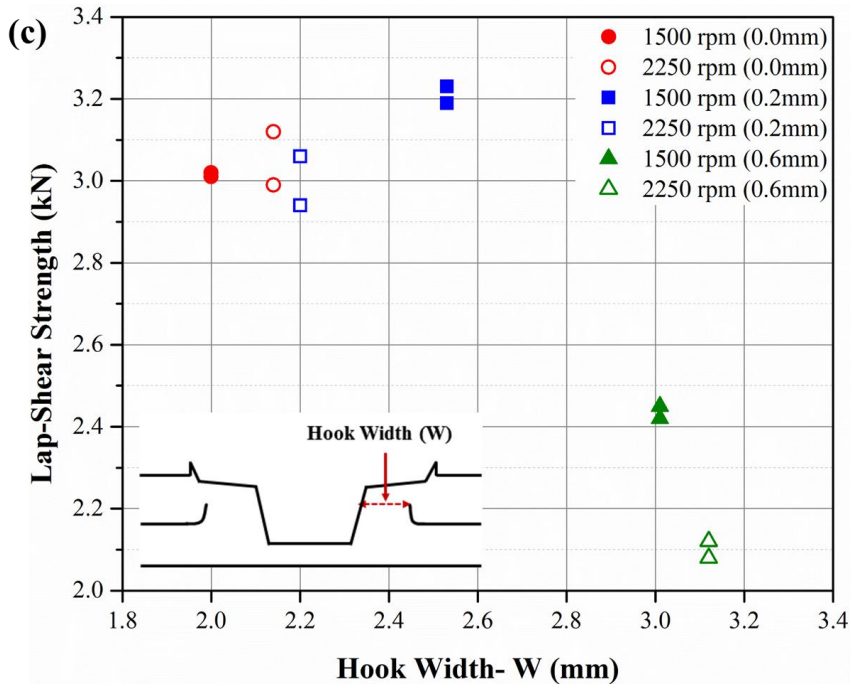

Figure 2-2 (c): Lap-shear strength as a function of tool hook width-W.

Figure 2-2(c) compares the lap-shear strength of individual coupons against the hook width. The hook width (W) was observed to increase with the increase in tool rotation speed as well as plunge depth. As the tool plunges into the bottom sheet, the downward force of the tool shoulder causes the interfacial hooks to be pushed away from the tool rotation axis. As a result, the hook width is increased as the shoulder plunge depth is increased. Despite that the results of a previous study [17] that suggested that the lap-shear strength increased with the increased hook width and large effective thickness, only a weak correlation was observed in this study. However,

we note that as the hook width increased, a decrease in the effective sheet thickness was observed, which is likely the reason the strength of the weld did not correlate well with the hook width.

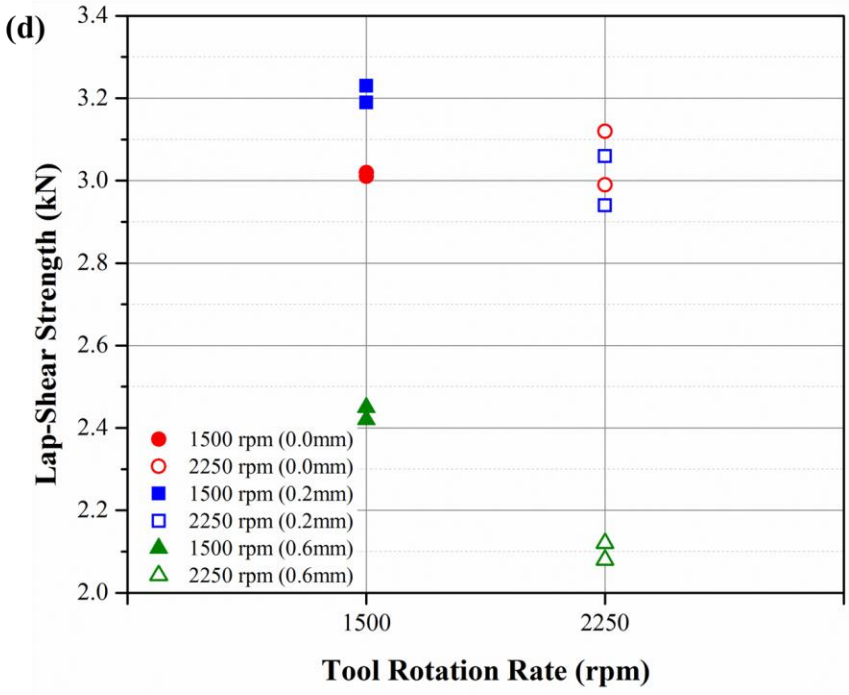

Figure 2-2 (d): Lap-shear strength as a function of tool rotation rate-rpm. The number shown in parenthesis denotes the shoulder plunge depth.

Figure 2-2(d) compares the lap-shear strength of individual coupons against to tool rotation rate. The variation in static strength between the two tool rotation rates for identical tool shoulder plunge depth is evidence of the influence of tool rotation rate on the microstructure. In fact, for the same shoulder plunge depth, the lower tool rotation rate (1500 rpm) exhibited better lap-shear strength compared to the higher tool rotation rate (2250 rpm).

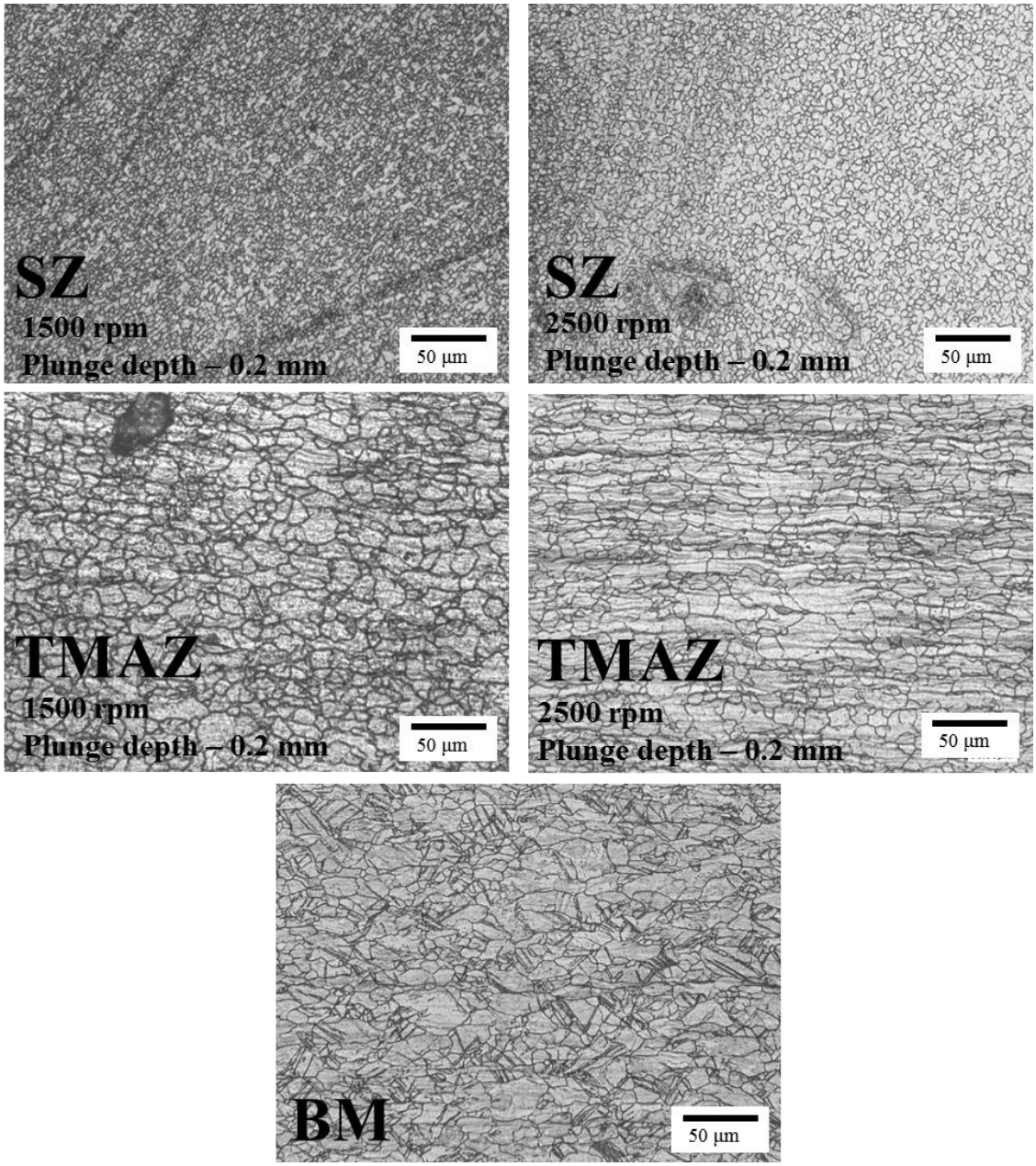

Figure 2-3: Representative microstructure of the friction stir spot welded lap-shear coupons in the stir zone (SZ), thermo-mechanically affected zone (TMAZ), and base material (BM). The tool rotation rate and shoulder plunge depth are indicated on the corresponding image.

This higher strength is due to the difference in microstructure; similar observations have been re- ported elsewhere [9, 19]. Figure 2-3 show representative microstructure for the lower (1500 rpm) and the higher (2250 rpm) tool rotation rate. Figure 2-3 show the grain structure in the stir zone (SZ) and thermo- mechanically affected zone (TMAZ) of the welds for 1500 rpm and 2250 rpm at a plunge depth of 0.2 mm. In addition, Fig. 2-3 shows the microstructure of the base material (BM). As commonly observed, the SZ, which is adjacent to the key-hole, experienced a high degree of plastic deformation resulting in formation of very fine grains com- pared to base material, which is characterized by larger irregularly shaped grains. The TMAZ, which is adjacent to the SZ and below the tool shoulder, experienced a high degree of heat, but less plastic deformation, and thus resulted in the formation of larger partially recrystallized grains in this region. In fact, it is clearly seen that the grains in the SZ and TMAZ experienced greater recrystallization at 2250 rpm tool rotation rate due to the increase heat generation compared to the welds made at 1500 rpm. This difference in grain structure resulted in the observed disparity of lap-shear strengths for the same plunge depth.

To further confirm the effect of the tool rotation rate on the microstructure, microhardness measurements of the SZ, TMAZ and BM of the top sheet, were performed. As shown in Fig. 2-4 the hardness near the keyhole in the SZ exhibited the highest hardness values due to presence of a very fine microstructure. The hardness was observed to decrease in TMAZ and the BM relative to the SZ. The decrease in the hardness measurements away from the keyhole is due to the presence of the larger partially recrystallized grains as shown in Fig. 2-3. Similar observations were made in FSSW of Mg AZ31 alloys [18, 19]. The microhardness measurements confirm that the lower

tool rotation rate (1500 rpm) produced a finer microstructure leading to better lap-shear strength for the same shoulder plunge depth compared to the higher tool rotation rate (2250 rpm).

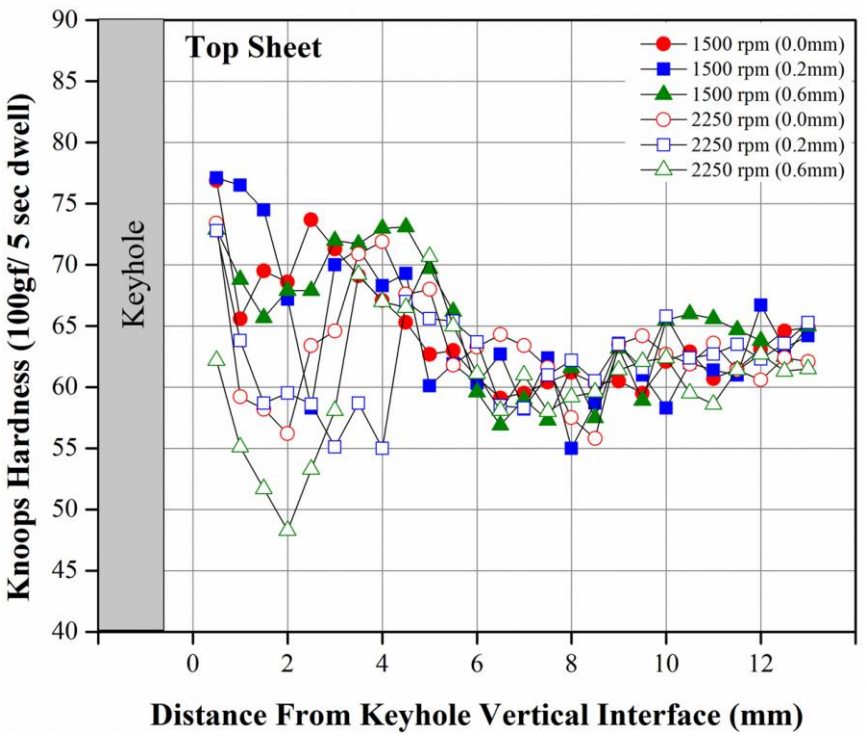

Figure 2-4: Microhardness profile of the FSSW specimens along weld cross section. The number shown in parenthesis denotes the shoulder plunge depth.

Figure 2-5 shows representative failure modes for the coupons fabricated at various tool rotation rates and plunge depth combinations. Note that the number in parenthesis in each image denotes the shoulder plunge depth. Two main types of failure modes were primarily observed. First, as shown in Fig. 2-5 (a), (d) and (e), failure occurred by interfacial shear failure. However, as shown in Fig. 2-5(b), (c) and (f), failure occurred by nugget pullout, where the crack propagated through the upper sheet. In fact, failure through the upper sheet, leading to nugget pullout, was dominant in coupons having a larger hook width and smaller effective sheet thickness. In contrast,

interfacial shear failure was dominant in coupons having a smaller hook width and larger effective sheet thickness. It is important to note that while the variation in the hook width did not have an affect on the lap-shear strength, the hook width appeared to have affected the failure mode. As shown in Fig. 2-5(a), (d), and (e), the welds with the smaller hook width failed by interfacial shear compared to the welds with larger hook width which failed by nugget pullout. With the exception of the best performing weld (1500 rpm and 0.2 mm shoulder plunge depth), higher lap-shear strength was observed for welds that failed by interfacial shear.

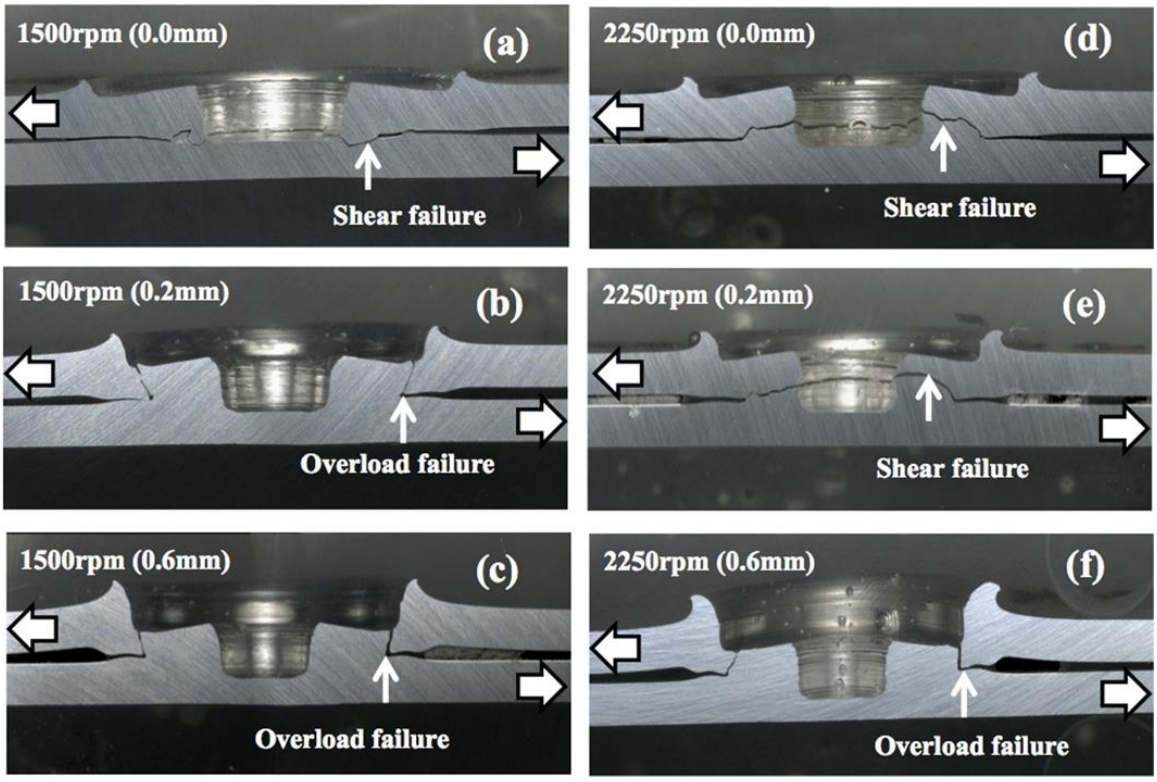

Figure 2-5: Lap-shear tensile failure modes of FSSW coupons welded at various tool speed and plunge depths. The number shown in parenthesis denotes the shoulder plunge depth and the horizontal arrows indicate the loading direction. The vertical arrows indicate the location of fracture initiation.

2.4. Conclusions

1. In this work, an investigation was carried out to quantify the influence of welding parameters on friction stir spot welding of a rare- earth containing ZEK100 Mg alloy. A summary of the main conclusions of this study are as follows: 1) Mg alloy ZEK100 sheets were successfully joined using FSSW.
2. An increase in tool rotation speed resulted in lower hardness measurements, larger hook height, and smaller effective sheet thick- ness and hook width.
3. Coupons with a large upper effective sheet thickness and a small hook height were found to have the highest lap-shear strength.
4. Lap-shear tensile experiments indicate that coupons welded at 1500 rpm and 0.2 mm tool shoulder plunge depth exhibited the highest lap-shear strength.
5. The interfacial shear failure was observed on coupons that contained large effective sheet thicknesses. Nugget pullout failure was observed in coupons that contained small upper effective sheet thickness and large hook width.

2.5. Bibliography

[1] S. Lee, Y.-H. Chen, J.-Y. Wang, J. Mater. Process. Technol. 124 (2002) 19.

[2] J.C. Mariusz Boba, Michael J. Worswick, Raja Mishra, in:, 9th Int. Conf. Magnes. Alloy. Their Appl., 2012, pp. 397–402.

[3] F. K. Chen, T. B. Huang, J. Mater. Process. Technol. 142 (2003) 643.

[4] K. Hantzsche, J. Bohlen, J. Wendt, K.U. Kainer, S.B. Yi, D. Letzig, Scr. M 63 (2010) 725.

[5] D.G.J. Griffiths, J. Robson, B. Davis, in:, 9th Int. Conf. Magnes. Alloy. Their Appl., 2012.

[6] J. Bohlen, M.R. Nürnberg, J.W. Senn, D. Letzig, S.R. Agnew, Acta Mater. 55 (2007) 2101.

[7] S. Kurukuri, D.G. Tari, M.J. Worswick, R.K. Mishra, J.T. Carter, in:, 9th Int. Conf. Magnes. Alloy. Their Appl., 2012, pp. 2–7.

[8] J.B. Jordon, M.F. Horstemeyer, S.R. Daniewicz, H. Badarinarayan, J. Grantham, J. Eng. Mater. Technol. 132 (2010) 041008.

[9] H.. Rao, J.. Jordon, M.. Barkey, Y.. Guo, X. Su, H. Badarinarayan, Mater. Sci. Eng. A 564 (2013) 369.

[10] N. Afrin, D.L.L. Chen, X. Cao, M. Jahazi, Mater. Sci. Eng. A 472 (2008) 179.

[11] Z. Zhang, X. Yang, J. Zhang, G. Zhou, X. Xu, B. Zou, Mater. Des. 32 (2011) 4461.

[12] Y.H. Yin, N. Sun, T.H. North, S.S. Hu, J. Mater. Process. Technol. 210 (2010) 2062.

[13] W. Yuan, R.S. Mishra, S. Webb, Y.L. Chen, B. Carlson, D.R. Herling, G.J. Grant, J. Mater. Process. Technol. 211 (2011) 972.

[14] S.M. Chowdhury, D.L. Chen, S.D. Bhole, X. Cao, Mater. Sci. Eng. A 527 (2010) 6064.

[15] C.I. Chang, C.J. Lee, J.C. Huang, Scr. Mater. 51 (2004) 509.

[16] H. Badarinarayan, Y. Shi, X. Li, K. Okamoto, Int. J. Mach. Tools Manuf. 49 (2009) 814.

[17] Y.H. Yin, N. Sun, T.H. North, S.S. Hu, Sci. Technol. Weld. Join. 15 (2010) 81.

[18] S.H. Chowdhury, D.L. Chen, S.D. Bhole, X. Cao, P. Wanjara, Mater. Sci. Eng. A 556 (2012) 500.

[19] K.N. Solanki, J.B. Jordon, W. Whittington, H. Rao, C.R. Hubbard, Scr. Mater. 66 (2012) 797.

CHAPTER 3

INFLUENCE OF STRUCTURAL INTEGRITY ON FATIGUE BEHAVIOR OF FRICTION STIR SPOT WELDED MG AZ31 ALLOY

Abstract

In this paper the fatigue behavior of the friction stir spot welded (FSSW) coupons of magnesium AZ31 alloy manufactured under different welding process conditions is investigated. Two sets of lap-shear coupons were made based on variation in plunge depth, tool rotation speed and tool geometry. Metallographic analysis of the untested FSSW coupons revealed differences in weld geometry and microstructure. Interfacial hooking of the faying surface was found to vary significantly between the two sets of process conditions. Microhardness test data revealed a large gradient in hardness profile. Results from the load controlled cyclic tests showed that lower tool rotation and shallower shoulder plunge depth led to better fatigue performance. Optical fractography of the fatigued coupons revealed that fatigue cracks initiated at the weld interface in both sets of coupons. However, the fracture mode showed variability between the two process conditions. The fractography analysis suggests that the effective top sheet thickness, interfacial hook and microstructure, which are largely determined by the process conditions, significantly affect the fatigue behavior of the friction stir spot welds in magnesium alloys.

3.1. Introduction

Friction stir spot welding (FSSW) is a thermo-mechanical process for spot lap-joining of sheet metals as shown in Fig. 3-1 [1,2]. The rotating tool comprises a probe pin that is plunged into two sheets of metal to be joined. The probe pin typically penetrates the upper sheet completely and then passes into the bottom sheet to various depths depending on process conditions.

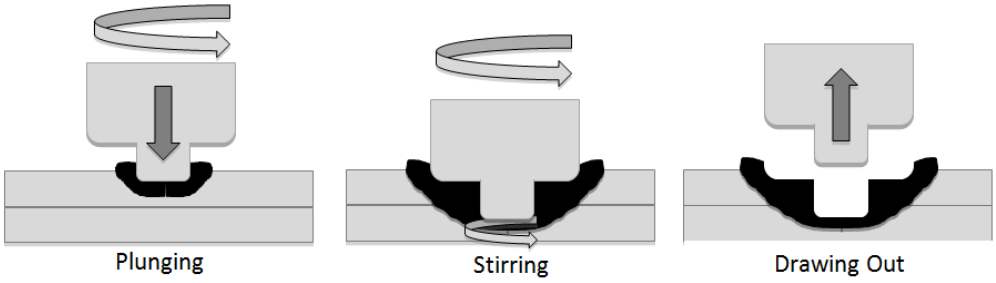

Figure 3-1: A schematic illustration of friction stir spot welding process.

Here, the downward force and rotational speed of the tool generates localized friction as the pin interacts with the upper sheet. The heat generated by friction softens the sheet materials adjacent to the tool and deforms plastically to form a solid state bond between the surface of upper and bottom sheet [3]. A longer dwell period typically provides the driving force for the upward displacement of the lower sheet material, which promotes good bonding [2]. Since the dwell time in a manufacturing setting is relatively short, e.g., 2 to 5 s, the tool rotation speed and plunging motion largely determines the heat generation [4], joint formation and weld mechanical properties [5]. In general, FSSW is free of defects commonly associated with fusion welding, mostly because the temperature attained during FSSW is less than the melting point of base materials. The other advantages of FSSW include no need of cooling agent, filler materials, or post weld treatment. In

addition, FSSW is more energy efficient and clean when compared to other types of spot welding techniques.

As industry continues the push for more fuel-efficient designs, magnesium alloys are receiving increased interest. Thus, FSSW is a favorable technique for spot welding lightweight metals, such as magnesium alloys. Some recent work on FSSW of magnesium AZ31 alloys has focused on the process-property-performance relation- ships [2,5–7]. One of the key findings was related to the size and shape of the interfacial hook. During FSSW, trapped oxide films present between the overlapping sheets are often displaced in an upward direction toward the top sheet into a ‘‘hook-like’’ shape. This hooking is largely due to the plastic flow of the material resulting from the downward plunge of the pin into the bottom sheet. In fact, higher joint static strengths were found when the hook region was curved more outwards from the tool axis and the distance from the hook extremity to the top surface of the weld was the greatest [7]. A similar observation was also found in aluminum alloys [8].

Regarding the effect of tool geometry, Badarinarayan et al. [9] noted that the triangular shaped tool head employed during FSSW significantly increased the lap-shear strength properties in Al 5083 sheets. Commin et al. [10] investigated the influence of the welding parameters on the microhardness evolution of FSW AZ31 Mg alloys and found that grain size increased with increase in heat input and resulted in a softer material in the thermomechanically affected zone (TMAZ). Xunhong et al. [11] found increased hardness in the nugget region of the weld where the grain size was much more refined than in the base metal or any other region of the weld.

While fundamental relationships governing the static strength of FSSW in magnesium alloys have been investigated, only a few studies exist regarding fatigue behavior and performance [12–14]. In lap- shear fatigue testing, fatigue cracks were found to initiate from this interfacial hook [13]. The coupons failed once the crack grew from the tip of the hook towards the nearest free surface. Hence, the geometry of the interfacial hook was found to be significant in determining the failure characteristics of the welded coupons [2,14]. However, beyond the work of Mallick and Agarwal [12], Jordon et al. [13], and Chowdhury et al. [14] the fundamental understanding of fatigue mechanisms in FSSW lap-joints is primarily restricted to aluminum alloys. Lin et al. [15,16] studied fatigue failures in friction spot welded aluminum 6111-T4 sheets processed using different geometrical tools. In addition, Lin et al. [15] compared the failure modes of FSSW made using different tool geometries. For spot welds created using a flat tool shoulder, cracks initiated from several locations compared to a concave tool shoulder. The amount of material deformation during the welding process due to the shape of the tool shoulder was identified as the likely reason for the difference in failure modes of the flat and concave tool. The fatigue cracks were observed to initiate near the possible original hook tip in the stir zone and propagated along the circumference of the nugget, then through the sheet thickness and finally along the width of the specimen [3].

While studies have been conducted on the influence of tool geometry on hook formation and fatigue life in FSSW Mg AZ31 alloy [2,7], no considerable study has been conducted on determining the influence of process conditions on fatigue life of FSSW Mg AZ31 alloy. In this paper, we attempt to correlate the fatigue life to the structural integrity of the weldment in FSSW Mg AZ31 alloy.

3.2. Material and Experiments

AZ31 Mg alloy sheets of 2.0mm thickness were chosen for the present study. Two sets of FSSW coupons were welded in an overlap configuration. For process 1, the individual sheet dimensions were: length of 100 mm, width of 35 mm, and a welded overlap area of 35x35 mm. For process 2, the individual sheet dimensions were: length of 100 mm, width of 38mm and a welded overlap area of 38x38 mm. For process 1, the FSSW tool was made from standard tool steel (H13) material with a shoulder diameter of 12mm and a cylindrical pin having a diameter of 5 mm, pin length of 3.2 mm, and left hand threads (M5), as shown in Fig. 3-2(a). For process 2, the FSSW tool is identical to the tool used in process 1; however the tool had a triangular pin as shown in Fig. 3-2(b). Both tools had a 101 concave shoulder as shown in Fig.3-2(c). Table 3-1 lists the process conditions used to join the two sets of lap-shear coupons employed in this study AZ31 Mg alloy sheets of 2.0 mm thickness were chosen for the present study. Figure 3-3 shows representative lap-shear samples from both process 1 and 2. For the fatigue tests, the lap-shear coupons were cyclically tested in an MTS 810 servo-hydraulic load frame under load control with a sinusoidal waveform at three different load ratios (0.1, 0.3, and 0.7).

Table 3-1: FSSW welding process parameters used in current study

Welding Parameters	**Process #1**	**Process #2**
Tool rotation (RPM)	1000	750
Tool Plunge Speed (mm/min)	20	20
Shoulder Plunge Depth (mm)	0.5	0.1
Dwell Time (sec)	2.5	2.5

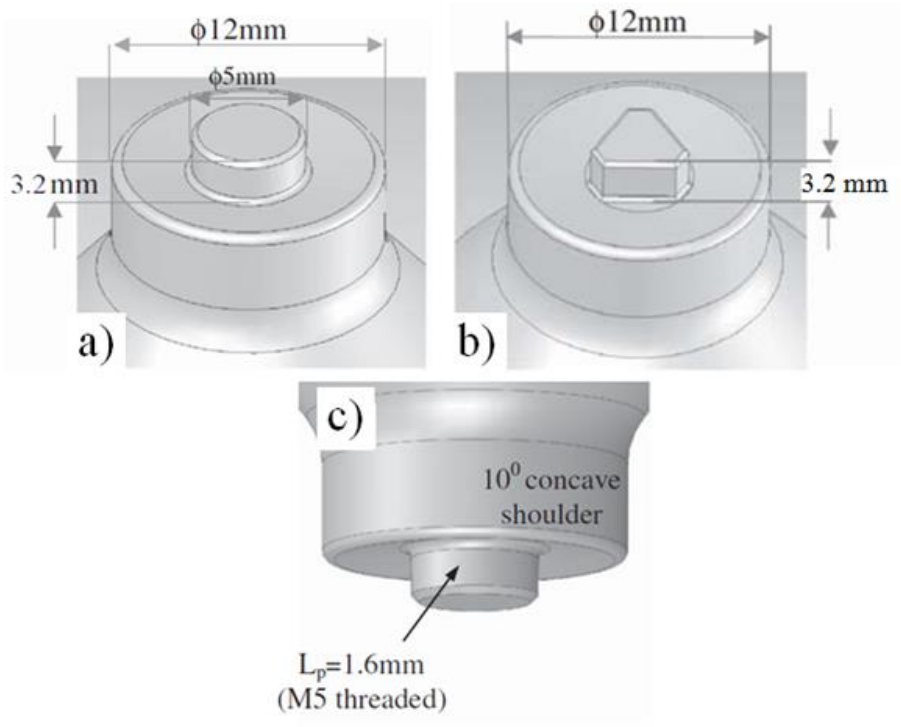

Figure 3-2: Schematic of the FSSW tool geometry employed for (a) process #1 and (b) process #2.

The fatigue tests were tested at frequencies that ranged from 5 to 30 Hz. While most of the tests were conducted at 10Hz, higher frequencies were employed for the low load amplitudes to expedite failure. Steel shims were employed in the test frame to prevent additional bending moments or loads. The grip-to-grip distance employed for each coupon was 110 mm. For weld characterization, samples were sectioned through the center of the weld nugget coupon and parallel to the loading direction. Samples were cold mounted in epoxy and then ground and polished. In order to reveal the microstructure of the FSSW coupons, the samples were etched using a 4.2 g picric acid, 10 ml acetic acid, 10 ml H2O, and 70ml ethanol [13,17]. Using a Keyence VHX-1000 digital optical microscope, key features of the weld were characterized including size and shape of the interfacial hook, the bond width, and effective sheet thickness. Typical optical micro- graphs

of the stir zone, thermomechanically affected zone (TMAZ), heat-affected zone (HAZ) and base metal were obtained.

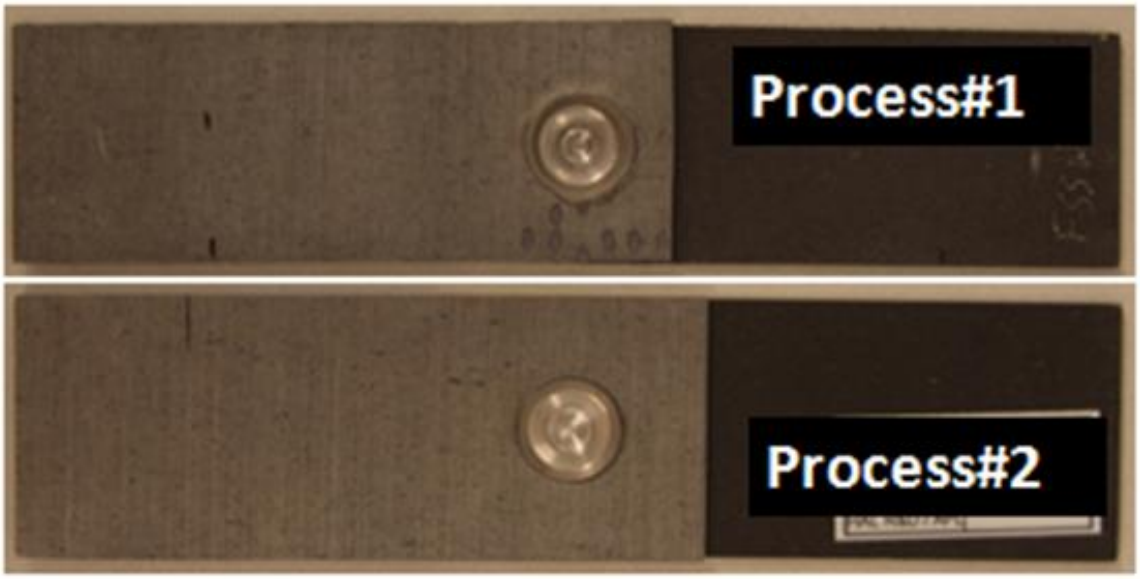

Figure 3-3: Representative lap-shear coupons produced from process #1 and process #2.

Microhardness measurements of representative weldments from process 1 and 2 were performed using a Wilson hardness testing machine. A load of 100 g and a dwell time of 5 s were employed to measure the Knoop hardness (HK) of the coupons. The hardness test was performed beginning near to the pinhole of each sample and advancing transversely towards the base metal. A total of 21 indents on the top and bottom sheet were made at approximately 0.5mm increments for both the processes. Representative fatigued coupons from process 1 and process 2 were also observed under the Keyence microscope to identify the failure modes at different cyclic load levels. In addition, fracture surfaces of failed fatigue coupons were examined under a Jeol 7000 scanning electron microscope (SEM) with the intent to evaluate the crack propagation rates between process 1 and 2.

3.3. Results and Discussion

3.3.1. Interfacial Hook and Geometrical Features

The as-welded coupons were observed under optical microscopy in order to measure and quantify key features of the weld nugget geometry. In typical FSSW joints, the faying surface oftentimes exhibits a hook-like shape as shown in Fig.3-4. This hooking of the faying surface is a result of trapped oxide films that are displaced upward due to the plastic flow of the material resulting from the downward plunge of the pin into the bottom sheet. In fact, the degree of oxide distribution at the faying surface is greatly influenced by the tool geometry and tool rotation speed [18]. For clarification purposes, the two peaks of the interfacial hooks are labeled as primary and secondary as marked in Fig.3-4. In both the processes, the primary and secondary hooks were observed. A smoother interface and more distinctive hook were observed in process 2. In contrast, the interfacial hook exhibited a more erratic path in process 1 and the distinction between the primary and secondary hooks was not as clear as in process 2. Further, the height of the hooks varied greatly between both processes, where in process 2 the hook heights were approximately three times as large as compared to process 1. Consequently, the link between the effective sheet thickness, T (see Fig. 3-5), and hook height are directly related to the shoulder plunge depth achieved during FSSW. If the tip-to-tip distance of the primary interfacial hooks is used to define the bond width, D2 (refer Fig. 3-5), process 2 had a slightly larger bond width. Dimension nomenclature of the various weld geometry measured in this study are indicated in Fig. 3-5 and the quantified results are shown in Table 3-2.

Table 3-2: Summary of dimensions of the FSSW features for process #1 and process #2 (refer Figure 3-5. for nomenclature).

Nomenclature	Process #1 (mm)	Process #2 (mm)
D1	10.8	11.0
D2	10.6	9.5
H1	0.15	0.63
H2	0.28	1.04
T	1.03	1.15

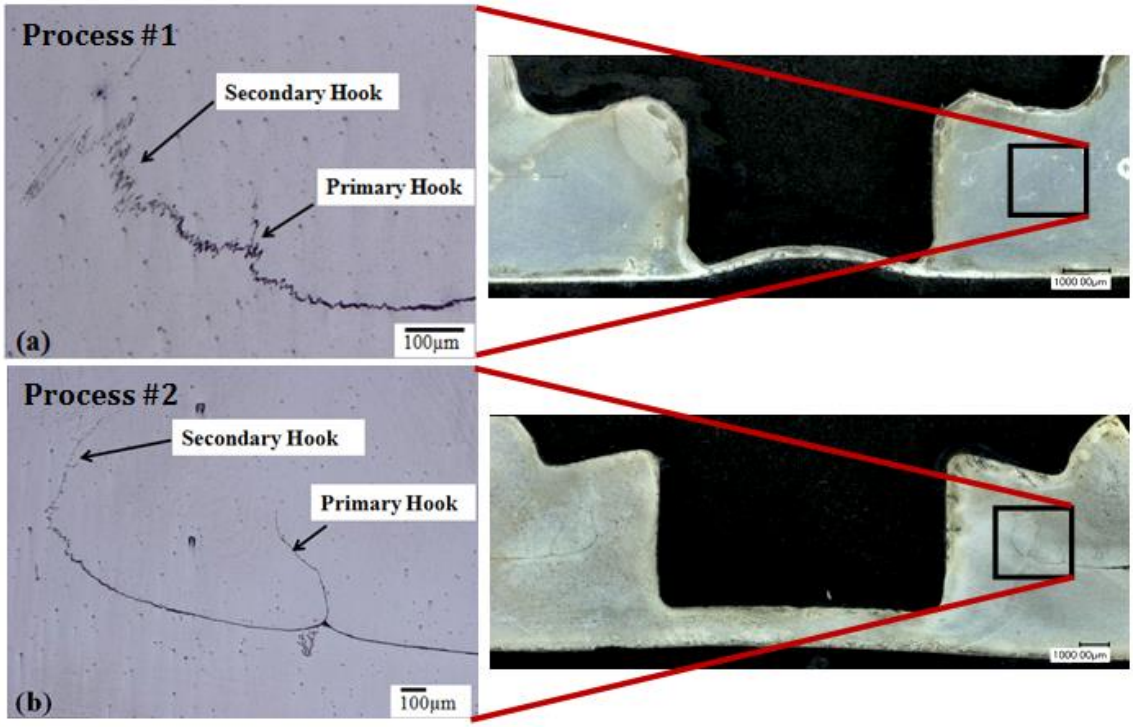

Figure 3-4 Figure 4. Magnified views of the primary and secondary hooks formed in (a) process #1 and (b) process #2.

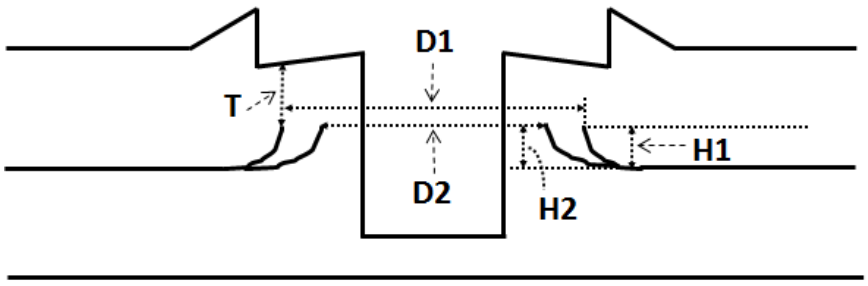

Figure 3-5: Schematic of key geometrical features FSSW coupon with dimension nomenclature. Refer Table 2 for dimensions.

3.3.2 Microstructure

Three microstructural zones (Fig. 3-6) including the stir zone, thermo-mechanically affected zone (TMAZ), and heat affected zone (HAZ), in addition to the base material, were identified in the top and bottom sheets of the coupons from both processes. The stir zone (SZ) is characterized by finer grains due to dynamic recrystallization as shown in Fig. 3-6(a) for process 1 and Fig. 3-6(b) for process 2. The TMAZ is characterized by larger recrystallized grains as shown in Fig. 3-6(c) for process 1 and Fig. 3-6(d) for process 2. The HAZ was characterized by the presence of both the base metal grains and partially recrystallized grains as shown in Fig. 3-6(e) for process 1 and Fig. 3-6(f) for process 2. The grain structure of the base metal as received is shown in Fig. 3-6(g) characterized by irregular grains. The grain size in the SZ and TMAZ in coupons fromprocess1 were generally larger compared to process 2 coupons. This can be attributed to the larger tool shoulder plunge depth and tool rotation (rpm) used in process 1 compared to process 2. In fact, higher tool rotation and larger tool plunge depth in process 1 generated more heat which contributed to greater recrystallization, whereas in process 2, a lower tool plunge depth and lower tool rotation speed generated less heat resulting in finer grain structure. This correlation of tool rotation speed to grain size has been reported elsewhere [11, 17].

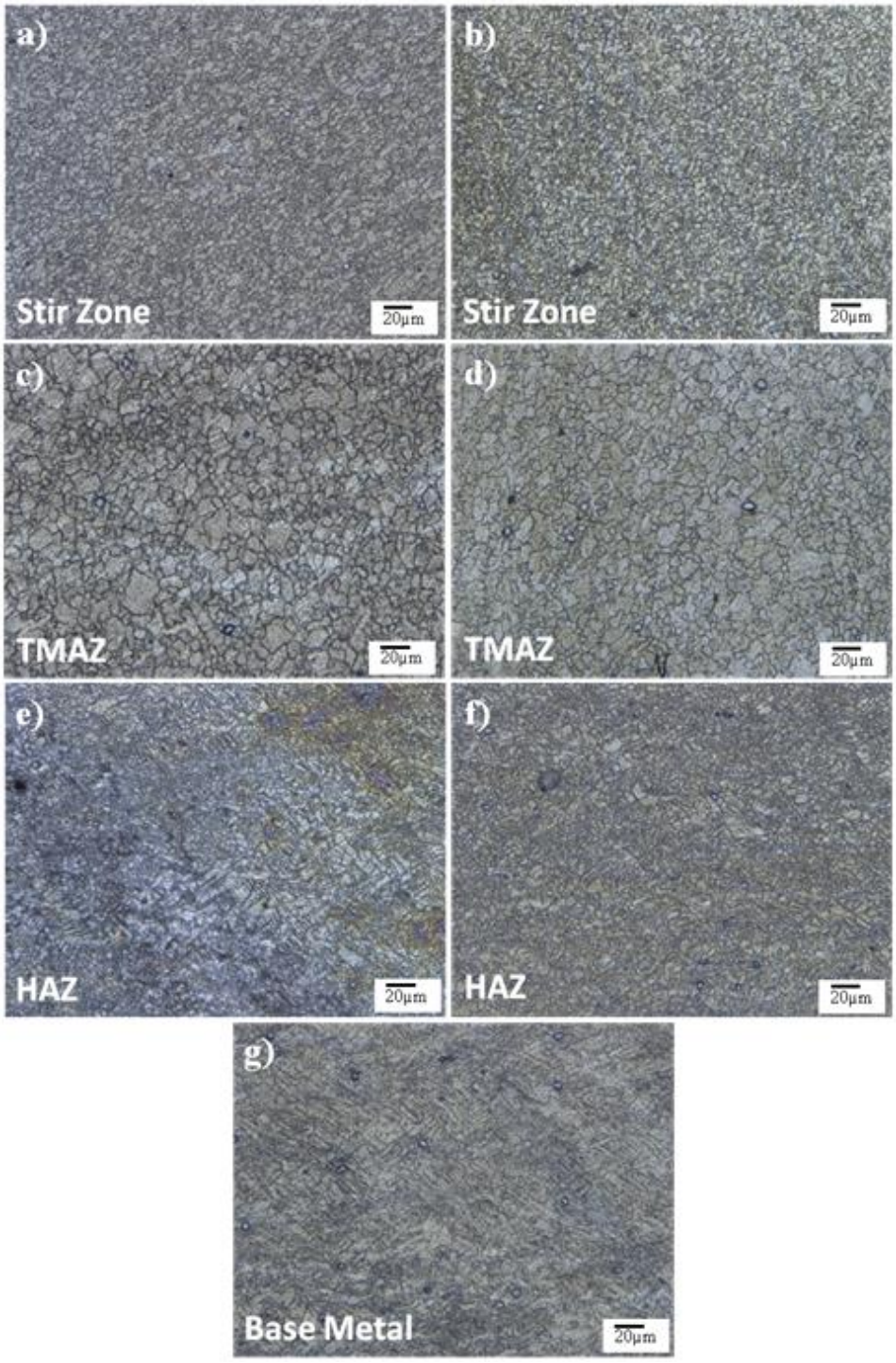

Figure 3-6: Microstructure features showing: (a) stir zone, (b) TMAZ, (c) and HAZ in coupons from process #1, and (d) stir zone (e), TMAZ, (f) HAZ in coupons from the process #2 and (g) Base Metal of the coupons.

3.3.3. Microhardness Profile

Fig. 3-7(a) shows the microhardness profile of the weldment comparing the bottom sheets from process 1 and process 2. Fig. 3-7(b) shows the microhardness profile of the weldment comparing the top sheets from process 1 and process 2. The horizontal axis in both Fig. 3-7(a) and (b) represent the axisymmetric distance from the center of the weldment (left side) and going outward away from the center of the weldment (right side). Microhardness mapping of the FSSW samples revealed the presence of a softer material response in the TMZ and harder material response in stir zone of the weldment in both processes. In addition, in both processes, a large gradient in relative hardness was observed moving from the stir zone towards the TMAZ. Furthermore, there was not a large difference in hardness values between the top and bottom sheet in the same coupon. Regarding differences between process 1 and 2, the most significant variation was in the stir zone, where the measured hardness in process 2 was approximately 20 percent higher compared to process 1 in the top sheet. This measured difference between process 1 and 2 in the stir zone was also observed in bottom sheet. The dissimilarity in measured hardness in the stir zones is directly related to the tool rotation, where Afrin et al. [17] showed that in FSW Mg AZ31B alloy made with a lower tool rotation speed (rpm) exhibited better tensile strength compared to welds made with higher tool rotation speed. A large gradient in hardness values between the stir and TMAZ was also observed. In contrast, the smallest grains and highest measured hardness was found in the stir zone, and the largest and lowest measured hardness was found in the TMAZ. Similar results were reported elsewhere [11, 18].

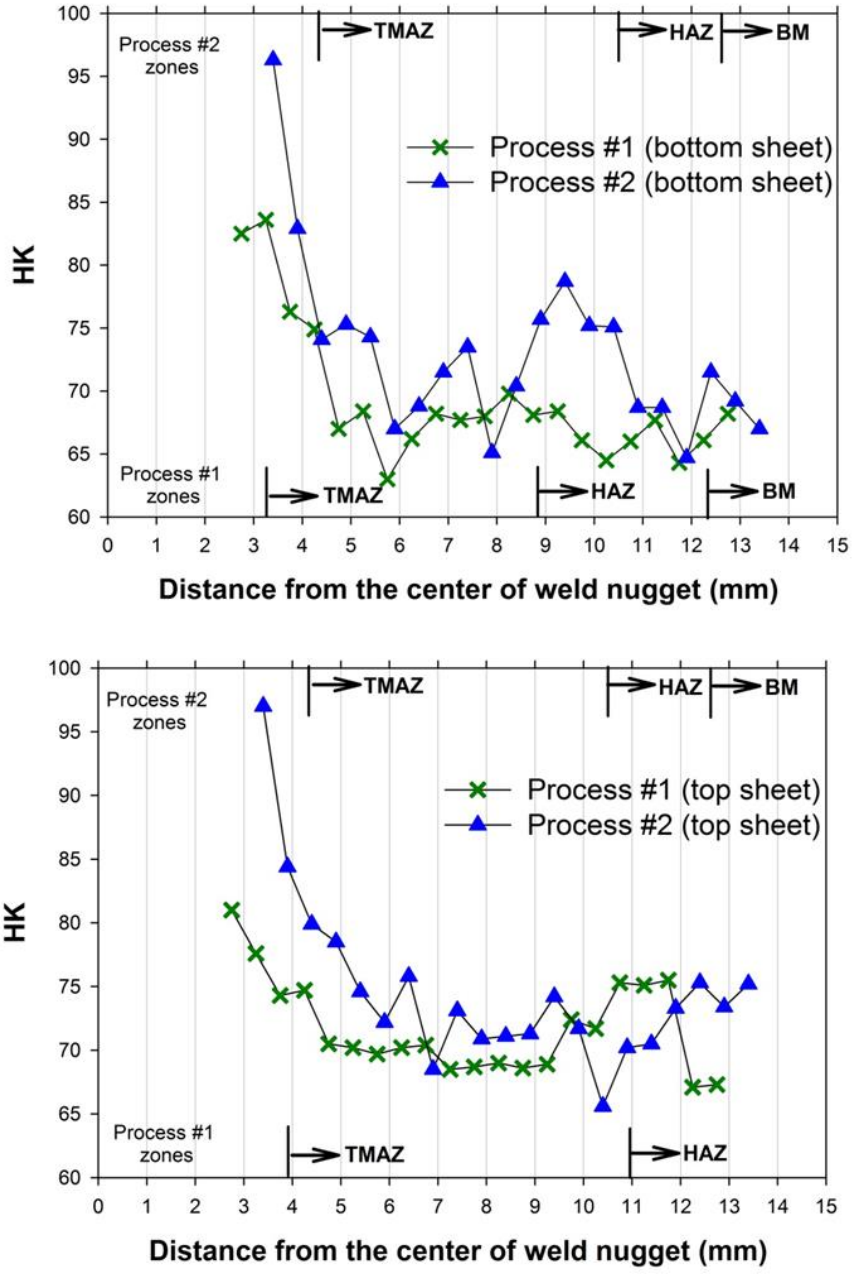

Figure 3-7: Microhardness profile across the friction stir spot welded specimens comparing hardness values of (a) top sheets of process #1 and process #2 (b) bottom sheets of process #1 and process #2.

3.3.4 Fatigue Tests

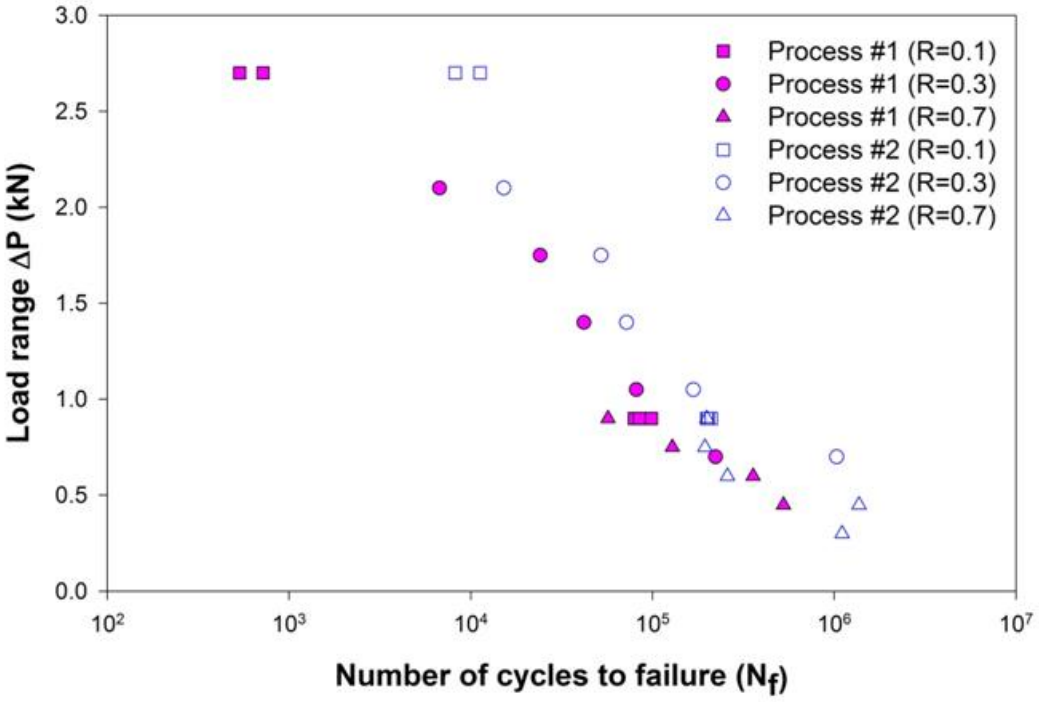

Figure 3-8: Experimental results of the load range versus the number cycles to failure for complete separation for friction stir spot weld lap-shear coupons tested at three load ratios (R=0.1, 0.3, 0.7).

Fig. 3-8 shows the results of the applied load range against the number of cycles to failure for the FSSW coupons. The load range tested for both processes was between 1 and 3 kN, and a range of load ratios of 0.1, 0.3, and 0.7. In general, the results of the lap-shear fatigue tests of the FSSW show that the number of cycles to final separation was greater for process 2 than process 1. In addition, the fatigue results confirm that the FSSW lap-shear coupons did not exhibit a load ratio effect commonly exhibited in base materials.

3.3.5. Failure Modes

Fig. 3-9 shows an overview of representative fractured FSSW coupons from both process 1 and 2. Several macro scale observations were made regarding the failure modes. It can be seen that the dominant crack originated from the interfacial hooks in coupons from the two processes. The mode of failure varied from nugget pullout, top sheet pullout, nugget shear failure and bottom sheet pullout for different loading conditions in the FSSW coupons of the two processes.

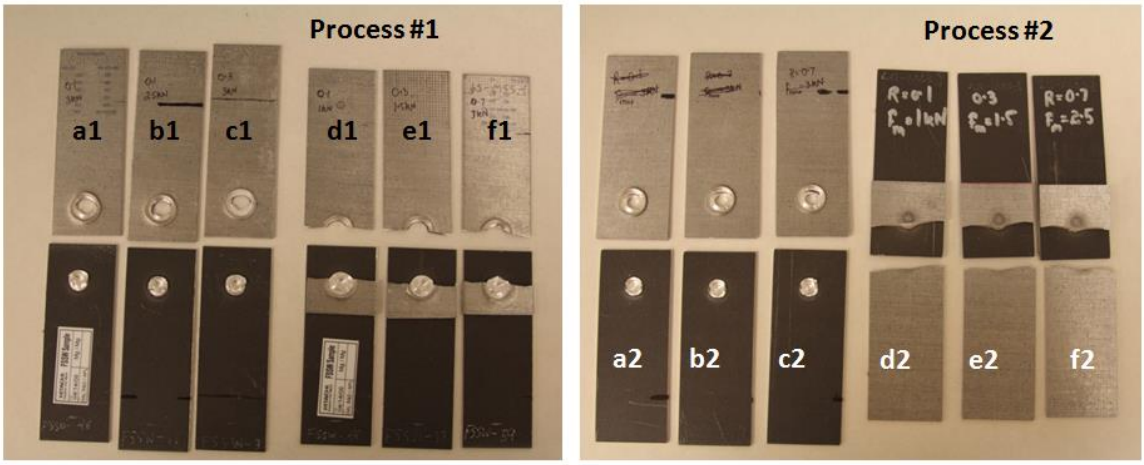

Figure 3-9: Representative fractured coupons tested at a range of maximum cyclic loads of 1-3 kN at R=0.1, 0.3, and 0.7 (Refer to Table 2 for a summary of failure modes).

Table 3-3 summarizes the failure modes for the FSSW Mg AZ31 coupons subjected to cyclic loading for both process 1 and process 2 based on the optical fractography conducted in this study. For the FSSW coupons from the process 1 tested at a maximum cyclic load of 2 kN or greater, fracture occurred by failure of the weldment.

Table 3-3: Summary of failure modes in coupons of process #1 and process #2

ID	Load Ratio (R)	Max Load (kN)	Failure Mode
Process #1			
a1	0.1	3	Dominant crack grew from primary hook into the top sheet, then halfway around the outer circumference of the nugget, finally failing by nugget pullout.
b1	0.3	2.5	
c1	0.7	3	
d1	0.1	1	Dominant crack grew from primary hook into the top sheet, halfway around the outer nugget circumference and then along the width of the top sheet.
e1	0.3	1.5	
f1	0.7	1	
Process #2			
a2	0.1	3	Dominant crack grew across the weld nugget and parallel to loading direction in mode II propagation.
b2	0.3	3	
c2	0.7	3	
d2	0.1	1	The Dominant crack grew from root of the secondary hook into the bottom sheet, propagated around the outer circumference of the nugget region and then along the width of the bottom sheet.
e2	0.3	1.5	
f2	0.7	2.5	

Below 2 kN, the joints failed with the dominating crack propagating through the sheet thickness from the primary hook into the top sheet then propagating along the outer circumference of the nugget. Halfway around the nugget circumference, the crack grew along the width of the top sheet and failed by top sheet pullout. This failure mode was similar to failure modes observed in aluminum FSSW lap-shear coupons [3].

As shown in Fig. 3-10(a), the nugget was seen to be intact in the remaining top and bottom sheet. Fig. 3-10(b) shows the location of the dominant crack propagation on the outer surface of the weld nugget. It is evident from Fig. 3-10(c) that the dominant crack propagated from the faying surface. Higher magnification of the region showed the dominant crack propagated from the primary hook into the top sheet thickness as seen in Fig. 3-10(d). No evidence of a secondary crack propagation or growth was found elsewhere in the weldment as shown in the magnified interfacial hook region in Fig. 3-10(e), which is located at the opposite side of the weldment (180 degrees around the circumference). At loads greater than 2 kN in process 1, the mode of failure varied where the dominant crack propagated from the sheet interface through the primary hook and top sheet thickness.

Coupons of process 1 failed by nugget pullout when the weldment reached the maximum load bearing capacity. Fractography of the tested FSSW coupon as seen in Fig. 3-11(a) and (b) show the nugget failure in the weldment. The cross-sectional view of the weldment revealed that dominant cracks propagated from the faying surface as shown in Fig. 3-11(c). A magnified view of the interfacial hook region (Fig. 3-11(d)) shows that the dominant crack propagated from the primary hook into the top sheet. Secondary cracks propagated on the opposite side of the weld nugget as seen in Fig. 3-11(e).

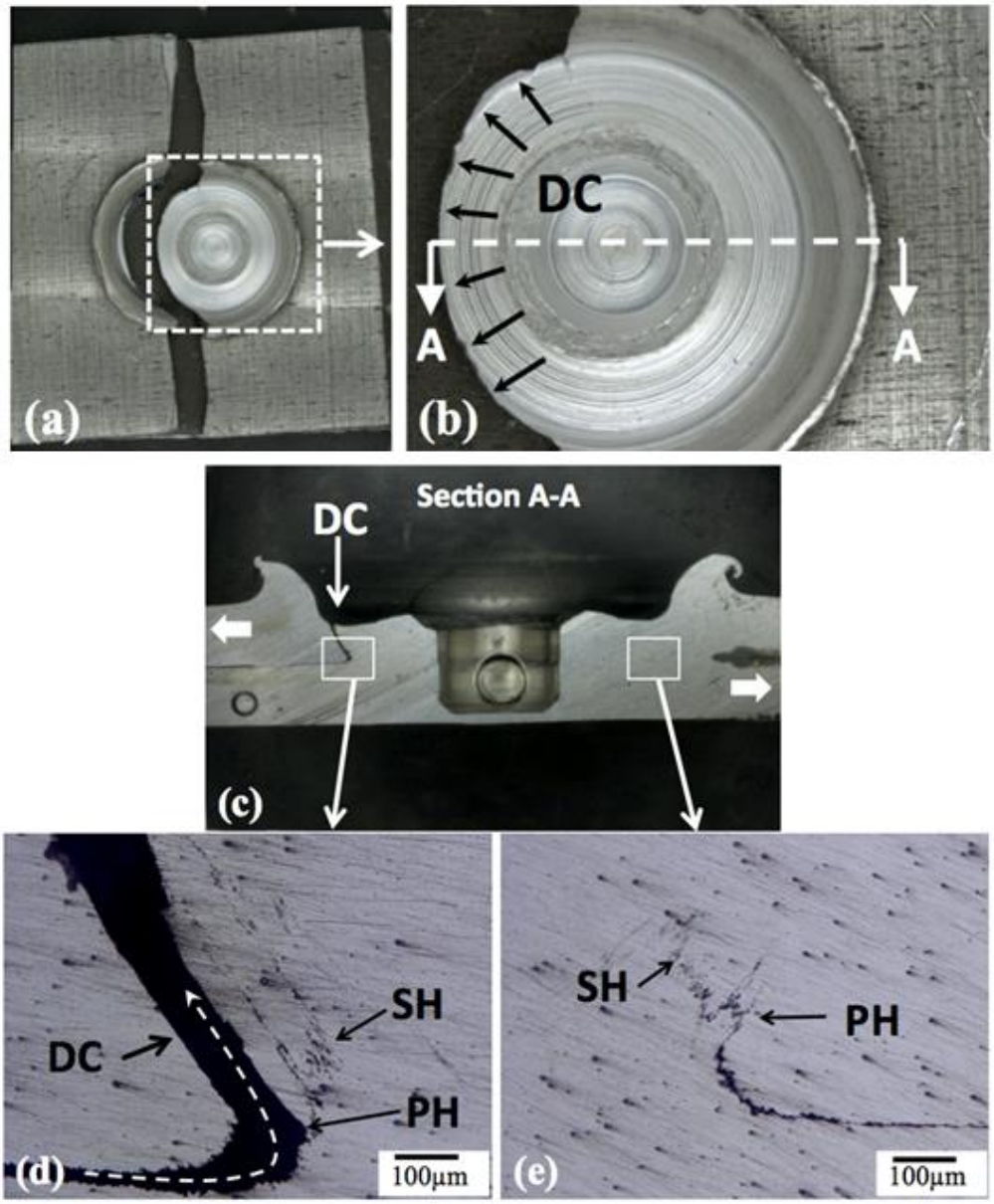

Figure 3-10: Crack propagation and failure mechanisms for process #1 coupon loaded at a maximum cyclic load of 1 kN at R=0.3. (a) An overview of the surface of the top sheet and (b) a magnified view of the location of surface crack initiation. (c) A section view of the weld nugget shows that the dominant crack (DC) propagated from the weld interface, and (d) and (e) show higher magnification images of the interfacial primary (PH) and the secondary (SH) hooks. Bold arrows in (c) indicate direction of applied loading.

However, these secondary cracks were non- dominant and did not contribute to final failure. These cracks either propagated at a significantly lower rate, or as the dominant crack became larger, it shielded the secondary crack.

For process 2 FSSW coupons tested below a maximum cyclic load of 2.5 kN, the coupons failed by bottom sheet failure as shown in Fig. 3-12(a). As in lower loads for FSSW coupons of process 1, the dominant cracks were not observed to propagate through the primary or secondary hooks. As shown in Fig. 3-12(b), secondary non-dominant cracks were observed to initiate to the top sheet, but did not contribute to the final separation of the coupon. Eyebrow cracks were seen on the top surface of the nugget caused due to the secondary cracks. A section view of the weldment confirmed that the dominant crack propagated into the bottom sheet as shown in Fig. 3-12(c). Magnified views of the interfacial hooks shown in Fig. 3-12(d) confirmed that secondary cracks on the opposite side of the weldment propagated into the top sheet from both primary and secondary hooks. However, these cracks did not contribute to the final failure. As seen in Fig. 3-12(e), the dominant crack grew from the root of the secondary hook towards the bottom sheet and then across the full width of the bottom sheet.

The FSSW coupons from process 2 tested above 2.5 kN failed by interfacial shear failure. Fig. 3-13(a) and (b) show the top surface of the coupons from process 2 with an eyebrow crack formed due to a secondary crack that propagated from the interfacial hooks. It is important to note that the top of the weldment remained intact and no separation of the top sheet was observed.

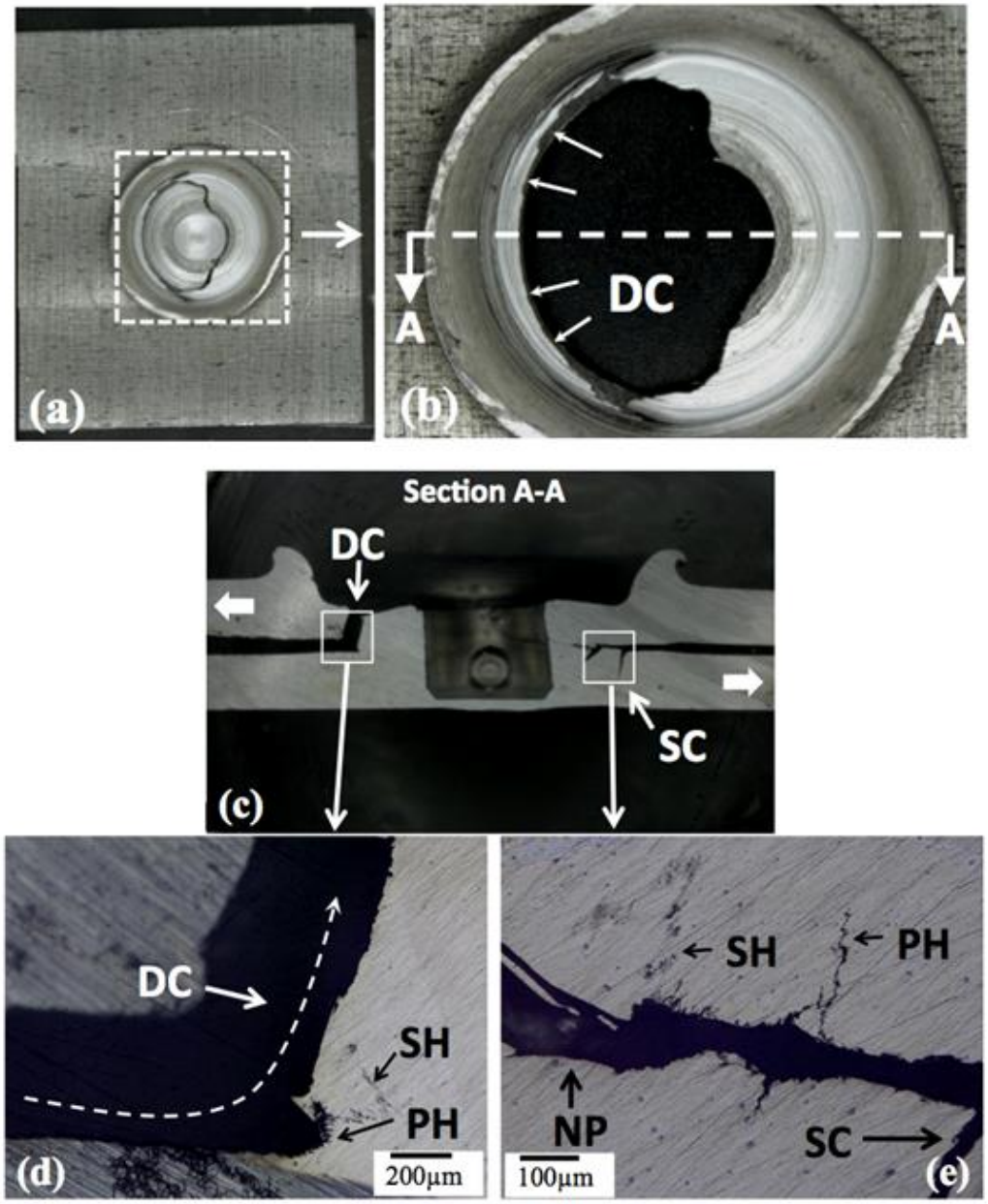

Figure 3-11 : Crack propagation and failure mechanisms for process #1 coupon loaded at a maximum cyclic load of 3 kN at R=0.3. An overview image of the (a) surface of the top sheet and (b) a magnified view of the location of surface crack initiation. (c) A section view of the weld nugget shows that the dominant crack (DC) propagated from the weld interface, and (d) and (e) show higher magnification images of the interfacial primary (PH) and the secondary (SH) hooks. Bold arrows in (c) indicate direction of applied loading.

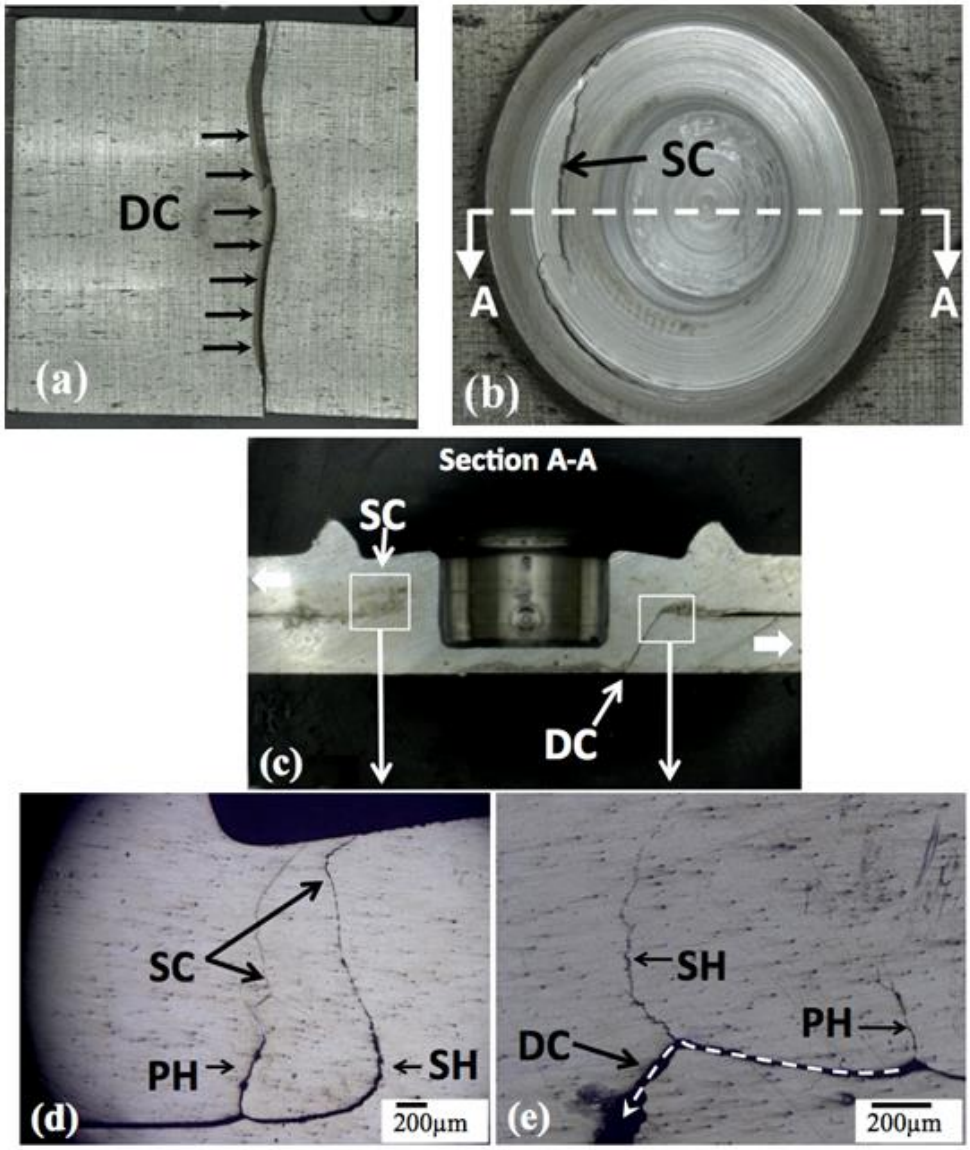

Figure 3-12: Crack propagation and failure mechanisms for process #2 coupon loaded at a maximum cyclic load of 1 kN at R=0.3. An overview image of the (a) surface of the bottom sheet showing the dominant crack and (b) top sheet showing a secondary crack. (c) A section view of the weld nugget shows that the dominant crack (DC) propagated downward into the bottom sheet and (d) and (e) show higher magnification images of the interfacial primary (PH) and the secondary (SH) hooks. Bold arrows in (c) indicate direction of applied loading.

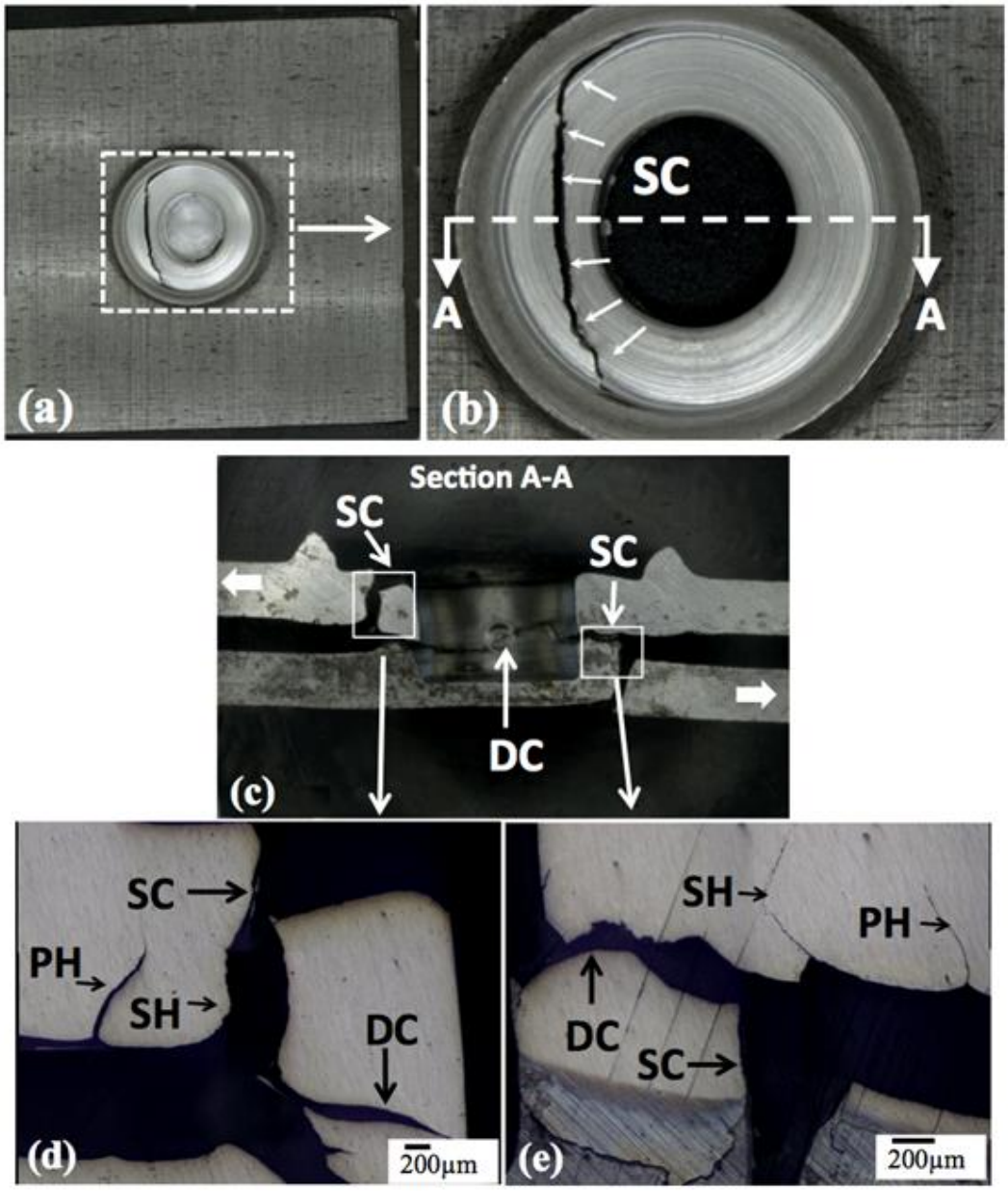

Figure 3-13: Crack propagation and failure mechanisms for process #2 coupon loaded at a maximum cyclic load of 3 kN at R=0.3. An overview image of the (a) surface of the top sheet and (b) a magnified view of the location of surface crack initiation of the secondary crack (SC). (c) A section view of the weld nugget shows that the dominant crack (DC) was primarily a mode II crack resulting in shear failure, and (d) and (e) show higher magnification images of the interfacial primary (PH) and the secondary (SH) hooking regions. Bold arrows in (c) indicate direction of applied loading.

The section view of the nugget region shows evidence of multisite cracking as seen in Fig. 3-13(c); however the dominant crack grew parallel to the loading direction in mode II as shown in Fig. 3-13(c). Fig. 3-13(d) and (e) show magnified views of the hook regions, showing the two sets of secondary crack propagation: one set showing cracks that grew into the top sheet from the interfacial hooks and the other set showing cracks that propagated to the bottom sheet. Also shown is that the dominant crack propagated through the wall of the keyhole. Analysis of the fractography results presented here gives an understanding of the underlining mechanisms of fatigue damage in FSSW lap-shear joints manufactured under various welding parameters. First, it is worth noting that Yin et al. [7] found that the monotonic strength of FSSW Mg AZ31 coupons increased when the bonded width is large, the distance from the hook extremity to the top surface of the weld was the greatest, and if the hook region is curved outward from the axis of the rotating tool.

In this study, the main difference between the two FSSW coupons are the welding parameters which in turn define the weld microstructure and welding geometry such as the effective sheet thickness, bond width and hook height. However, in lieu of establishing an empirical relationship between welding process parameters, geometrical and microstructural features, and fatigue performance as a way to explain the differences in two set of welds, we focus on the mechanics of fatigue crack damage. As such, the basic concepts of linear elastic fracture mechanics provide the basis for the discussion related to the fractography. If the spot weld is analyzed in terms of a stress intensity factor, we would expect process 2 to exhibit better fatigue resistance since the effective top sheet thickness was slightly larger in process 2 (1.15mm) compared to process 1 (1.03mm). In the lap-joint configuration, the effective top sheet thickness largely determines the global stress field, which in turn affects the driving force behind crack

initiation and crack propagation. When we consider process 1, the smaller effective top sheet thickness would likely produce a higher stress intensity factor compared to the bottom sheet, which would drive the dominant crack to propagate through interfacial hook and into the top sheet.

Likewise, in process 2, it is the effective top sheet thickness that again determines the fracture mode under cyclic loading. The stress intensity factor is lower in process 2 due to the thicker effective top sheet thickness. This lower stress intensity would reduce the driving force for dominant mode I crack growth through the top sheet and allow for an alternate location of crack initiation and crack growth. This was confirmed experimentally, where at the higher maximum cyclic loads, the dominant crack was observed to be a predominantly mode II type crack, which resulted in better fatigue lifetimes. At lower maximum cyclic loads, the initial cycles likely do not fully open the interfacial hook, which further repressed the stress intensity factor and allowed for the dominant crack to propagate through the bottom sheet as observed experimentally and shown in Fig. 3-12.

3.3.6. Fatigue Crack Propagation

In order to estimate crack growth rates and to confirm fracture modes in both sets of coupons, representative fracture surfaces of the FSSW coupons were imaged using SEM under high magnification with the intent to measure striation spacing. As shown in Fig. 3-14(a), the striation spacing was in the range of 1–1.6 mm for process 1 coupons tested at a maximum cyclic load of 1 kN. At higher loads, the striation spacing was observed to be in the 3.3–3.5 mm range, as shown in Fig. 3-14(b). In FSSW coupons from process 2 tested at a maximum cyclic load of 1

kN, the average striation spacing was around 0.80 mm and in coupons tested at 3 kN, the striation spacing was approximately 0.60 mm as shown in Fig. 3-14(c) and (d).

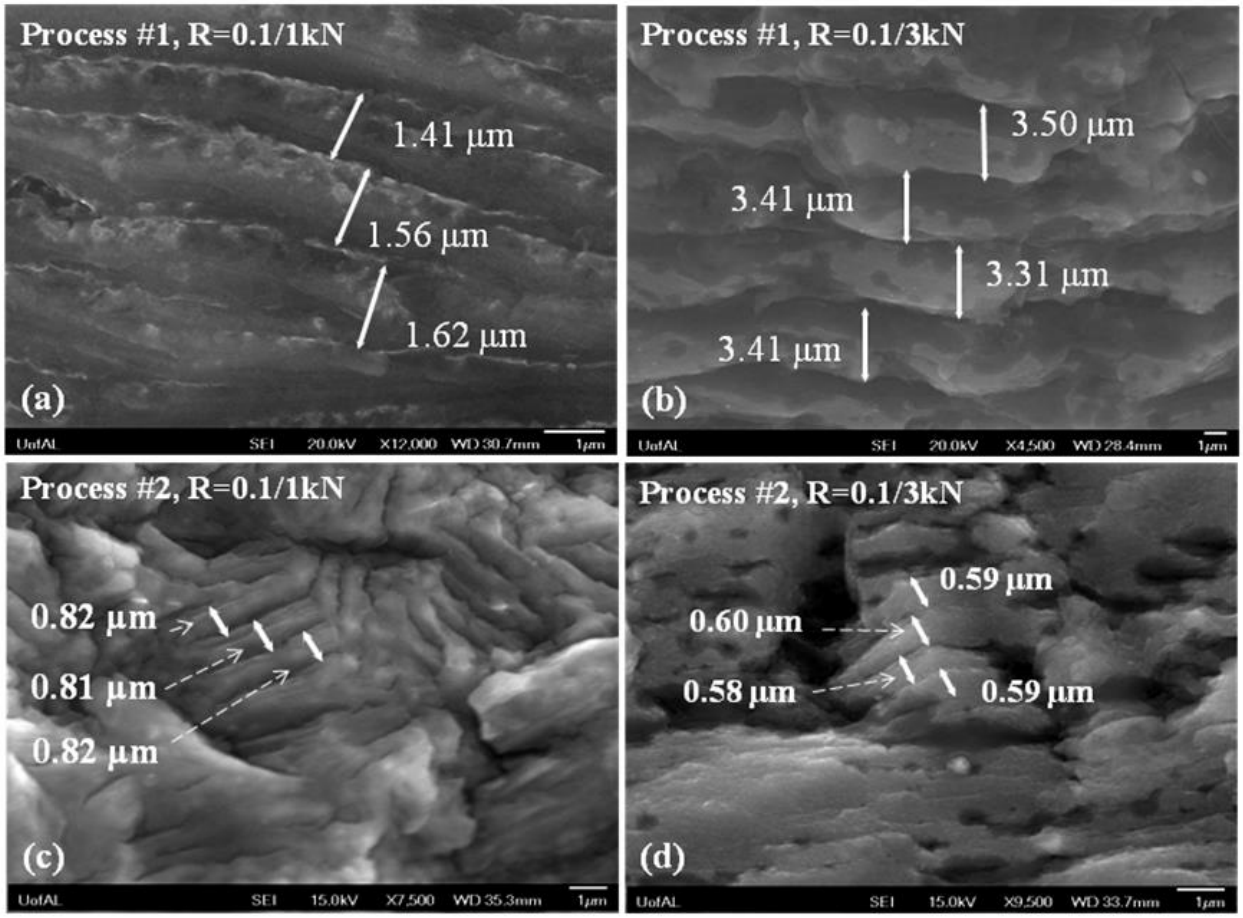

Figure 3-14: Scanning electron microscope images of striation spacing for: (a) process #1 coupons tested at maximum cyclic load of 1 kN, (b) process #1 coupons tested at maximum cyclic load of 3 kN, (c) process #2 coupons tested at maximum cyclic load of 1 kN, and (d) process #2 coupons tested at maximum cyclic load of 3 kN. Each of these coupons were tested at R=0.3.

We note that the difference between the 1 and 3 kN for process 2 is small and this observed difference could likely be due to scatter . We also note that the striations were less distinct in

process 2 and as such, were considerably more difficult to locate compared to process 1. The striation measurements aided in estimating the rate of the crack propagation in the FSSW coupons between the two processes. In general, cracks propagated at a higher rate in process 1 compared to process 2 as shown in Fig. 3-15. This generally faster propagation rate supports the hypothesis that the effective top sheet thickness and the larger microstructure gradient contributed to the difference in fatigue performance observed for process 1 and 2.

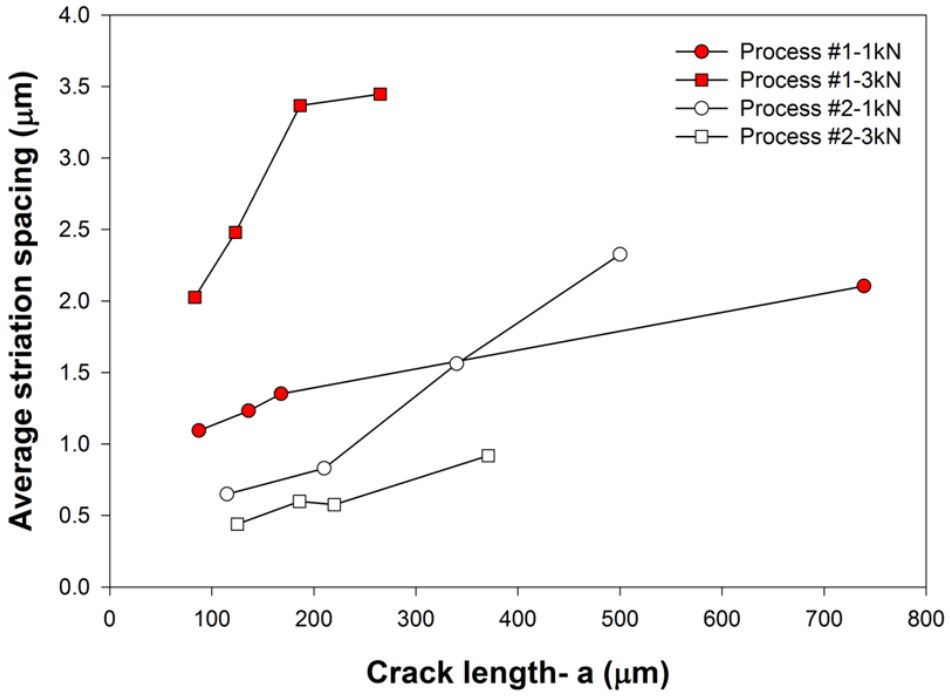

Figure 3-15: Plot indicating crack growth rate in coupons of process #1 and process #2.

3.4. Conclusions

In this study, the influence of microstructural and geometrical features on fatigue lifetimes are evaluated on two different sets of friction stir spot welded lap-shear coupons. Several differences in the initial state of the weld structure including microstructure, size and shape of the

interfacial hooks and the effective top sheet thickness were observed between the two processes. Fractography analysis conducted in this study suggests that the microstructure and effective top sheet thickness largely determine the failure mode, which in turn influence fatigue failure. While the height of the interfacial hook was greater in the process with better fatigue performance, it was the larger effective top sheet thickness that promoted crack propagation modes more favorable to greater fatigue resistance. As such, the shoulder plunge depth during the friction stir welding process may likely be the dominant design factor in producing durable spot welds using this joining technique.

3.5. Bibliography

[1] S.M. Chowdhury, D.L. Chen, S.D. Bhole, X. Cao, Mater. Sci. Eng. A 527 (2010) 6064.

[2] Y.H. Yin, N. Sun, T.H. North, S.S. Hu, J. Mater. Process. Technol. 210 (2010) 2062.

[3] D. A. Wang, C. H. Chen, J. Mater. Process. Technol. 209 (2009) 367.

[4] A. Gerlich, P. Su, T.H. North, J. Mater. Sci. 40 (2005) 6473.

[5] Y.H. Yin, N. Sun, T.H. North, S.S. Hu, Mater. Charact. 61 (2010) 1018.

[6] N. Sun, Y.H. Yin, a. P. Gerlich, T.H. North, Sci. Technol. Weld. Join. 14 (2009) 747.

[7] Y.H. Yin, N. Sun, T.H. North, S.S. Hu, Sci. Technol. Weld. Join. 15 (2010) 81.

[8] H. Badarinarayan, Y. Shi, X. Li, K. Okamoto, Int. J. Mach. Tools Manuf. 49 (2009) 814.

[9] H. Badarinarayan, Q. Yang, S. Zhu, Int. J. Mach. Tools Manuf. 49 (2009) 142.

[10] L. Commin, M. Dumont, J.-E. Masse, L. Barrallier, Acta Mater. 57 (2009) 326.

[11] W. Xunhong, W. Kuaishe, Mater. Sci. Eng. A 431 (2006) 114.

[12] P. Mallick, L. Agarwal, Soc. Automot. Eng. Warrendale, PA (2009).

[13] J.B. Jordon, M.F. Horstemeyer, S.R. Daniewicz, H. Badarinarayan, J. Grantham, J. Eng. Mater. Technol. 132 (2010) 041008.

[14] S.H. Chowdhury, D.L. Chen, S.D. Bhole, X. Cao, P. Wanjara, Mater. Sci. Eng. A 556 (2012) 500.

[15] P. Lin, J. Pan, T. Pan, Int. J. Fatigue 30 (2008) 74.

[16] P. Lin, J. Pan, T. Pan, Int. J. Fatigue 30 (2008) 90.

[17] N. Afrin, D.L.L. Chen, X. Cao, M. Jahazi, Mater. Sci. Eng. A 472 (2008) 179.

[18] C.I. Chang, C.J. Lee, J.C. Huang, Scr. Mater. 51 (2004) 509.

CHAPTER 4

EFFECT OF PROCESS PARAMETERS ON MECHANICAL PROPERTIES OF FRICTION STIR SPOT WELDED DISSIMILAR ALLOYS

Abstract

Friction stir spot welding was applied to dissimilar cast magnesium alloy AM60B and rolled aluminum alloy 6022-T4 under various welding conditions. The influence of welding parameters such as the tool rotation rate and tool shoulder plunge depth on lap-shear failure load was examined. Welds were made at 1000, 1500, 2000 and 2500 rpm tool rotation rate and various tool shoulder plunge depths from 0 mm to 0.9 mm. The cross section of each weld nugget exhibited the formation of intermetallic compounds (IMC) in the stir zone. An increase in tool rotation rate decreased the width of the stir zone and resulted in lower lap-shear failure load. The stir zone width increased and interlocking of IMCs was observed with increase in tool shoulder plunge depth at 1000 rpm tool rotation rate. High lap-shear failure load was achieved in FSSW coupons having a large stir zone width with formation of discontinuous IMCs at the tip of the interfacial hook. An average lap-shear failure load of 2.5 kN was achieved for welds made at 1000 rpm tool rotation rate and 0.9 mm tool shoulder plunge depth. The present study suggests that the mechanical properties of the dissimilar FSSW alloys are greatly influenced by the stir zone width, interfacial hooks and the IMCs which are all weld process dependent.

4.1. Introduction

Automotive industries around the globe have increased the application of light weight magnesium and aluminum alloys in place of steel to produce more economical and better performing vehicles [1]. The traditional joining method used in automotive industry is resistance spot welding, which works well for steel but not suitable for aluminum or magnesium alloys [1–3]. Friction stir spot welding (FSSW) is a variant of the friction stir welding (FSW), a solid-state welding technique developed by The Welding Institute, UK in 1991[4]. A typical FSSW setup consists of a rotating tool with a probe pin that is plunged into two sheets of metal to be joined. The probe pin typically penetrates the upper sheet completely and then passes into the bottom sheet to various depths depending on process conditions. Here, the downward force and rotational speed of the tool generates localized friction as the pin interacts with the upper sheet. The heat generated by friction softens the sheet materials adjacent to the tool and deforms plastically to form a solid state bond between upper and lower sheets [5]. Essentially the welding process condition such as the tool rotation rate, tool shoulder plunge depth and dwell time determine the heat generation, weld mechanical properties and joint formation [6,7]. In addition to welding process conditions, the weld tool geometry plays a crucial role in material mixing and material flow. Tools with concave tool shoulder are found to produce weld joints with higher static strength compared to tools with convex or flat tool shoulder [6,8,9]. The effect of tool pin design on the weld strength of the FSSW joints has been well documented [6,9–11]. FSSW are characterized by unique feature known as the interfacial hooks formed at the faying surface. This hooking feature is a result of trapped oxide films that are displaced upward due to the plastic flow of the material resulting from the downward plunge of the pin into the lower sheet. The interfacial hooks are proven to influence

the failure load of the weld. A smaller hook height is observed to lead to better mechanical properties compared to welds with relatively large hook height [12–15]. The degree of oxide distribution at the faying surface is greatly influenced by the tool geometry and tool rotation rate [16]. Most research conducted on FSSW is relatively confined to joining of similar alloys of aluminum or magnesium. To utilize the optimum physical, mechanical and chemical properties of these alloys, there is increased interest to use in combination of aluminum and magnesium. The challenge of joining these dissimilar alloys lies in the formation of the brittle intermetallic compounds (IMC) in the stir zone along with the geometrical features of the weld.

With limited research conducted in solid-state joining of dissimilar alloys, most have reported about the formation IMCs and its effect on the weld joint strength [17–23]. Constitutional liquefaction occurred in the joints during the welding of Mg and Al alloys and the IMCs ($Al_{12}Mg_{17}$, Al_3Mg_2) were produced at the weld interface [19–23]. These IMCs are brittle and much harder compared to the base material and act as sites for easy crack growth. In FSSW of AA5083 to AZ31, presence of a thick layer of IMCs in a defect-free weld was reported. The thickness of the IMC was observed to have negligible influence on the lap-shear strength of the weld but the distribution of these IMCs did affect the weld strength [17]. On contrary, in FSW of AZ31B and AA5083, the lap-shear strength of welds decreased with the increase in thickness of IMCs, due to the weakened mechanical interlock between Mg and Al alloys [20]. Lee et al. [18] observed that with increase in tool plunge depth, the area of IMCs increased and so did the lap-shear strength of welded low carbon steel and Al-Mg alloy. Beyond certain tool plunge depth, the lap-shear strength decreased as a result of upper plate thinning. The thickness of the IMC layer increased with increase in tool rotation rate and tool dwell time which reduced the lap-shear strength of the FSSWed AA6K21 Al alloy and AZ31 Mg alloy. This reduction in strength was observed due to

the cracking in IMCs as the frictional heat increased with an increase in tool rotation rate and dwell time [19]. In fatigue testing of FSSWed dissimilar AZ31 to AA5754, the failure occurred due to nugget debonding where the IMC layer was present [23]. Yin et al. [24] observed that the interfacial hooks formed in FSSW AZ91 and AZ31 Mg alloys curved inwards towards the axis of the tool and hence the distance from the tip of the hook to the keyhole periphery influenced the strength of the weld joint. This distance greatly increased for welds made using a tool having a triangular threaded pin compared to welds made using a non-threaded pin tool. In general, welds made with triangular pin tools have displayed a larger bond width and better lap-shear strength compared to welds made using cylindrical pin tool [6,25]. While limited work has been done on FSSW of dissimilar Al/Mg alloys, and the fundamental understanding of critical role of IMCs on weld strength is still lacking. In this work, an effort has been made to explore the influence of the welding conditions on IMC formation as well as lap-shear tensile properties between FSSW of cast Mg alloy AM60B and rolled AA6022-T4.

4.2. Materials and Experiment

A cast AM60B plate having a thickness of 3.1 mm was FSSW to 1.5 mm-thick rolled AA6022-T4 sheet was used in this study. The FSSW tool used in this study as shown in Fig. 4-1 was made of standard tool steel (H13) and constituted a concave tool shoulder and a triangular pin with grooved surface. The geometrical features and dimensions of the FSSW tool are listed in Table 1. FSSW was conducted by stacking the magnesium sheet on top of aluminum sheet with lap-shear overlapping of 30x30 mm. In-house designed clamps were used to clamp the sheets during the FSSW as shown in Fig. 4-2(a). Four spot welds were made on each set of sheet as shown

in Fig. 4-2(b). Four individual test coupons were water jet cut from the FSSW plates and the final dimension of the test coupons are shown in Fig. 4-2(c).

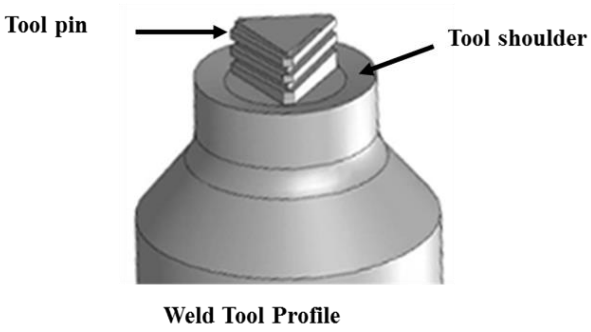

Figure 4-1: FSSW tool profile used in this study

Table 4-1: Information of the FSSW tool material and geometric feature employed in this study

Tool material	H13 Tool steel	
Tool profile	Shoulder shape	concave
	Shoulder diameter	12 mm
	Pin shape	Triangular
	Pin diameter	tri. = 5.4 mm (eq.);
	Pin length	3.5 mm
	Pin surface	grooved

One of the research goals of this study is to identify the ideal welding parameters for optimal weld strength. The course of isolating the weld process parameters was carried out in two stages; stage I, the optimum weld tool rotation rate was quantified and in stage II, the ideal tool shoulder plunge

depth was identified. In stage I, a set of FSSW coupons were prepared at different tool rotation rates, 1000/1500/2000/2500 rpm and tool shoulder plunge depth of 0.2/0.4/0.6 mm. The coupons were subjected to tensile test and the optimum tool rotation rate was identified based on the weld strength.

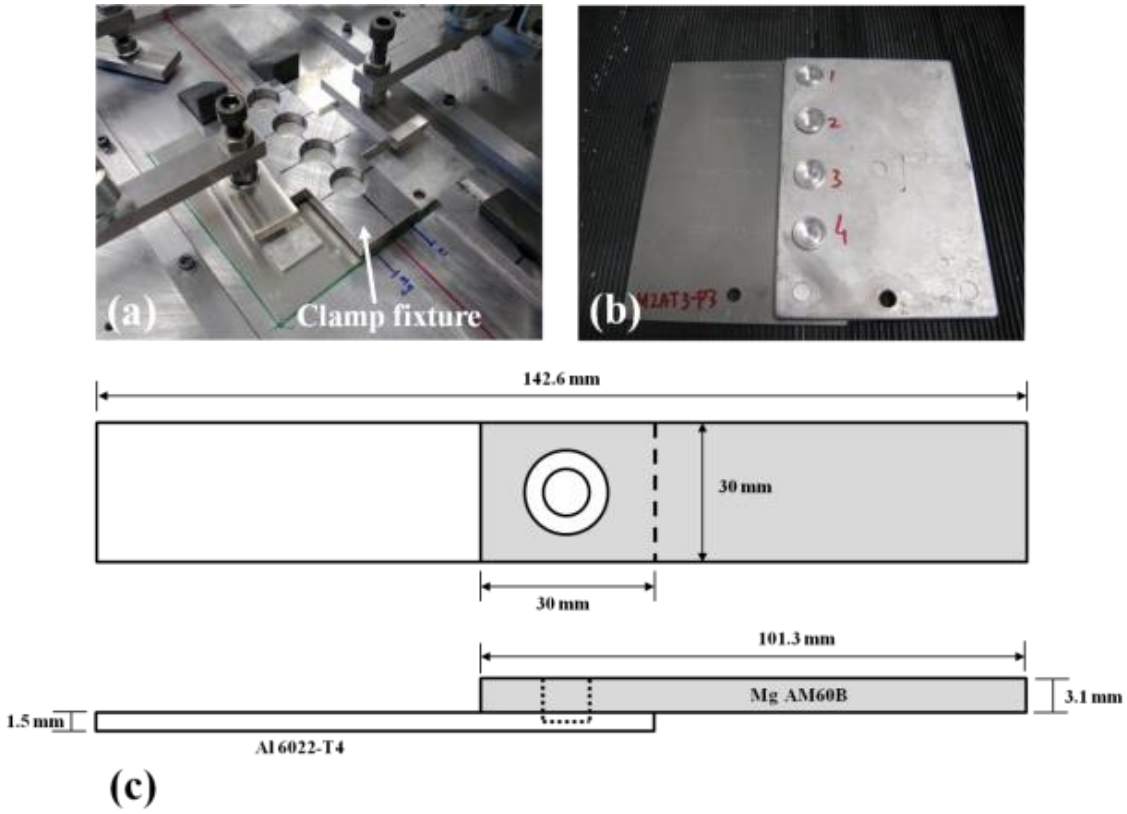

Figure 4-2: Representation of (a) Clamp fixture (b) Finished FSSWed magnesium to aluminum sheet before water-jet cut (c) geometrical dimensions of the FSSW test coupon.

In stage II, the final set of FSSW coupons were prepared using the tool rotation rate quantified in stage I and then by varying the tool shoulder plunge depth. The process window indicating various welding parameters employed in this two-stage study is shown in Table 4-2. A constant tool plunge speed of 12 mm/min was maintained in both stages of the welding.

Table 4-2: FSSW process parameters employed in current study

Phase 1			
Tool rotation rate (rpm)	**Tool shoulder plunge depth (mm)**	**Dwell time (s)**	**Plunge speed (mm/min)**
1000	0.2/0.4/0.6	1	12
1500	0.2/0.4/0.6	1	12
2000	0.2/0.4/0.6	1	12
2500	0.2/0.4/0.6	1	12
Phase 2			
1000	0.0/0.3/0.6/0.9	1	12

The lap-shear tensile tests were conducted at room temperature on an Instron screw-drive machine (Model 1123) with a constant cross head speed of 2 mm/min. At each stage of study, selected tested and un-tested coupons were cross-sectioned through the center of the welds and cold mounted in epoxy. The mounted specimens were mechanically grinded and polished with 0.05 µm final finish for weld geometry, IMCs and failure modes analysis. In order to reveal the microstructure and IMCs, AM60B was etched using an acetic picral solution (4.2 g picric acid, 10 ml acetic acid, 10 ml H_2O, and 70ml ethanol) and the AA6022-T4 was etched with 20% NaOH solution (caustic etching). The macro and microstructures of welds and failure modes were analyzed using the optical microscope. The microstructures of the as-received cast AM60B and AA6022-T4 are shown in Fig. 4-3 (a) and Fig. 4-3(b) and (c) respectively. The grain structure in cast AM60B comprises of a combination of irregular sized globular grains and large dendrites. Cast pores or voids were also observed all through the sheet. The AA6022-T4 rolled aluminum

alloy shows large globular grains on the surface and elongated grains along the rolling direction of the sheet. To analyze the IMCs and its composition, untested FSSW coupons were examined under Jeol 7600F SEM with EDS capabilities.

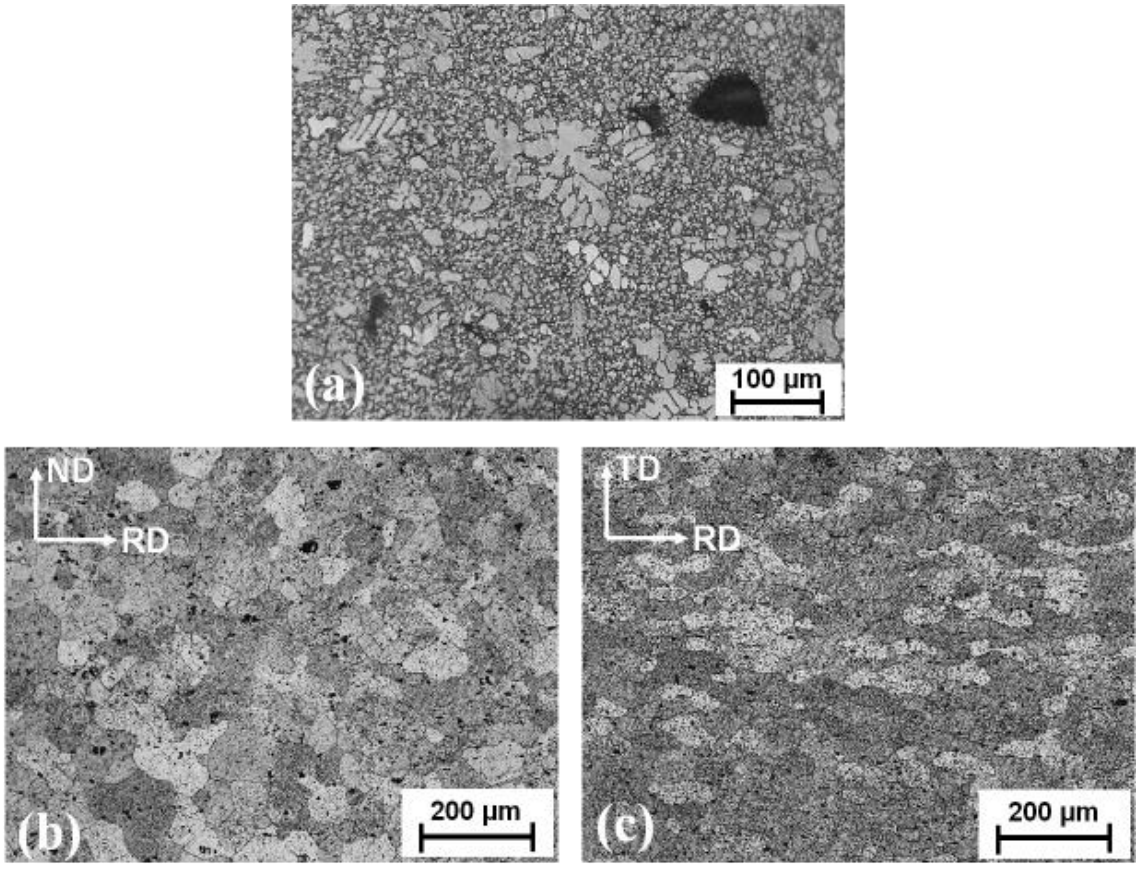

Figure 4-3: Microstructure of the as-received (a) magnesium AM60B, (b) and (c) aluminum 6022 -T4.

4.3. Results and Discussion

To isolate the ideal tool rotation rate, welded coupons were produced under different welding parameters and lap-shear tested. Figure 4 shows the failure load as a function of tool shoulder plunge depth at various tool rotation rates. The results indicate that welds made at 1000

rpm tool rotation rate had a higher failure load compared to welds made at other tool rotation rates when the shoulder plunge depth is between 0.2 and 0.6 mm. Though there is slight scatter in the results for each individual welded coupon, the failure load decreased gradually with increase in tool rotation rate.

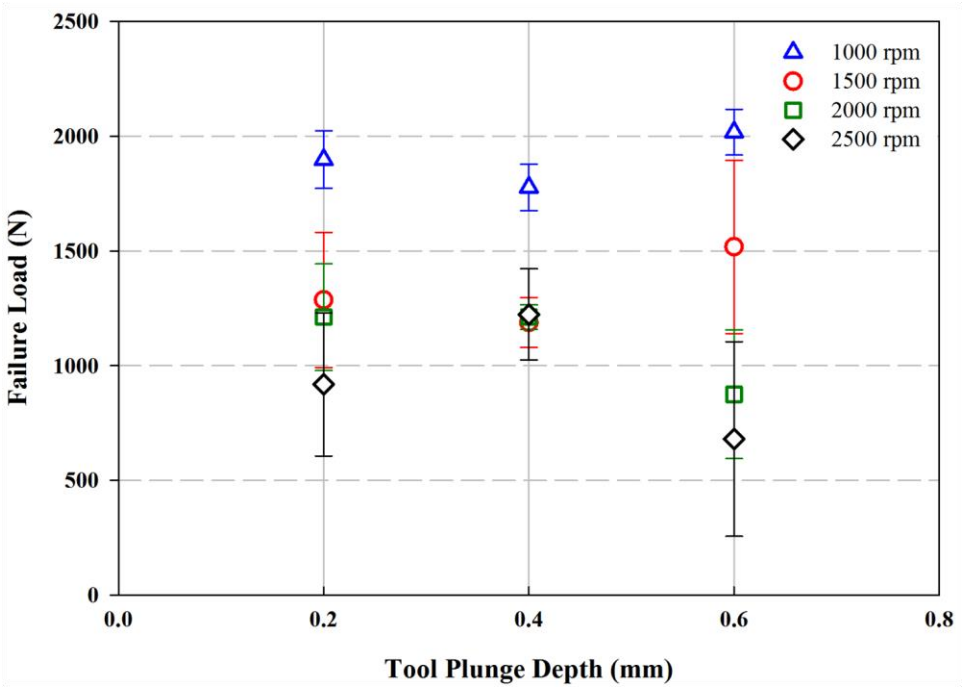

Figure 4-4: Stage I lap-shear failure load of spot welds as a function of tool shoulder plunge depth under various tool rotation rates.

The failure load of welds made at 1000 rpm and 1500 rpm tool rotation rate initially decreased with an increase in tool shoulder plunge depth. At 2000 rpm tool rotation rate, the failure load decreased with increase in tool shoulder plunge depth. While for welds produced at 2500 rpm tool rotation rate, the failure increased with increased tool shoulder plunge depth and then decreased drastically with increase in tool shoulder plunge depth. The decrease in failure load can be attributed to the size and microstructure of the stir zone as well as the hook features of faying

surface. It has been well documented in FSSW of similar alloys, that the tool rotation rate and tool shoulder plunge depth influence the hooking geometry and microstructure which in-turn affect the mechanical properties [12, 15, 24, 26–28]. Since in stage I the identification of the ideal tool rotation is the primary goal, the influence of the tool rotation rate on physical and mechanical properties of welds will be discussed. The influence of the tool shoulder plunge depth on the physical and mechanical properties of welds will be discussed later in this section.

4.3.1. Influence of Tool Rotation Rate on Mechanical Property and Macro Features of the Weld

One of the major issues in welding dissimilar materials is the formation of the IMCs in the stir zone [18–20, 29–31]. For brevity purpose, the discussion on formation of IMCs with respect to tool rotation rate will not be discussed and hence the macro features such as the hook geometry, the weld bond width and stir zone will be emphasized. The cross section analysis of the untested weld coupons suggests that the failure load are highly influenced by the size of the stir zone, the hook geometry and weld bond width. Figure 4-5 compares cross-sections of the untested welds made at 0.6 mm tool shoulder plunge depth but various tool rotation rates. Figures 4-5(a), (b) and (c) show macrographs of the weld cross section and the numbered box in each picture indicates the stir zone which is enlarged and presented in Fig. 4-5(d), (e) and (f) respectively. The distance from the tip of the hook to key-hole interface is addressed as the weld bond width. It is evident from the Fig. 4-5(d), (e) and (f) that geometrical features like the bond width, stir zone size, hook height and orientation vary from one weld to another, indicating the dominant influence of tool rotation rate on material flow and mixing. In the current study, the stir zone size and weld bond width of welds decreased with increase in the tool rotation rate. A similar phenomena has been reported in FSSW of magnesium alloy [32].

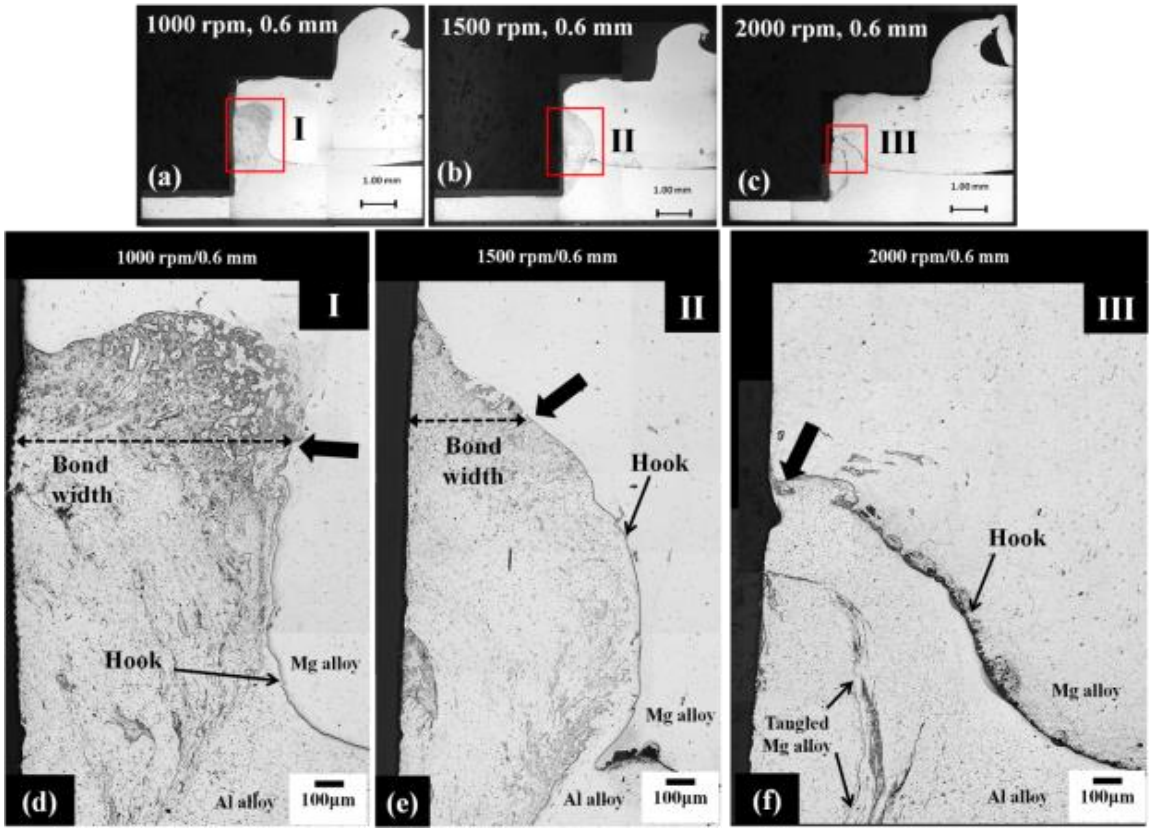

Figure 4-5: Representative cross sections of unetched and untested welds made at (a) 1000 rpm, 0.6 mm plunge depth (b) 1500 rpm, 0.6 mm plunge depth (c) 2000 rpm, 0.6 mm plunge depth. (d), (e) and (f) are magnified views of region I, II and III indicating the geometrical features of each weld with bold arrow in each picture indicating the point of termination of the interfacial hook. The dotted horizontal line indicates the weld bond width region in each weld.

The weld bond width is the region in the weld nugget where a complete bonding of materials occurs when plastically deformed material from the upper and lower sheet flows and mixes together with the aid of the probe pin. The amount of plastic deformation is dominated by the amount of the frictional heat generated. During FSSW, a major portion of the frictional heat is generated when the tool shoulder comes in contact with the upper sheet and the amount of frictional heat generated is influenced by the tool rotation rate. While the tool shoulder predominantly

determines the frictional heat generated, the probe pin influences the material flow and mixing during the FSSW [6, 12, 25, 27]. Increasing the tool rotation rate introduces higher frictional heat [16, 33, 34] and strain rate [33, 34] in the weld nugget. This reduces the viscosity of the material right under the tool shoulder and material adjacent to pin in the key-hole region [32]. The reduced viscosity sabotages the material mixing in the stir zone by introducing slippage between the pin and the materials adjacent to it. The function of the pin which is to stir and mix the materials from upper and lower sheets is thus weakened. This is clearly evident from Fig. 4-5(e) and (f) where the stir zone becomes narrower and the weld bond width reduces as the soft material from the bottom of the pin is extruded and flows locally around the periphery of the key-hole. With a weaker bonding and narrower stir zone, the welds failed at much lower loads. At 1000 rpm tool rotation rate, the frictional heat generated is sufficient to plastically deform the material around the pin while maintaining high viscosity between the pin surface and the material around it. Materials right adjacent to pin sticks to the pin surface and rotates at the same rate as the tool which results in breaking of the interface and mixing of materials from the upper sheet and lower sheet [35], thus a large weld bond width and stir zone as seen in Fig. 4-5(d). While the stir zone size or weld bond width is one of the factors that influence the lap-shear strength of the welds, the role of hook geometry will be investigated.

During FSSW, trapped oxide films present between the overlapping sheets are often displaced in an upward direction towards the upper sheet into a ‘‘hook-like’’ shape. This hooking is largely due to the plastic flow of the material resulting from the downward plunge of the pin into the lower sheet [15]. In FSSW higher joint strengths were found when the hooks oriented outwards from tool rotation axis and away from key-hole compared to hooks that terminate very close to key-hole [6, 13, 24, 25]. The bold arrows in Fig.4- 5(d), (e) and (f) indicate ending of hook

in each weld and the distance from the tip of the hook to the key-hole interface is determined as weld bond width (highlighted in dotted line). Yin et al. [24] indicated that the lap-shear strength of spot welds between AZ91 and AZ31 increased as the weld bond width increased. It is evident from Fig. 4-5(d) that the hook orients outwards from the tool axis and terminates away from the key-hole for welds made at l000 rpm. With the increase in tool rotation rate (1500 rpm and 2000 rpm), the hook orients towards tool axis and terminates much closer to the key-hole as seen in Fig. 4-5(e) and (f). At higher tool rotation rate (2000 rpm), continuous hooking to the key-hole indicates that the softer material in the bottom aluminum alloy sheet was simply extruded without breaking the oxide layer in the bottom sheet. In other words, the top magnesium alloy sheet and bottom aluminum sheet did not mix and a clear bifurcation at the faying surface exists indicating insufficient bonding between the two sheets. These interfacial hooks act as preexisting cracks and the failure of the welds occurred when the crack progressed through the tip of the hook to the nearest free surface [6, 12, 14, 15, 25].

4.3.2. Influence of Tool Shoulder Plunge Depth on Formation of IMCs and Weld Bond width

With the isolation of the tool rotation rate in the first stage, the task was to identify the ideal tool shoulder plunge depth. Figure 4-6 presents the lap-shear tensile result for welds produced at 1000 rpm and various tool shoulder plunge depths. It is quite evident that the lap-shear failure load increased with increase in plunge depth. This is attributed to weld geometric features as well as the formation of IMCs. Since most of the welds in this study failed when cracks propagated from the interfacial hook into the key-hole through the stir zone and ultimately detached due to shear overload, the influence of effective upper sheet thickness on failure load is not of importance. Hence the weld bond width and hook geometry are analyzed. Few studies on FSSW of similar

alloys [6, 36, 37] have indicated that the increase in plunge depth improved tensile strength of the welds. Similar finding has also been reported in FSSW of dissimilar metals [17, 18]. The increase in plunge depth during FSSW of dissimilar metals increased the formation of IMCs and at the same time formed a strong interlock bond thereby improving the weld strength.

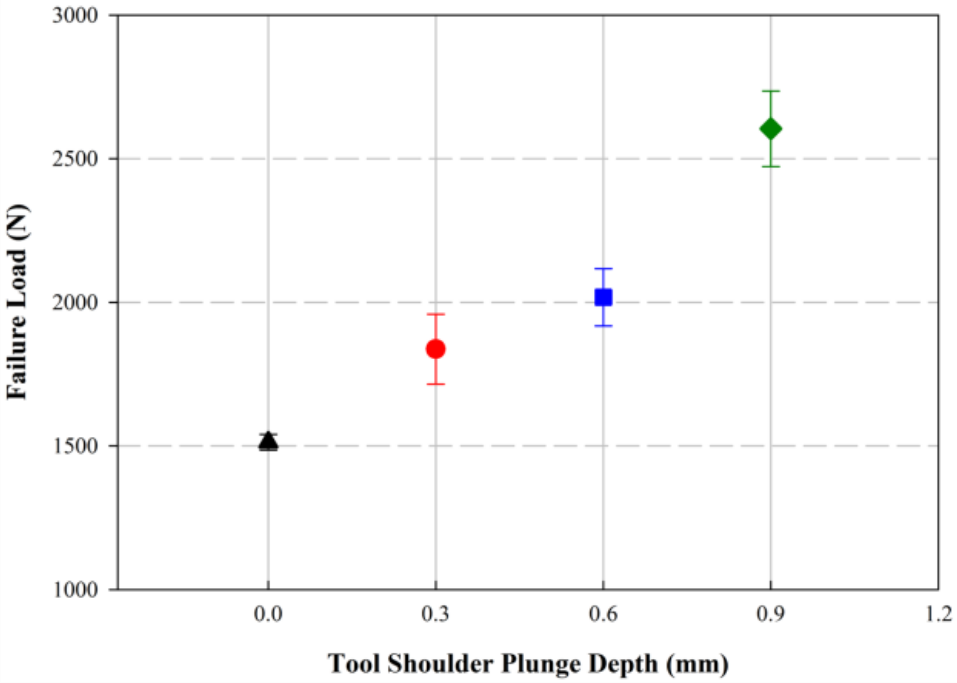

Figure 4-6: Stage II lap-shear failure load of spot welds as a function of tool shoulder plunge depth at 1000 rpm tool rotation rate.

Yin et al. [13] proposed that the weld strength in FSSW can be increased if welds are produced with large bond width and smaller hook height and larger effective sheet thickness. The transverse cross-sections of untested and unetched representative welds produced under various tool shoulder plunge depths are shown in Fig. 4-7. Figures 4-7(a), (b) and (c) present cross-sections of welds produced at 0.0 mm, 0.6 mm and 0.9 mm tool shoulder plunge depth respectively and the rectangular box in each picture indicates the stir zone which is enlarged and shown in Fig. 4-7(d),

(e) and (f) respectively. It is quite evident that the stir zone size increased with increase in tool shoulder plunge depth. It has to be noted that the thickness of the upper sheet (magnesium alloy) is 3.1 mm which is twice the thickness of the lower aluminum sheet.

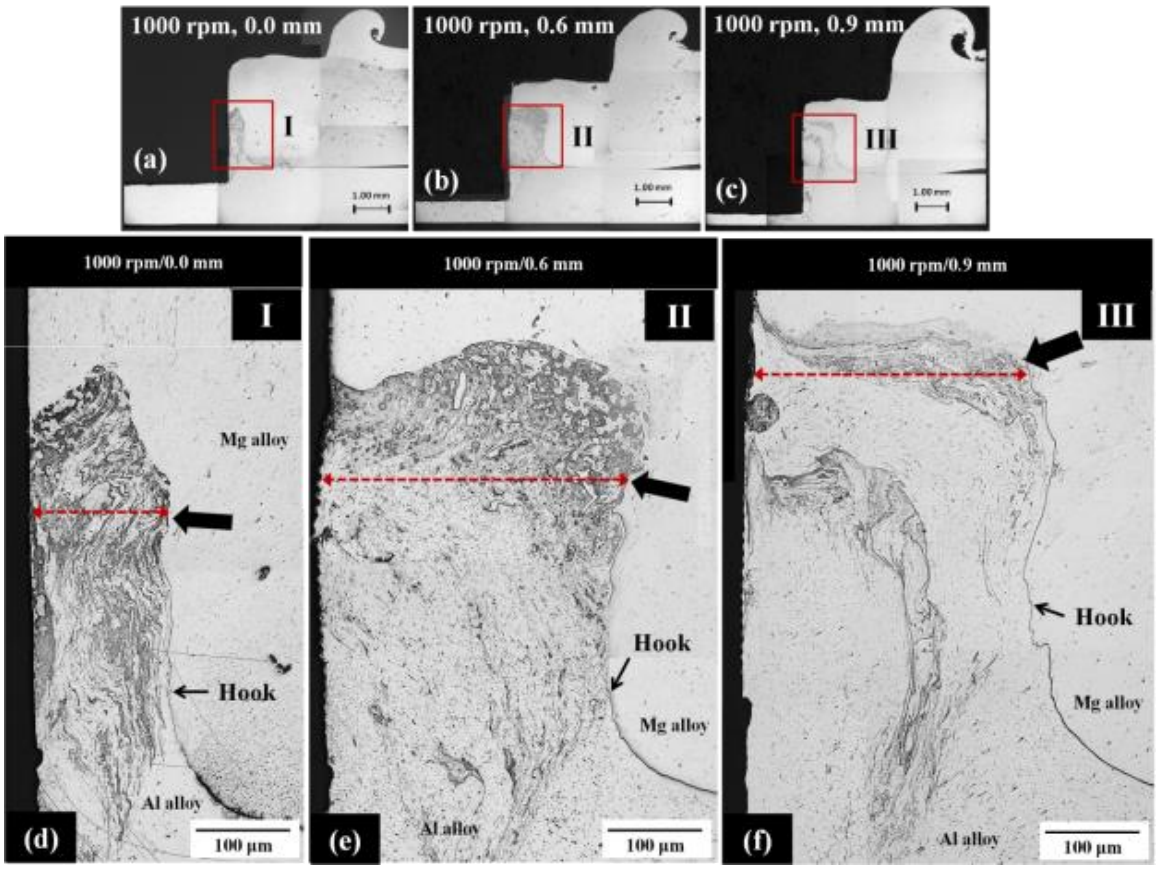

Figure 4-7: Representative cross sections of unetched and untested FSSW coupons produced at 1000 rpm and various plunge depths (a) 0.0 mm (b) 0.6 mm (c) 0.9 mm (d), (e) and (f) are magnified views of region I, II and III indicating the geometrical features of each weld with bold arrow in each picture indicating the point of termination of the interfacial hook.

As previously discussed, the bold arrow in each figure indicates the ending of interfacial hook and the horizontal dotted line highlights the approximate weld bond width in each weld. The weld bond width increased with increase in tool shoulder plunge depth as the aluminum from the lower sheet

was extracted and pushed upwards towards the upper sheet where it mixed with the magnesium forming a strong weld bond. Hence from Fig. 4-7 it can be inferred that the weld bond width increased with increase in tool plunge depth and the interfacial hook terminated away from the key-hole surface and thereby increasing the weld strength.

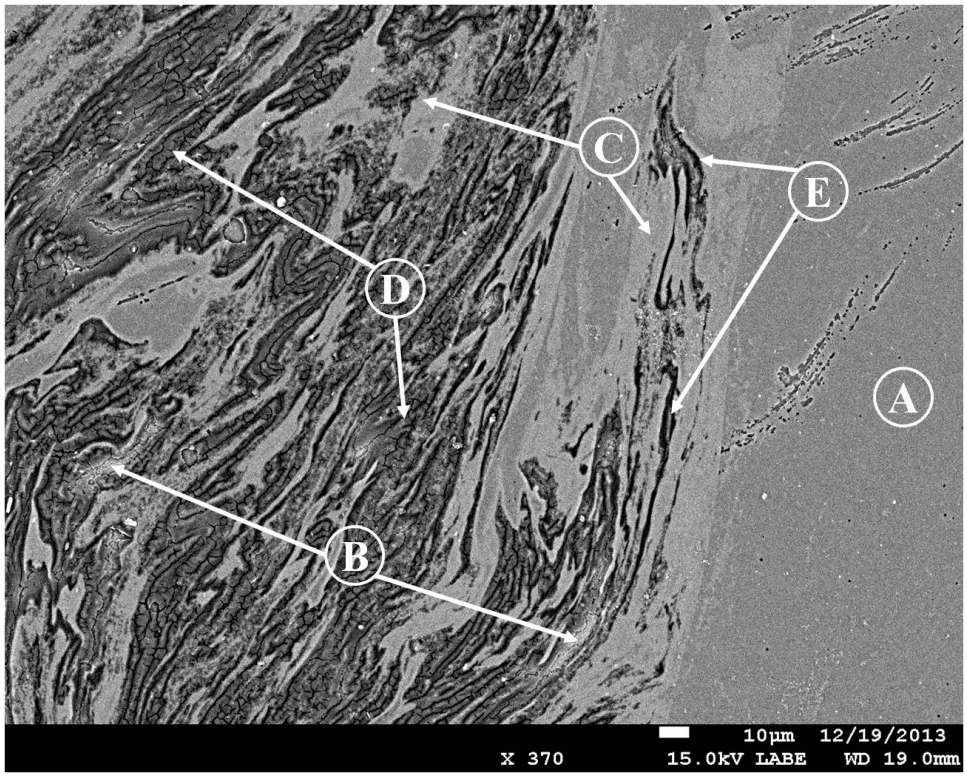

Figure 4-8: Representative cross sections indicating different regions in the stir zone. Each region is characterized by a different phase for which the composition is giving in table 4-3.

As discussed earlier in this section, one of the other important factors that influence the weld strength in a dissimilar weld is the formation of IMCs. The formation of IMCs during FSSW and FSW of magnesium and aluminum alloys has been discussed in detail elsewhere [17, 19–22,29]. The two IMCs that are often observed during welding of magnesium and aluminum alloys are Al_3Mg_2 and $Al_{12}Mg_{17}$ respectively in aluminum rich side and magnesium rich side of the weld.

For comparative study only two welding conditions will be discussed, 0.0 mm and 0.9 mm plunge depth at 1000 rpm. Table 4-3 gives an overview of main compositions (weight %) measured at various regions of interest in the stir zone of the two welds using EDS. Figure 4-8 indicates the different regions identified in the stir zone of the weld. Though visually each phase can be distinguished from each other, EDS was performed on all the samples to clarify the composition. To keep the discussion simple, the compositions for all of the analyzed weld samples are hence not discussed or mentioned in this paper and only a representative composition of different phases are mentioned in table 4-3.

Table 4-3: Composition (weight %) measured using EDS at various locations in the stir zone of the welds.

Region	Phase	Mg (Wt %)	Al (Wt %)	O (Wt %)	Total
A	AM60B	90.43	8.96	0.65	100.0
B	6022-T4	0.96	98.54	0.51	100.0
C	Al_3Mg_2	36.74	61.8	1.46	100.0
D	$Al_{13}Mg_{17}$	79.82	19.28	0.9	100.0
E	Al_3Mg_2 + Oxide	13.45	67.74	18.81	100.0

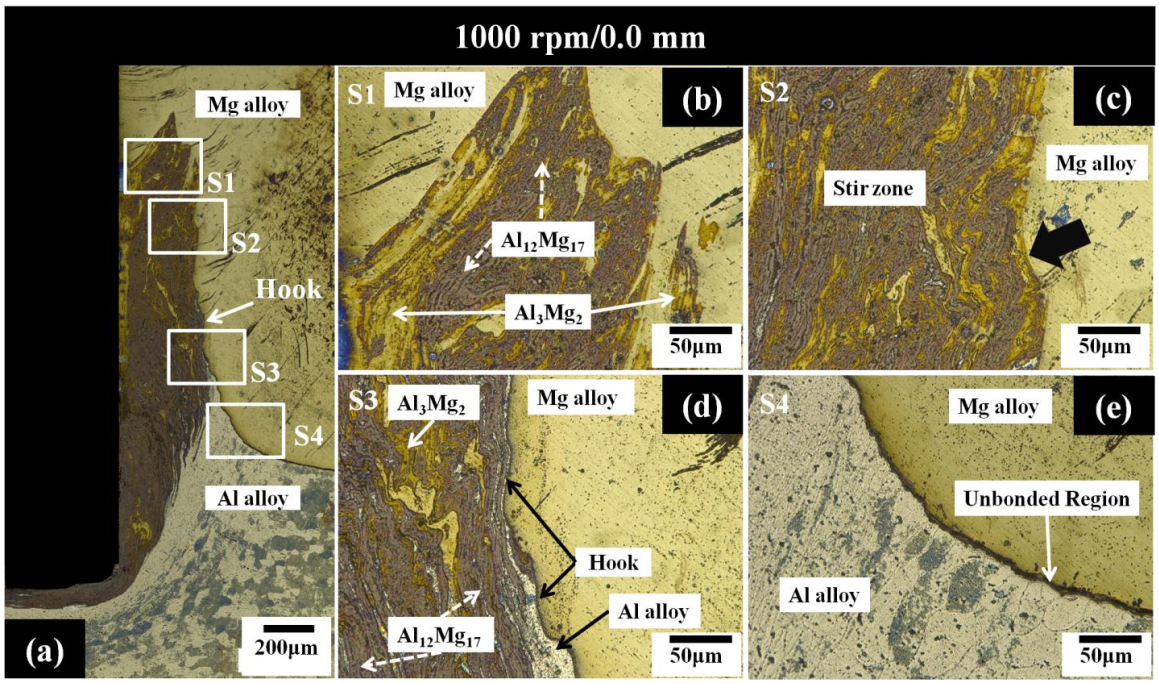

Figure 4-9: Microstructure of the weld nugget region in weld made at 1000 rpm and 0.0 mm plunge depth (a) Macrograph of the stir zone region, (b) region S1 indicating the interlocking in the weld bond width region, (c) region S2, bold arrow indicates the point of termination of the interfacial hook, (d) region S3 indicating the interfacial hook and (e) S4 indicating the unbounded region along the faying surface.

Figure 4-9 shows the microstructure and IMCs formed in welds produced at 0.0 mm. Figure 4-9(a) shows an overview of cross section of the weld with several areas of interest (S1, S2, S3 & S4) highlighted by rectangular boxes. Figure 4-9(b) shows a magnified view of region S1 (the weld bond width region). It is evident the bonding of the magnesium and aluminum sheet exists in form of a mechanical interlock between the IMCs and the top magnesium sheet. The interlocking of the IMCs with the native metal has shown to improve the weld strength [20, 29, 38]. The darker region in the stir zone is composed of $Al_{12}Mg_{17}$ and the lighter region mostly around the periphery of the stir zone is composed of Al_3Mg_2 as indicated in Fig. 4-9(b) and Fig. 4-9(c) (region S2). The bold arrow in Figure 9(c) indicates the point where the interfacial hook terminates, after which

there exists continues phase between the magnesium alloy and Al_3Mg_2 which extends into the stir zone forming an interlock with the $Al_{12}Mg_{17}$. Figures 4-9(d) (region S3) shows the region where the interfacial hook exists which is formed when the aluminum alloy from the bottom sheet is extracted upwards into the magnesium alloy. The interfacial hook (aluminum alloy) forms a weak bond with the magnesium alloy due to presence of the Al_3Mg_2 between the two materials (Fig. 4-10(d), (e)). As in FSSW of similar metals, there exists an unbounded region at faying surface of the two sheets as seen in Fig. 4-9(e) (region S4).

The SEM images in Fig.4-10 provides a better perspective of the regions of interest very clearly differentiating the various regions in the stir zone. $Al_{12}Mg_{17}$ is distinguished as the darker region and Al_3Mg_2 is the lighter region at the periphery of the stir zone. Sato et al. [17] reported similar contrast between the two IMCs. Figure 4-10(b) (region S5) is the region at top of the stir zone and the enlarged section of the dotted rectangular region is shown in Fig. 4-10(c) shows the mechanical interlocking between the native magnesium alloy and the IMCs in the stir zone of the weld. As mentioned earlier the interfacial hook is composed of the extruded aluminum alloy which forms a kissing bond with the magnesium alloy as shown in Figure 10(d) (region S6). The dotted rectangular box region is enlarged to show the presence of the thin shinny layer of Al_3Mg_2 at the interface between the hook and the magnesium alloy. Previous studies have shown the formation of thin layer of $Al_{12}Mg_{17}$ at the interface of the two sheets [17, 19, 21]. In current study Al_3Mg_2 is formed at the interface between the aluminum and magnesium sheets which may be due to the fact that the aluminum alloy is extruded upwards and constitutionally contributes to a greater weight % compared to magnesium.

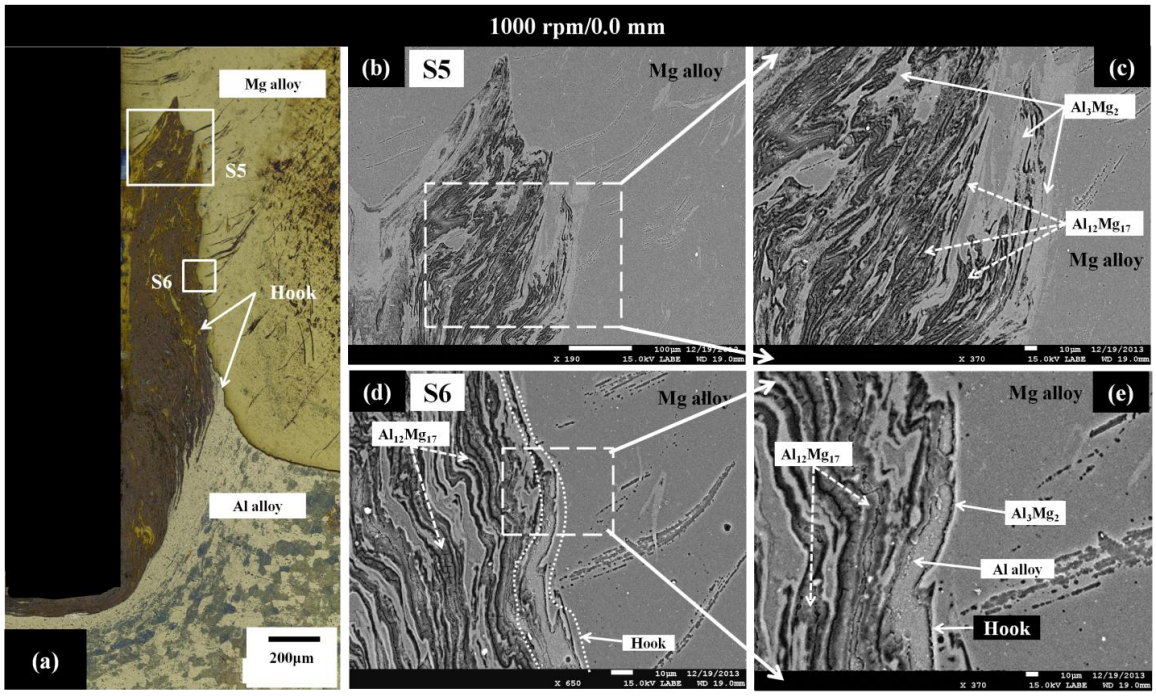

Figure 4-10: SEM images of the weld nugget region in welds produced at 1000 rpm and 0.0 mm plunge depth (a) Non-SEM macrograph of the stir zone region , (b) region S5 indicating the interlocking in the weld bond width region (c) magnified view of dotted rectangular region in S5 showing the continues phase (continues phase is confusing reader, we need another term or quantitative composition) between the magnesium and Al_3Mg_2 , (d) region S6 indicating the interfacial hook (e) magnified region in the dotted rectangular box in region S6 showing the composition of the hook and presence of Al_3Mg_2 between the magnesium and aluminum alloy.

For welds made at 0.9 mm tool shoulder plunge depth, the formation of IMCs was similar to what has been observed at 0.0 mm plunge depth. One of the primary differences is the increase in stir zone size and weld bond width as previous discussed. Figure 4-11(a) shows the transverse cross section of the etched weld with numerous rectangular boxes indicating the area of interests in the stir zone (T1, T2, T3 & T4). Figure 4-11(b) (region T1) presents the weld bond width region with IMCs forming a mechanical interlock with the native magnesium alloy. Compared to welds

produced at 0.0 mm plunge depth, the weld bond width and the size of the IMCs is much larger in welds produced at 0.9 m plunge depth.

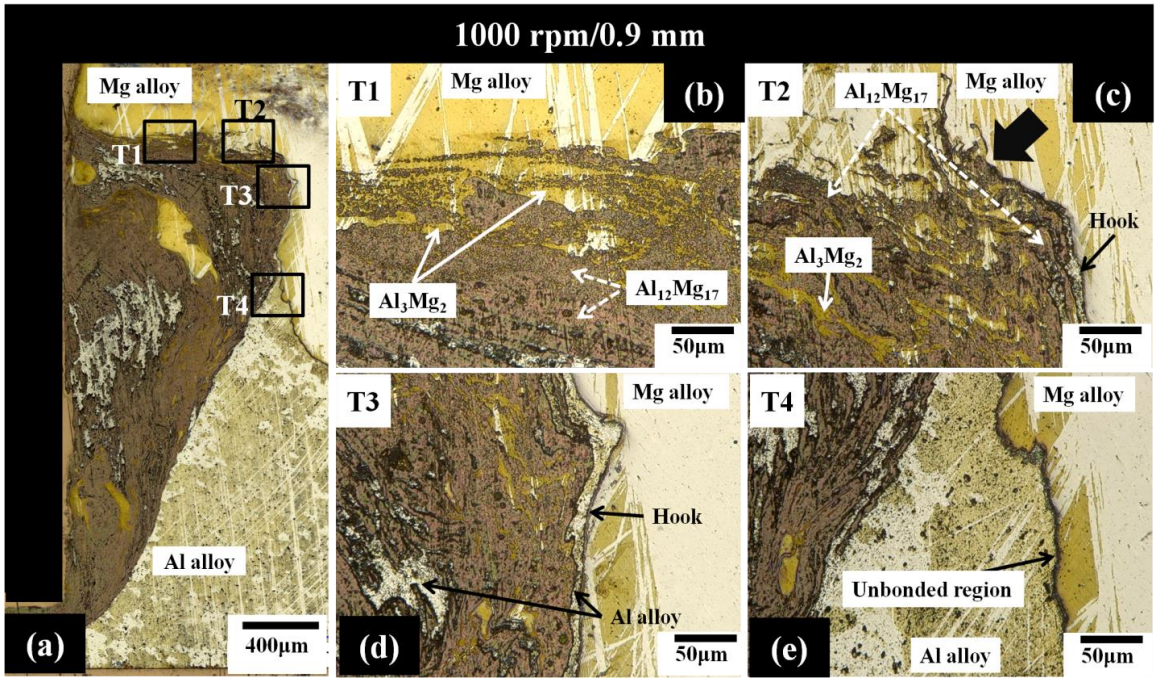

Figure 4-11: Microstructure of the weld nugget region in welds produced at 1000 rpm and 0.9 mm plunge depth (a) Macrograph of the stir zone region, (b) region T1 indicating the interlocking in the weld bond width region (c) region T2, bold arrow indicates the point of termination of the interfacial hook (d) region T3 indicating the interfacial hook (e) T4 indicating the unbounded region along the faying surface.

Earlier work by Lee et al. [18] indicated that the tensile strength of FSSW steel and Al-Mg alloy increased with plunge depth. With an increase in plunge depth, the stir zone size of the weld increased and the bonding of the native alloy with the IMCs in the stir zone increased. In this study the strong bonding in the weld region as mentioned earlier is due to mechanical interlocking between and the magnesium alloy and the IMCs in the stir zone. As seen Fig. 4-11(b) where the magnesium alloy (top sheet) forms a mechanical interlock with the IMCs in the stir zone. The

IMCs in the stir zone of the welds produced at 0.9 mm are thicker and continuous, but thinner and discontinuous at the weld bond width region. IMCs are brittle in nature and reduce the ductility of the welds when formed at interface or stir zone which results in reduced weld strength.

A thinner and discontinuous IMCs in the weld bond region provides better ductility compared to continuous thicker IMCs and thereby increasing the tensile strength of the welds [19, 20, 38]. In Fig. 4-11(c) (region T2) the bold arrow indicates the termination of the interfacial hook. It is clearly seen that the hook terminates away from the keyhole surface thereby increasing the weld bond width. Similar to welds produced at 0.0 mm plunge depth, the region T3 in Fig. 4-11(d) and T4 in Fig. 4-11(e) shows the interfacial hook formed by the extruded aluminum alloy and the unbonded region at the faying surface.

Figure 4-12 presents SEM images of the weld nugget, Fig. 4-12(a) shows the etched cross section with rectangular boxes indicating region of interest (T5 & T6). The weld bond width region seen in Fig. 4-12(b) (region T5) shows continuous thick $Al_{12}Mg_{17}$ just below periphery or boundary of the stir zone and smaller agglomerates of $Al_{12}Mg_{17}$ at the periphery of the stir zone in the weld bond width region. This is evident in Fig. 4-12(c) where the agglomerates of $Al_{12}Mg_{17}$ is formed in continues solution of Al_3Mg_2. The darker regions are the α-Mg+ $Al_{12}Mg_{17}$ eutectic structure formed due to the constitutional liquation mechanism [17,29]. In Fig. 4-12(d) (region T6) the interfacial hook terminates just before the weld bond width (indicated by bold arrow). An enlarged view of the area indicated in the dotted rectangular box in Fig. 4-12(d) is shown in Fig. 4-12(e). The interfacial hook is formed by the extruded aluminum alloy and a thin layer of Al_3Mg_2 is formed between the out layer of the hook and magnesium.

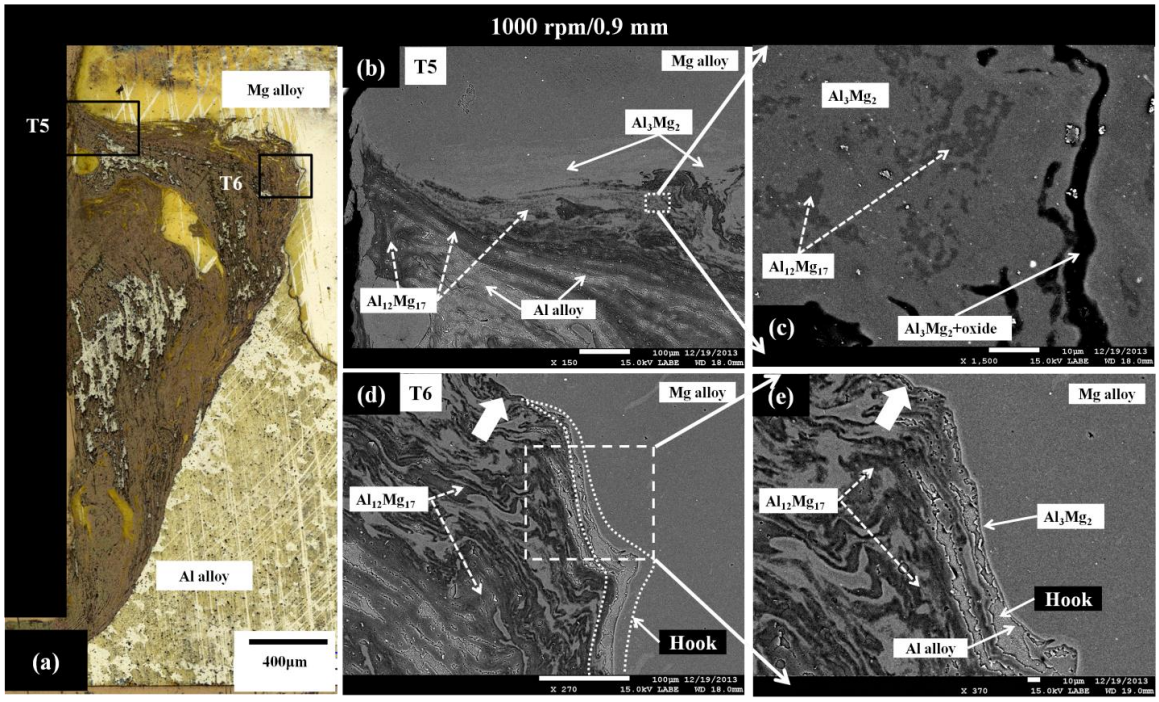

Figure 4-12: SEM images of the weld nugget region in FSSW coupon produced at 1000 rpm tool rotation rate and 0.9 mm plunge depth (a) Non-SEM macrograph of the stir zone region with rectangular boxes indicating various regions of (b) region T5 indicating the interlocking in the weld bond width region (c) magnified region in the dotted rectangular region of T5 showing the agglomerated $Al_{12}Mg_{17}$ in Al_3Mg_2 (d) region T6 indicating the interfacial hook (e) magnified region in the dotted rectangular box in region T6 showing the composition of the hook and presence of Al_3Mg_2 between the magnesium and aluminum alloy.

The cross sections of failed welds in Fig. 4-13(a) and Fig. 4-13(b) indicate that cracks propagate through the weak interfacial hook on end of the weld nugget. The regions indicated in the rectangular box in Fig. 4-13(a) and Fig. 4-13(b) are magnified to show the crack propagation in the weld nugget in Fig. 4-14 and Fig. 4-15 respectively. The failure mode in both welds is very similar. Once the crack grew halfway around the keyhole, the weld failed due to shear overload through the other side of the weld nugget.

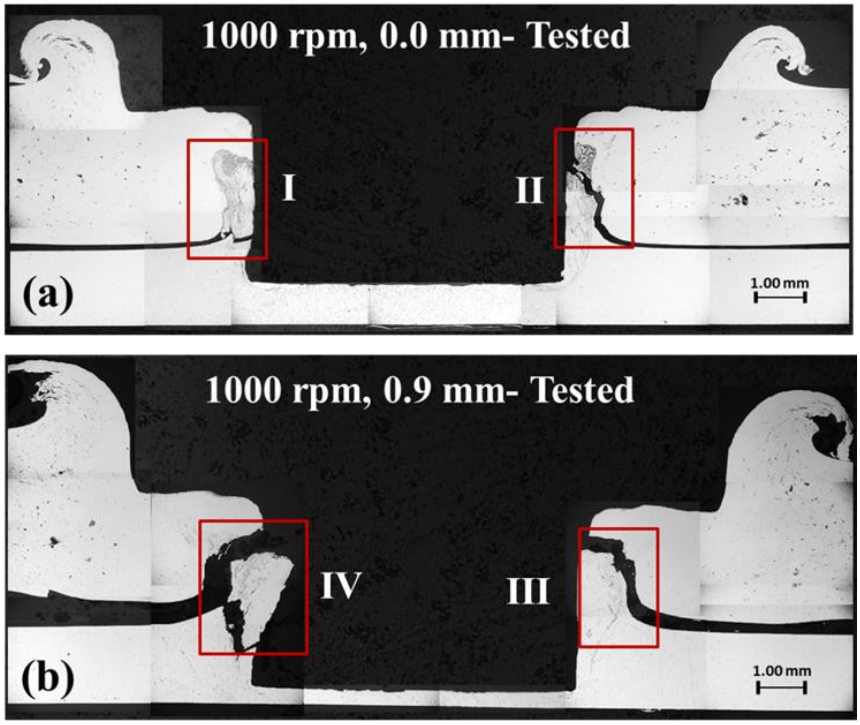

Figure 4-13: Cross sections of the failed spot welds at (a) 1000 rpm and 0.0 mm tool shoulder plunge depth, (b) 1000 rpm and 0.9 mm tool shoulder plunge depth. The rectangular boxes in each picture indicate the stir zone where the cracks progressed and failure occurred.

Figures 4-14(a) and Fig. 4-15(a) shows macrographs of the weld nugget region with the primary crack (PC) propagating through the faying surface and along the interfacial hook, and finally reaching the keyhole surface. The cracking through the base of the stir zone on the other side of the weld nugget indicates the shear over load failure (SOF). The brittle thin layer of Al_3Mg_2 at the interface of the hook and the magnesium alloy provides easy path for the already existing crack to propagate without any hindrance as seen in Fig. 4-14(c) and Fig. 4-15(c). Once the PC reaches the tip of the interfacial hook, continuous phase between the Al_3Mg_2 and magnesium alloy and interlocking of the Al_3Mg_2 in the stir zone with $Al_{12}Mg_{17}$ gives resistance for the crack to propagate effortlessly.

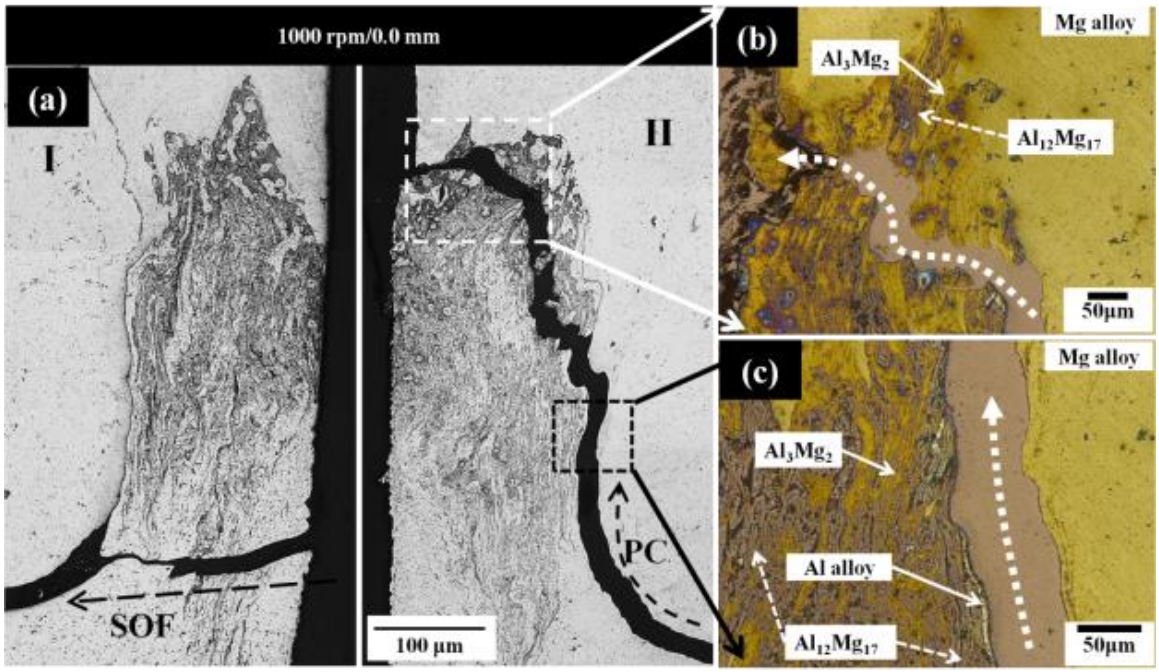

Figure 4-14: Magnified regions of the stir zone in failed weld produced at 1000 rpm and 0.0 mm plunge depth (a) region I and region II indicating the primary crack (PC) on one side of the weld nugget and shear over load failure (SOF) on the other side of the nugget (b) magnified view of the weld bond width area indicating the path of PC propagation (c) magnified view of the interfacial hook signifying the PC propagating through the IMC Al_3Mg_2.

From Fig. 4-14(b) it is evident that the thick continuous IMCs formed at the periphery of the stir zone coupled with smaller weld bond width provided an easier path for the PC to propagate resulting in lower lap-shear strength. In Fig. 4-15(b) discontinuous IMCs coupled with larger weld bond width provided higher resistance for the PC to propagate which resulted in welds with higher lap-shear strength. The study indicates that the formation of IMCs and the weld geometry together influence the lap-shear strength in FSSW dissimilar alloys.

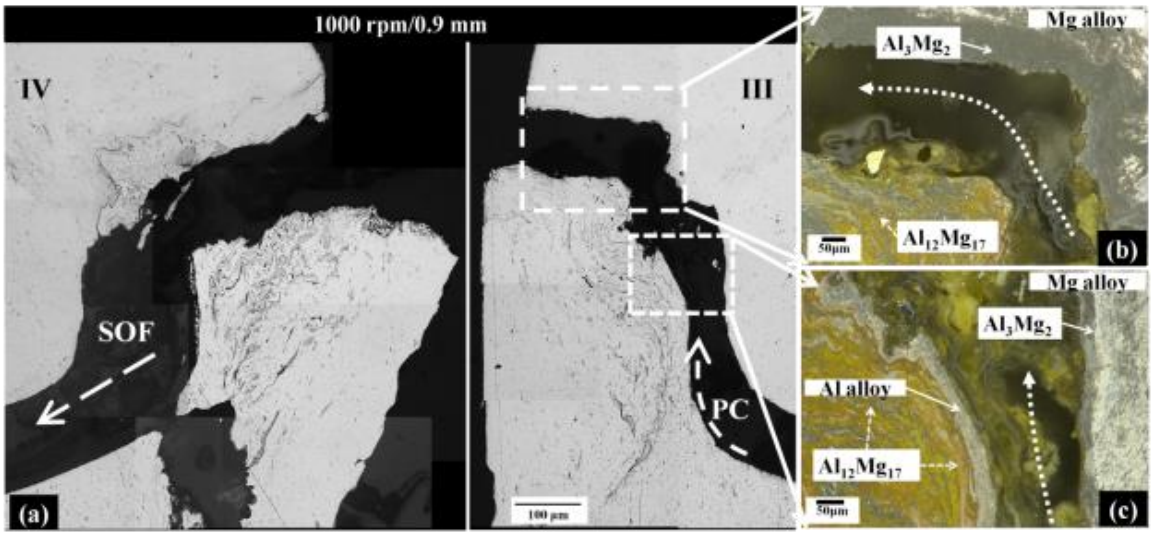

Figure 4-15: Magnified regions of the stir zone in failed FSSW coupons produced at 1000 rpm and 0.9 mm plunge depth (a) region III and region IV indicating the primary crack (PC) on one side of the weld nugget and shear over load failure (SOF) on the other side of the nugget (b) magnified view of the weld bond width area indicating the path of PC propagation (c) magnified view of the interfacial hook signifying the PC propagating through the IMC Al_3Mg_2.

4.4. Conclusions

In this study the effect of welding parameters on mechanical properties of the FSSW dissimilar alloys was investigated. An optimum process condition for FSSW cast AM60B to AA6022-T4 was identified. The following conclusions are made:

1. It is feasible to join via FSSW cast AM60B Mg alloy to AA6022-T4 Al alloy with good mechanical properties under certain weld process parameters for a given tool.
2. With the increase in tool rotation rate for the same tool plunge depth, the weld bond width decreased due to localized material flow and reduced material mixture in the stir zone. This

decrease in weld bond width results in lower lap-shear failure load of the FSSW dissimilar welds.

3. The lap-shear failure load of FSSW dissimilar alloys depends on both the geometrical feature as well as the formation of the IMCs in the stir zone.
4. The lap-shear failure load of the FSSW coupons increased with increase in tool shoulder plunge depth at 1000 rpm tool rotation rate. The weld bond width increased with increase in tool shoulder plunge depth thereby improving the lap-shear strength of the weld coupons.
5. The IMCs are formed in the stir zone. A continuous, thick layer of IMCs resulted in reduced weld strength while discontinuous, thinner layers of IMCs resulted in improved weld strength.
6. The interlocking of the base alloy with the IMCs in the stir zone improves the weld strength considerably. This interlocking can be achieved only with good material mixture.
7. The mechanical properties of the FSSW dissimilar alloys depend on the weld geometry and the IMCs formed in the weld nugget. These dominant features of the FSSW are all weld process parameter dependent, such as the tool rotation rate and the tool shoulder plunge depth. With the precise weld process parameters it is possible to produce sound FSSW joints in dissimilar alloys of magnesium and aluminum.

4.5. Bibliography

[1] G.S. Cole, A.M. Sherman, Mater. Charact. (1995) 3.

[2] P. Thornton, A.R. Krause, R.G. Davies, Weld. J. 75 (1996) 101s.

[3] A. Gean, S.A. Westgate, J.C. Kucza, J.C. Ehrstrom, Weld. Journal- New York 78 (1999) 80s.

[4] W. Thomas, E. Nicholas, J. Needham, M. Murch, P. Templesmith, C. Dawes, Friction Stir Butt Welding, G.B. Patent 9125978.8, 1991.

[5] D. A. Wang, C. H. Chen, J. Mater. Process. Technol. 209 (2009) 367.

[6] H. Badarinarayan, Y. Shi, X. Li, K. Okamoto, Int. J. Mach. Tools Manuf. 49 (2009) 814.

[7] A. Gerlich, P. Su, T.H. North, J. Mater. Sci. 40 (2005) 6473.

[8] P. Lin, J. Pan, T. Pan, Int. J. Fatigue 30 (2008) 90.

[9] Q. Yang, X. Li, K. Chen, Y.J. Shi, Mater. Sci. Eng. A 528 (2011) 2463.

[10] W. Yuan, R.S. Mishra, S. Webb, Y.L. Chen, B. Carlson, D.R. Herling, G.J. Grant, J. Mater. Process. Technol. 211 (2011) 972.

[11] S.M. Chowdhury, D.L. Chen, S.D. Bhole, X. Cao, Mater. Sci. Eng. A 527 (2010) 6064.

[12] Y.H. Yin, N. Sun, T.H. North, S.S. Hu, J. Mater. Process. Technol. 210 (2010) 2062.

[13] Y.H. Yin, N. Sun, T.H. North, S.S. Hu, Sci. Technol. Weld. Join. 15 (2010) 81.

[14] J.B. Jordon, M.F. Horstemeyer, S.R. Daniewicz, H. Badarinarayan, J. Grantham, J. Eng. Mater. Technol. 132 (2010) 041008.

[15] H. Rao, J. Jordon, M. Barkey, Y. Guo, X. Su, H. Badarinarayan, Mater. Sci. Eng. A 564 (2013) 369.

[16] C.I. Chang, C.J. Lee, J.C. Huang, Scr. Mater. 51 (2004) 509.

[17] Y.S. Sato, A. Shiota, H. Kokawa, K. Okamoto, Q. Yang, C. Kim, Sci. Technol. Weld. Join. 15 (2010) 319.

[18] C. Lee, D. Choi, Y. Yeon, S. Jung, Sci. Technol. Weld. Join. 14 (2009) 216.

[19] D. H. Choi, B. W. Ahn, C.Y. Lee, Y.M. Yeon, K. Song, S.-B. Jung, Intermetallics 19 (2011) 125.

[20] N. Yamamoto, J. Liao, S. Watanabe, K. Nakata, Mater. Trans. 50 (2009) 2833.

[21] A. McLean, G.L.F. Powell, I.H. Brown, V.M. Linton, Sci. Technol. Weld. Join. 8 (2003) 462.

[22] Y.C. Chen, K. Nakata, Scr. Mater. 58 (2008) 433.

[23] S.H. Chowdhury, D.L. Chen, S.D. Bhole, X. Cao, P. Wanjara, Mater. Sci. Eng. A 556 (2012) 500.

[24] Y.H. Yin, N. Sun, T.H. North, S.S. Hu, Mater. Charact. 61 (2010) 1018.

[25] H. Badarinarayan, Q. Yang, S. Zhu, Int. J. Mach. Tools Manuf. 49 (2009) 142.

[26] K.N. Solanki, J.B. Jordon, W. Whittington, H. Rao, C.R. Hubbard, Scr. Mater. 66 (2012) 797.

[27] N. Sun, Y.H. Yin, a. P. Gerlich, T.H. North, Sci. Technol. Weld. Join. 14 (2009) 747.

[28] Z. Zhang, X. Yang, J. Zhang, G. Zhou, X. Xu, B. Zou, Mater. Des. 32 (2011) 4461.

[29] V. Firouzdor, S. Kou, Metall. Mater. Trans. A 41 (2010) 3238.

[30] S. Kou, Weld. J. 88 (2009) 213.

[31] X.J. Cao, M. Jahazi, Mater. Sci. Forum 638-642 (2010) 3661.

[32] W. Yuan, R.S. Mishra, B. Carlson, R. Verma, R.K. Mishra, Mater. Sci. Eng. A 543 (2012) 200.

[33] A. Gerlich, M. Yamamoto, T. North, Metall. Mater. Trans. A 38 (2007) 1291.

[34] A. Gerlich, P. Su, T.H. North, Sci. Technol. Weld. Join. 10 (2005) 647.

[35] H. Schmidt, J. Hattel, J. Wert, Mater. Sci. Eng. 12 (2004) 143.

[36] S. Bozzi, L. Helbert-Etter, T. Baudin, V. Klosek, J.G. Kerbiguet, B. Criqui, J. Mater. Process. Technol. 210 (2010) 1429.

[37] H.M. Rao, R.I. Rodriguez, J.B. Jordon, M.E. Barkey, Y.B. Guo, H. Badarinarayan, W. Yuan, Mater. Des. 56 (2014) 750.

[38] V. Firouzdor, S. Kou, Metall. Mater. Trans. A 41 (2010) 2914.

CHAPTER 5

EFFECT OF WELD PROCESS PARAMETERS ON LAP-SHEAR STRENGTH OF FRICTION STIR LINEAR WELDED ALUMINUM 60022 T4 TO MAGNESIUM AM60B

Abstract

The lap-shear strength of friction stir linear welded (FSLWed) aluminum 6022 to cast magnesium AM60B alloy under varying weld process conditions were examined. A process window was developed to initially identify the potential weld process conditions. Several welded joints were produced by varying the tool rotation rate and tool traverse speed while keeping the plunge depth constant. The welds were produced in such a manner that the advancing side of the weld was at the free end of the lap-shear coupon and the retreating side of the weld was at the loading side of the coupon. Welds produced at 1500 rpm tool rotation speed and at 50 mm/min and 75 mm/min tool traverse speed had the highest failure load at approximately 3.5 kN. Furthermore, analysis of the cross section of the untested coupons suggest the welds made at 1500 rpm tool rotation rate and 75 mm/min tool traverse speed produced welds with negligible voids compared to welds made at 1500 rpm and 50 mm/min traverse speed. Cross sections of the tested coupons indicate the failure or dominant crack initiated at the advancing side and progressed through the weld nugget which were marked by presence of intermetallic compounds (IMCs). This study demonstrates the feasibility of welding dissimilar materials by FSLW process under selective weld process conditions with promising results.

5.1. Introduction

One of the ways to make present day cars and trucks environmentally friendly is by improving the fuel efficiency. Hence automotive industries around the globe are looking into lightweight materials for mass saving and thereby improving the fuel efficiency of the cars, trucks and other automobiles. Light weight alloys based on magnesium and aluminum has found a favorable place to replace the existing heavy steel based alloys. The use of magnesium in automotive industry is hindered by the fact that the traditional welding technique are difficult to use on the lightweight alloy [1–3]**.** The alternative joining method that has emerged and proven to be a viable technique is friction stir welding (FSW). Friction stir welding was developed by The Welding Institute, UK in 1991 and is a novel solid state welding technique [4]. FSW consists of a rotating tool with a probe pin which is plunged between two sheets of material to be joined. The downward movement of the tool provides the forging force while the friction between the tool shoulder and the material surface generates frictional heat. The transverse movement of the tool along the material surface forms a weld joint between the two materials to be joined.

For most part, the FSLW process has been extensively studied in joining aluminum to aluminum alloys [5–8] and magnesium to magnesium alloys [9–13]. At times owing to design constraints, two or more alloys may be used in combination. To exploit the optimum physical, mechanical and chemical properties of these alloys, there is increased interest to join aluminum and magnesium in combination. The challenge of joining the dissimilar alloys lies in the formation of the brittle intermetallics (IMC) in the weld zone. With limited research conducted in solid state joining of dissimilar alloys, most have reported about the formation IMCs and its effect on the weld joint strength [14–21]. Constitutional liquation occurred in the weld joints during the welding

of Mg and Al alloys and the IMCs ($Al_{12}Mg_{17}$, Al_3Mg_2) were produced at the weld interface [14,16,20–27]. During FSLW of aluminum to magnesium, the temperatures attained in the stir zone is far below melting point, but liquation is likely to occur in the stir zone where temperatures can reach up to 450^0C which is the eutectic temperature in Al-Mg binary phase diagram. Upon cooling, the liquid formed in the stir zone solidify into Al_3Mg_2 at the Al rich side of the weld and $Al_{12}Mg_{17}$ at the Mg rich side of the weld [25–28]. The formation of IMCs have shown to reduce the weld strength in both the spot and liner welds of dissimilar alloys [14,16,23,25,27,28].

As in conventional FSW of similar alloys, the weld process conditions and tool design have been observed to significantly influence the weld strength. Yamamoto et al. [16] observed in FSW Al-Mg alloy, as the thickness of the IMCs formed at the faying surface of the two sheets increased, the lap-shear strength of the weld decreased. The thickness of IMCs was influenced by the frictional heat input, a higher heat input resulted in thicker IMCs thereby reducing the weld strength. A very high tool rotation rate and low tool traverse speed introduced a high frictional heat favoring the formation of thicker IMCs. While a low tool rotation rate and high tool traverse speed introduced week bonding due to insufficient frictional heat. Firouzdor et al. [28] studied the effect of material position during the friction stir linear welding. The butt weld configuration yielded better weld strength compared to welds made in lap-shear mode configuration. The weld strength in butt welded aluminum to magnesium alloy increased when the magnesium was placed on the ascending side of the weld and aluminum on the retreating side. The position of magnesium on the ascending side of the weld favored frictional heat input which was just sufficient to plastically deform the material and at the same time suppressed the formation of IMCs at the interface. Defects were observed in FSLW of aluminum to magnesium alloys when the tool rotation rate was 800 rpm and the defect free welds were obtained when the tool rotation rate

increased beyond 1000 rpm [24]. In FSLW of aluminum to magnesium in butt weld configuration, the joint strength increased when the tool pin was centered or offset into magnesium alloy and a lower weld strength was observed when the tool pin was offset into the aluminum alloy [17].

Though FSLW has been studied extensively on similar alloys, there has been very few studies on FSLW of dissimilar alloys. The available research data on FSLW dissimilar aluminum to magnesium is more or less confined to butt weld configuration [15–17,23,24,27,29] and very few on lap-shear configurations [25,26,28]. Most of these studies have indicated the formation of IMCs and its effect on the weld strength, however not many studies indicate the influence of welding process conditions such as, tool rotation rate and tool traverse speed on weld strength. The authors in this current study have attempted to investigate the influence of these weld process conditions on the formation of the IMCs and its influence on the weld strength in FSLW dissimilar alloys of aluminum and magnesium alloys in lap-shear configuration.

5.2. Materials and Experiment

A rolled AA6022-T4 aluminum alloy of 1.5 mm in thickness was FSW to cast AM60B magnesium alloy of thickness 3.5 mm. The FSW tool used in this study shown in Fig. 5-1 was made of standard tool steel (H13) and constituted a concave tool shoulder and a triangular pin. The geometrical features and dimensions of the FSW tool are listed in Table 5-1. The aluminum sheet was placed on top of the magnesium sheet with an overlay of 30 mm and the tool was made to traverse from one end of the sheet to other as shown in Fig. 2(a).

Table 5-1: Information of the FSSW tool material and geometric feature employed in this study

Tool material	H13 Tool steel	
Tool profile	Shoulder shape	concave
	Shoulder diameter	12 mm
	Pin shape	Triangular
	Pin diameter	tri. = 5.4 mm (eq.);
	Pin length	2.4 mm

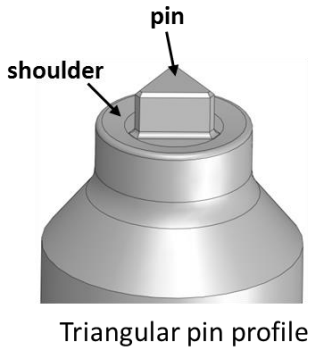

Figure 5-1: FSLW tool profile

The sheets were clamped together using an in-house designed clamp fixture as shown in Fig. 5-2(b). The tool rotation was in a counter clock wise direction and welds were produced in a manner such that the advancing side (AS) was at the free end of the coupon and retreating side (RS) was on the loading side of the coupon as shown in Fig. 5-2(c). One of the research goals of this study is to identify the ideal welding parameters for optimal weld strength. As such, a process window was developed as shown in Fig. 5-3(a) and several test welds were made to identify the feasible welding process conditions as shown in Fig. 5-3(b).

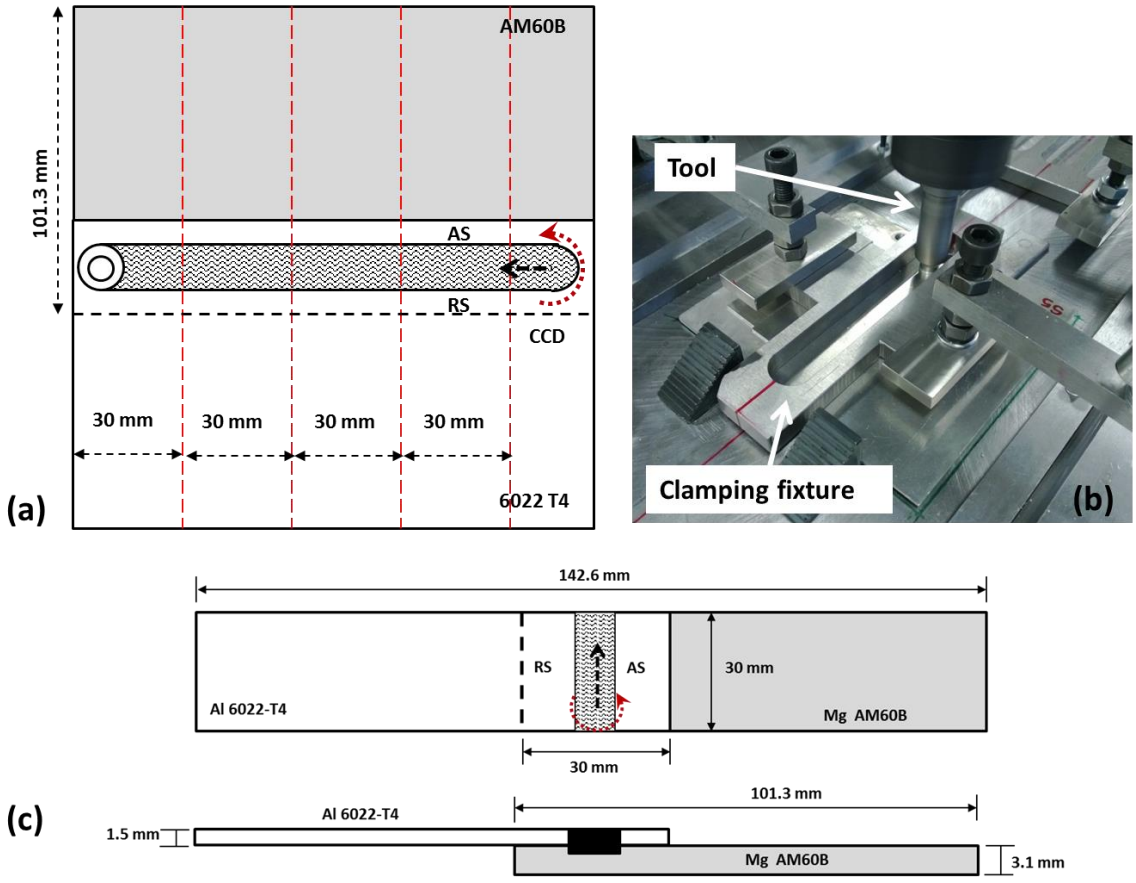

Figure 5-2: Representation of (a) The FSLW methodology indicating the tool traverse direction, tool rotation direction and geometrical dimensions of the welding condition (b) clamping fixture employed in this study (c) geometrical dimensions of the FSSW test coupon after water-jet cut.

A tool shoulder plunge depth of 0.2 mm and 3^0 tool tilt angle was maintained for all the welding conditions. The lap-shear tensile tests were conducted at room temperature on Instron screw-drive machine (Model 1123) with a constant cross head speed of 2 mm/min. At each stage of study, selected tested and un-tested coupons were cross-sectioned through the center of the welds and cold mounted in epoxy. The mounted specimens were mechanically grinded and finely polished using 0.05 µm aluminum oxide. Since two different materials were polished

simultaneously, only de-ionized water was used through the polishing steps. In order to reveal the microstructure and IMCs, AM60B was etched using an acetic glycol solution (20 ml acetic acid, 1 ml HNO_3, 20 ml H2O, and 60ml ethylene glycol) and the AA6022-T4 was etched with 20% NaOH solution (caustic etching). The macro and microstructures of welds and failure modes were analyzed using the optical microscope. Casting pores or voids were also observed in as received AM60B sheet. To analyze the IMCs and its composition, untested FSSW coupons were examined under Jeol 7000F SEM with EDS capabilities.

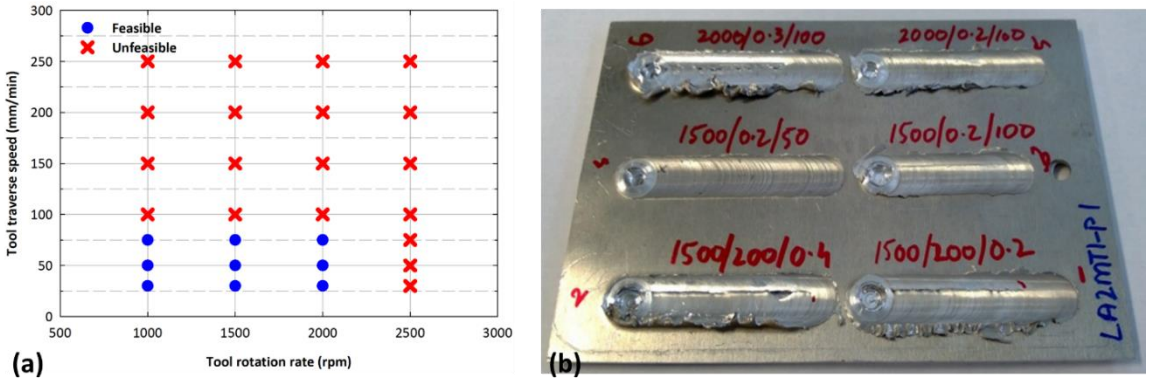

Figure 5-3: (a) Plot showcasing the process condition window (b) raw welds produced to develop the process condition window.

5.3. Results and Discussion

Two major factors influence the weld strength in FSLW dissimilar joints, the macro features such as the hook geometry and effective sheet thickness and micro features such as the IMCs in the stir zone. During FSLW the faying surface on ascending side (AS) forms into a 'hook' like feature which points upwards towards the top sheet and the retreating side forms a cold lap feature and may extend across to weld nugget towards the AS [30]. To understand the different orientation of AS and RS hook, a schematic is shown in Fig. 5-4.

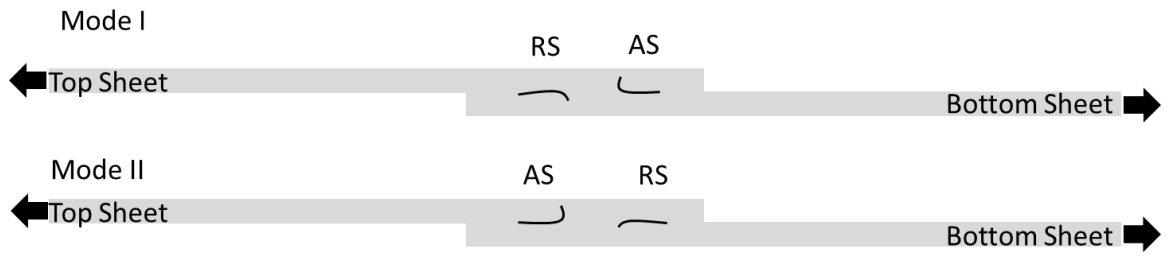

Figure 5-4: Schematic of RS and AS loading in a FSLW in lap-shear configuration.

Mode I has RS on the top sheet and is on the loading side of the coupon, while in Mode II, the AS is on the loading side of the coupon. Previous studies on FSLW of similar alloys indicated the lap-shear strength of the joints increased when the RS of the weld was subjected to loading that is in Mode I [8, 30, 31]. Yuan et al. [30] observed in FSLW of Mg alloys, the weld strength was higher when the RS cold lap feature terminated away from the AS hook and weld strength decreased when the RS cold lap feature terminated very close to AS hook. In this current study, all the test coupons were produced in Mode I, where the RS on the top sheet was loaded. Since in this study, the welds failed by shear overload through the weld nugget, the influence of effective sheet thickness will not be discussed. For brevity purpose, the microstructure of the weld with the best weld performance will be discussed later in this section.

5.3.1. Lap-Shear Tensile Strength and Macro Features

The lap-shear tensile strength of the FSLW coupons produced under different welding conditions were tested. The results are plotted and shown in Fig. 5-5(a) for welds produced at 1000 rpm, Fig. 5-5(b) for welds produced at 1500 rpm and Fig. 5-5(c) for welds produced at 2000 rpm and varying tool traverse speed (TTS) ranging from 30 mm/min to 75 mm/min. At 1000 rpm, the welds produced at TTS of 30 mm/min had the highest lap-shear strength and the weld strength

plummeted with increase in TTS. For welds produced at 1500 rpm, a trivial increase in the lap-shear strength was observed when the TTS increased from 30 mm/min to 50 mm/min and then dropped negligibly at 75 mm/min TTS. For welds produced at 2000 rpm tool rotation rate, the lap-shear strength increased with the increase in TTS from 30 mm/min to 50 mm/min and decreased steeply on further increase in TTS to 75 mm/min. The cross section of the untested coupons produced at 1000 rpm and varying TTS is shown in Fig. 5-6.

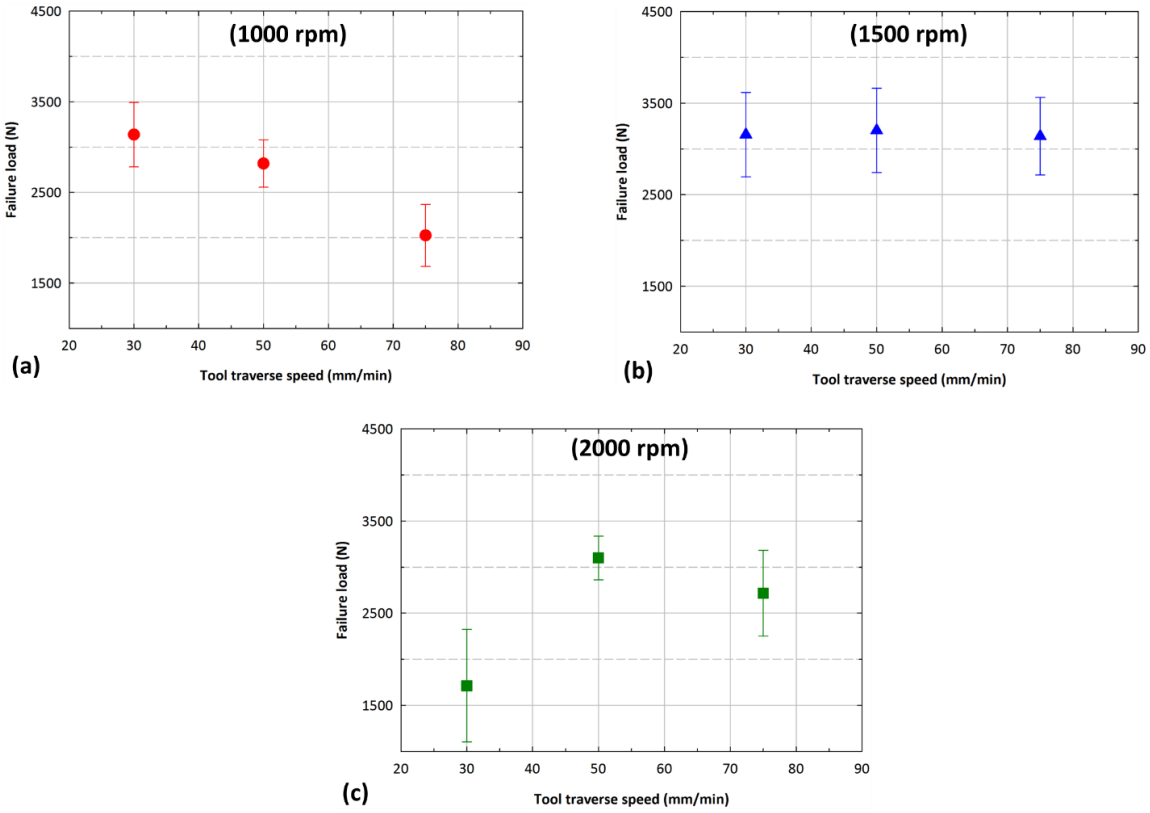

Figure 5-5: Lap-shear test data for welds produced at different tool rotation rate and varying tool traverse speed (a) 1000 rpm (b) 1500 rpm and (c) 2000 rpm.

It is a well-known fact that a higher tool rotation rate [10,21,32–36] and lower TTS [8,11,13] introduces more frictional heat and results in greater plastic deformation of the materials in the stir zone. As seen in Fig. 5-6(a) for welds produced at 1000 rpm and 30 mm/min TTS, the RS cold lap

feature terminates in the stir zone and does not continue across the weld nugget towards the AS hook. As the TTS increases at the same tool rotation rate of 1000 rpm, the amount of frictional heat generated reduces resulting in insufficient material mixture resulting in weaker bond.

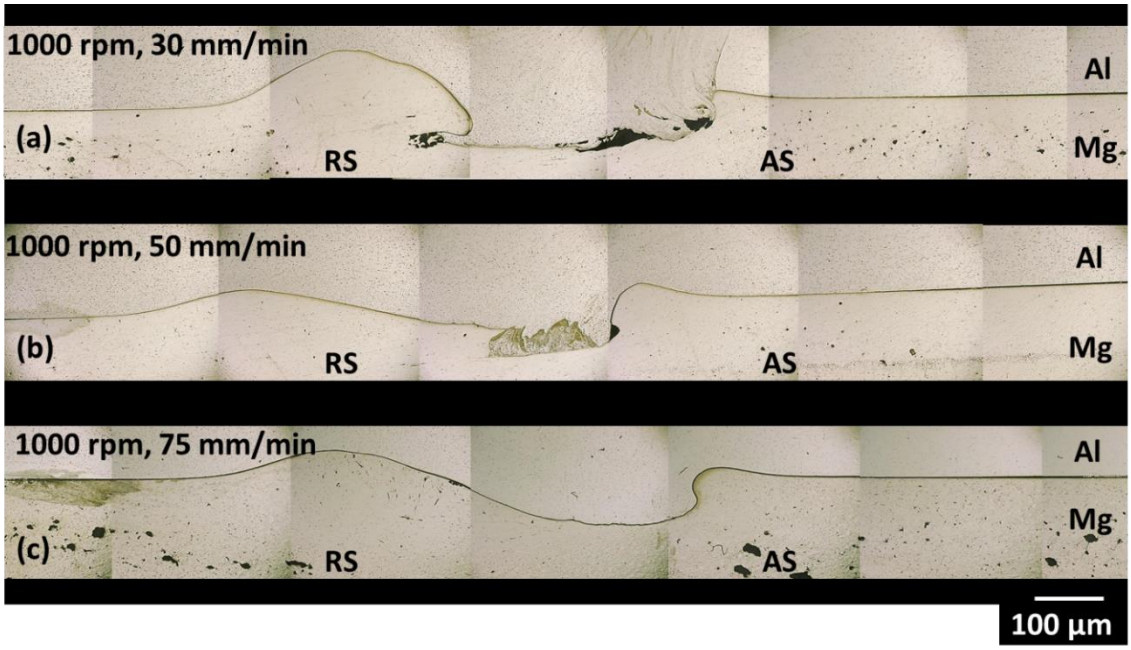

Figure 5-6: Cross section of the untested weld samples produced at 1000 rpm (a) 30 mm/min traverse speed (b) 50 mm/min traverse speed (c) 75 mm/min traverse speed.

This is clearly observed in Fig. 5-6(b) for welds produced at 50 mm/min TTS, the RS cold lap feature terminates very close to AS hook and the stir zone size decreased which resulted in lower weld strength. With further increase in TTS to 75 mm/min, the RS cold lap feature extended all the way through the weld nugget and fused with the AS hook as seen in Fig. 5-6(c). It is a strong indication that at faster TTR, the amount of frictional heat generated is much lower which resulted in insufficient material mixture leading to poor weld strength. At 1000 rpm tool rotation rate, relatively lower frictional heat is generated, to counter the lower frictional heat, a slower TTS

introduces more frictional heat resulting in localized plastic deformation resulting in superior weld strength.

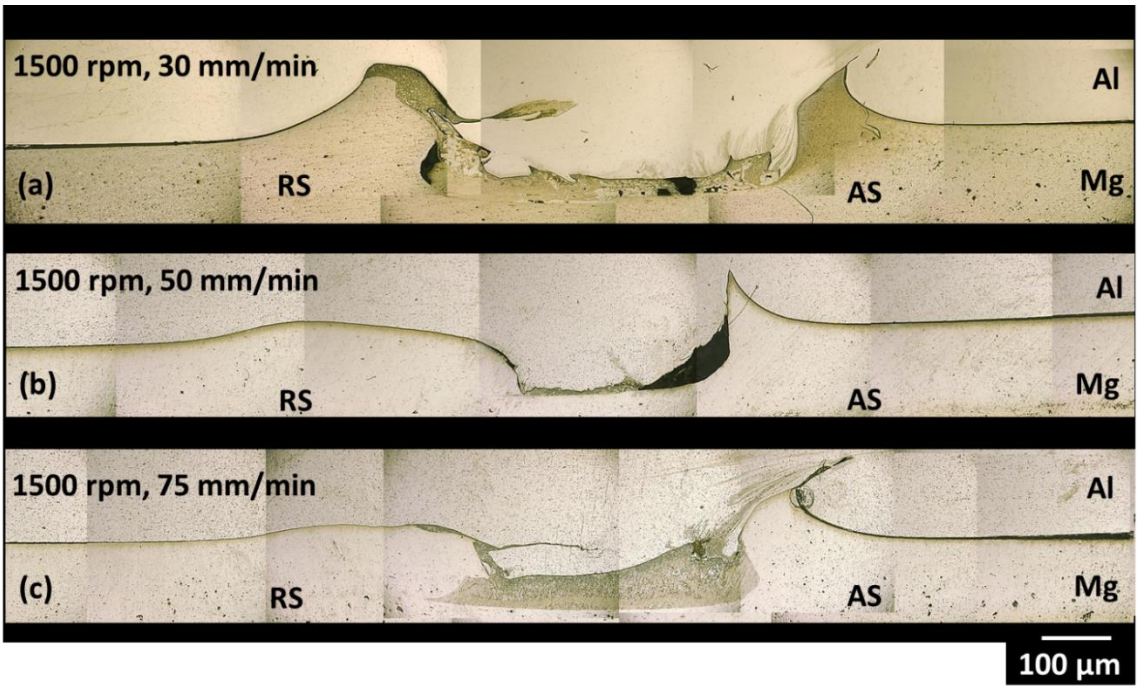

Figure 5-7: Cross section of the untested weld samples produced at 1500 rpm (a) 30 mm/min traverse speed (b) 50 mm/min traverse speed (c) 75 mm/min traverse speed.

The cross section of the untested weld coupons produced at 1500 rpm and varying TTS are shown in Fig. 5-7. In general, welds produced at 1500 rpm tool rotation rate showed superior and consistent weld strength for all the three TTS. Welds produced at 30 mm/min TTS (Fig. 5-7(a)) the RS cold lap feature terminated away from the AS hook in the weld nugget. With the increase in the TTS, the cold lap feature on RS was more suppressed and terminated in the weld nugget away from the AS hook. The formation of weld voids or channel defects were prominent in lower TTS at 30 mm/min as seen in Fig. 5-7(a) and 50 mm/min as seen in Fig. 5-7(b). At 75 mm/min

TTS (Fig. 5-7(c)), the weld voids are very small or negligible. This suggests the TTS has a high impact on the frictional heat generated in the weld nugget, very high frictional heat leads to insufficient material being retrieved back into weld nugget causing voids and channel defects in the welds. For welds made at 2000 rpm and varying TTS, the presence of voids in the weld nugget indicates a very high frictional input heat due to high tool rotation rate. Welds produced at 30 mm/min had the lowest weld strength of all the welds produced at varying TTS.

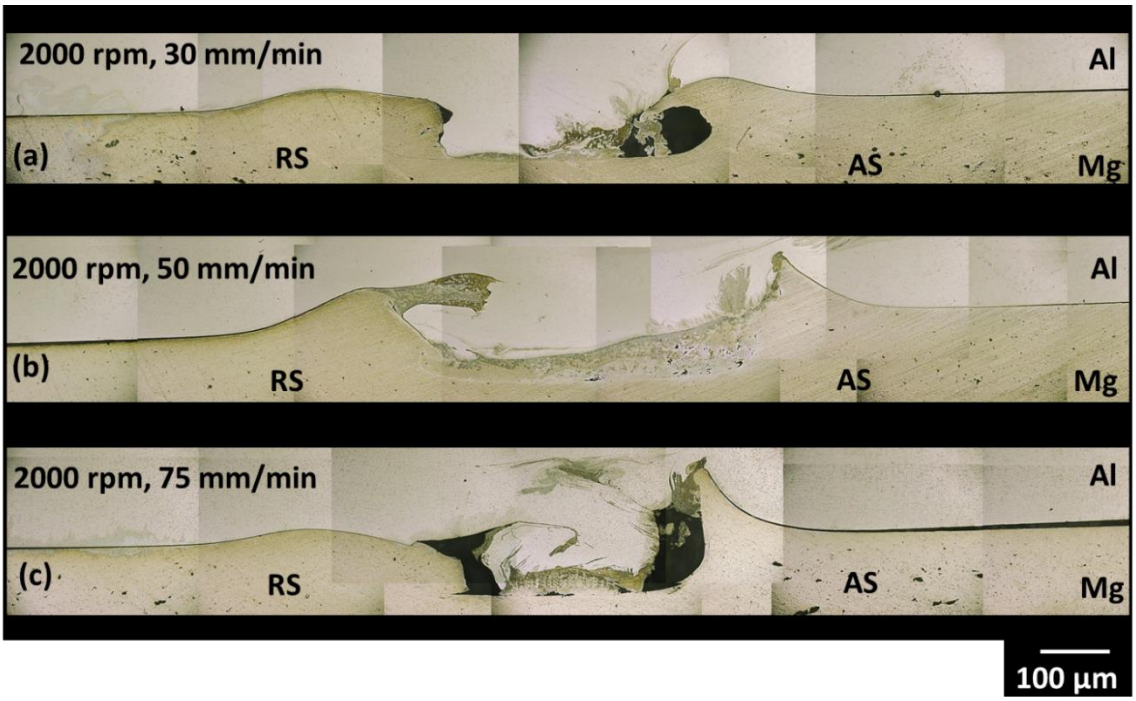

Figure 5-8: Cross section of the untested weld samples produced at 2000 rpm (a) 30 mm/min traverse speed (b) 50 mm/min traverse speed (c) 75 mm/min traverse speed.

The cross section of the untested weld coupon produced at 30 mm/min TTS indicates presence of large voids at the AS of the weld nugget as seen in Fig. 5-8(a). The cause for lower weld strength may be due to formation of voids or channel defects along with geometry of the AS hook which is curved towards the weld nugget. Since all the welds in this study failed through shear overload,

the AS hook pointing inwards into the weld nugget facilitates the crack growth through faying surface. With increase in TTS to 50 mm/min, the weld strength considerably increased. The cross section of the untested weld in Fig. 5-8(b) indicates a good weld bond in stir zone free of any channel defects and geometrical features of the RS cold feature and AS hook in favor of high weld strength. Welds produced TTS of 75 mm/min had the lowest weld strength and the cross section of the weld revels large voids on AS and RS indicating insufficient material mixture as seen in Fig. 5-8(c). The higher TTS may have resulted in insufficient material mixture resulting very small weld bond widths and large voids/channel defects.

Welds produced at 1500 rpm showed very consistent lap-shear strength compared to welds produced at 1000 rpm and 2000 rpm. Hence 1500 rpm was identified as the ideal tool rotation rate. The 30 mm/min and 50 mm/min TTS was left out of further study for two reasons; one due to presence of voids in the weld nugget which may have undesirable influence on the fatigue life of these welds and second due to fact that it would take longer period of time to produce a weld at 30 and 50 mm/min compared to welds produced at 75 mm/min TTS which is of economic importance to manufacturing industry.

5.3.2. Microstructure Analysis

The microstructure of the untested weld coupons reveled the formation of IMCs in the stir zone of the weld nugget and along the faying surface. The etched untested weld sample (Fig. 5-9(d)) indicates the RS cold lap feature, AS hook and a thick layer of IMCs in the stir zone of the weld nugget. Two kinds of IMCs were observed, $Al_{12}Mg_{17}$ on Mg rich side and Al_3Mg_2 on Al rich side of the weld. The discussion is kept simple to the exact composition and structure of IMCs to be discussed later in this section.

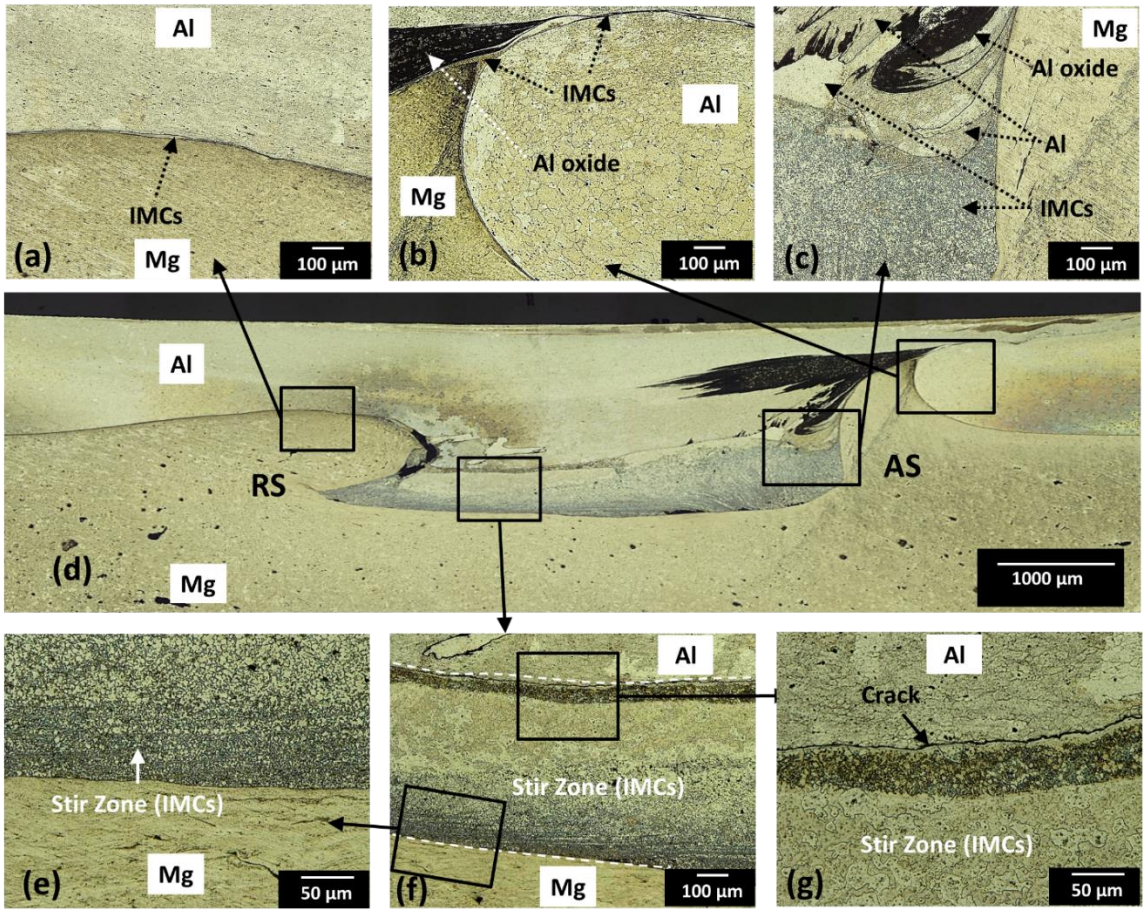

Figure 5-9: Cross section of the etched weld sample produced at 1500 rpm and 75 mm/min tool traverse speed (a) cold lap feature on the RS of the weld (b) AS of the weld with hook (c) magnified view of the AS towards the bottom of the weld nugget (d) cross section of the weld showing the various geometrical features of the FSLW (e) magnified view of the interface between the magnesium and IMC (f) magnified view of the sandwiched IMC layer between aluminum and magnesium (g) magnified view of the interface between the aluminum and the IMC in the stir zone.

Along the faying surface on the AS and the RS a thin layer of IMCs are formed as shown in Fig.5-9(a) and Fig. 5-9(b). Since the two surfaces are clamped together, there is possibility of diffusion of Mg and Al atoms at the faying surface right under the tool shoulder. The faying surface under the tool shoulder can attain favorable temperatures for the formation of IMCs. On the

advancing side of the weld, adjacent to the AS hook on the Al sheet, a dark region was observed as shown in Fig. 5-9(c) and Fig. 5-9(d). Firouzdor et al. [25] observed a similar dark region on the AS in FSLW of Al to Mg and quantified it as the Al oxide layer. The AS hook is formed of the Mg from the bottom sheet which was extruded by the rotating tool pin as seen in Fig. 5-9(b). The AS hook is separated from the faying Al surface by a thin layer of IMCs, where the dimensions of these IMCs will be discussed later in this section. The stir zone of the weld nugget is characterized by presence of a thick layer of IMCs (~0.4 mm-0.8 mm) which extends from the AS to the RS of the weld nugget. Closer to the AS, the thickness of the IMCs is much larger compared to thickness of IMCs near to the RS. This is due to the fact the extracted material from the AS is suppressed on the RS by the tool shoulder. As seen in Fig. 5-9(c) the thin IMCs layer continue from the AS hook and continue into the stir zone in the weld nugget. Figure 5-9(f) shows the layer of IMCs formed in the stir zone sandwiched between the top Al and Mg sheet. The IMCs in the stir zone is close to the bottom Mg sheet shown in Fig. 5-9(e), and has no visible crack between the native Mg and the IMCs indicating a continuous bonding between the two materials. While the interface between the IMCs and the top Al sheet has a prominent visible crack as seen in Fig. 5-9(g), the hypothesis is the weld tool pin does not completely penetrate the bottom Mg sheet, while it completely penetrates the top Al sheet during the welding process. This process introduces a mixture rich in liquefied Al in the stir zone close to the top portion of the weld tool pin while the Mg in the bottom sheet comes directly under the weld tool pin surface. The rotating motion of the tool pin extracts the plastically deformed Mg and pushes upwards into the Al rich mixture in the stir zone leading to the formation of IMCs. This action does not break the Mg completely but rather extracts the Mg which mixes with liquefied Al in the stir zone. This thick layer of IMCs in the stir zone is the bonding agent which holds the top Al sheet and bottom Mg sheet together.

Three different regions in the stir zone were observed under SEM to analyze the chemical composition of the IMCs. Table 5-2 provides the different chemical composition of the phases that were analyzed under SEM using EDS technique. Figure 5-10(a) shows the regions A1, A2 and A3 where the EDS analysis were performed. Region A1 shown in Fig. 5-10(b) is from near to the Al and thick IMCs interface where a clear distinction between the native Al and IMCs can be observed. The crack between the IMCs and native Al indicates a partial bonding between the two interfaces. On top of IMCs is phase R1 which is native Al alloy and phase R3 is Al3Mg2 rich in Al.

Table 5-2: Composition (weight %) measured using EDS at various locations in the stir zone of the welds (instead of using phase, it is necessary to use actual locations)

Region	Phase	Mg (Wt %)	Al (Wt %)	O (Wt %)	Total
R1	Al 6022-T4	2.9	93.9	3.5	100.0
R2	Mg AM60B	0.96	98.54	0.51	100.0
R3	Al_3Mg_2 + Al Eutectic	33.3	61.8	4.9	100.0
R4	Primary Al_3Mg_2	39.9	57.2	2.9	100.0
R5	Primary $Al_{12}Mg_{17}$	54.0	43.6	2.3	100.0
R6	$Al_{12}Mg_{17}$ + Mg Eutectic	71.6	28.4	0.0	100.0

A closer look at the interface between the two materials shows traces of layers of Al3Mg2 on surface of the native Al alloy as seen in Fig. 5-10(c). At the center of the IMCs layer, region A2 shows the two IMCs phases clearly distinguishable from each other. The lighter region, phase R5 is the primary Al12Mg17 while the darker region, phase R4 is the primary Al3Mg2 as seen in Fig. 5-10(d). Similar observations were made in earlier studies of FSWed Al to Mg [14,25,27].

This clearly shows the stirring action of the weld tool pin causes the two liquefied Al and Mg to mix with each other, which on cooling forms into Al3Mg2 in the Al rich side and Al12Mg17 on the Mg rich side of the weld. The clear distinction between the two phases of IMCs can be appreciated in Fig. 5-10(e) where the lighter region, phase R5 coexists with the darker region, phase R4. Region A3 in Fig. 5-10(f) shows the lower IMC layer near to the Mg sheet. Unlike at the interface between the Al and IMCs, there is no visible crack between the interface of Mg and IMCs in the stir zone. The un-pitted region in Fig. 5-10(f) is phase R2 the base Mg AM60B alloy, while the pitted region above are the IMCs. The magnified area of the pitted region in Fig. 5-10(g) shows a layer of primary Al12Mg17 (phase R5) characterized by what appears to be strands of Al12Mg17 and the pitted region (R6) is the Al12Mg17 + Mg eutectic. Sato et al. [27] noted after constitutional liquation cools to solid phase, liquid →Al12Mg17 +Mg after primary solidification of Al12Mg17.

The continuity between the base Mg sheet and the IMCs in the stir zone indicates the tool pin did not completely penetrate the Mg sheet rather, the material from the Mg close to tool pin bottom surface liquefies and is pushed upwards towards the Al rich mixture. Throughout this process, small amounts of liquefied Al mixes with the Mg which on cooling solidified into Al12Mg17. The shear force near to top portion of the tool pin is much higher than at the bottom surface of the tool pin. This introduces a very high shear force in the top Al sheet that the materials around the top portion of tool undergoes sever deformation compared to materials under the tool pin surface.

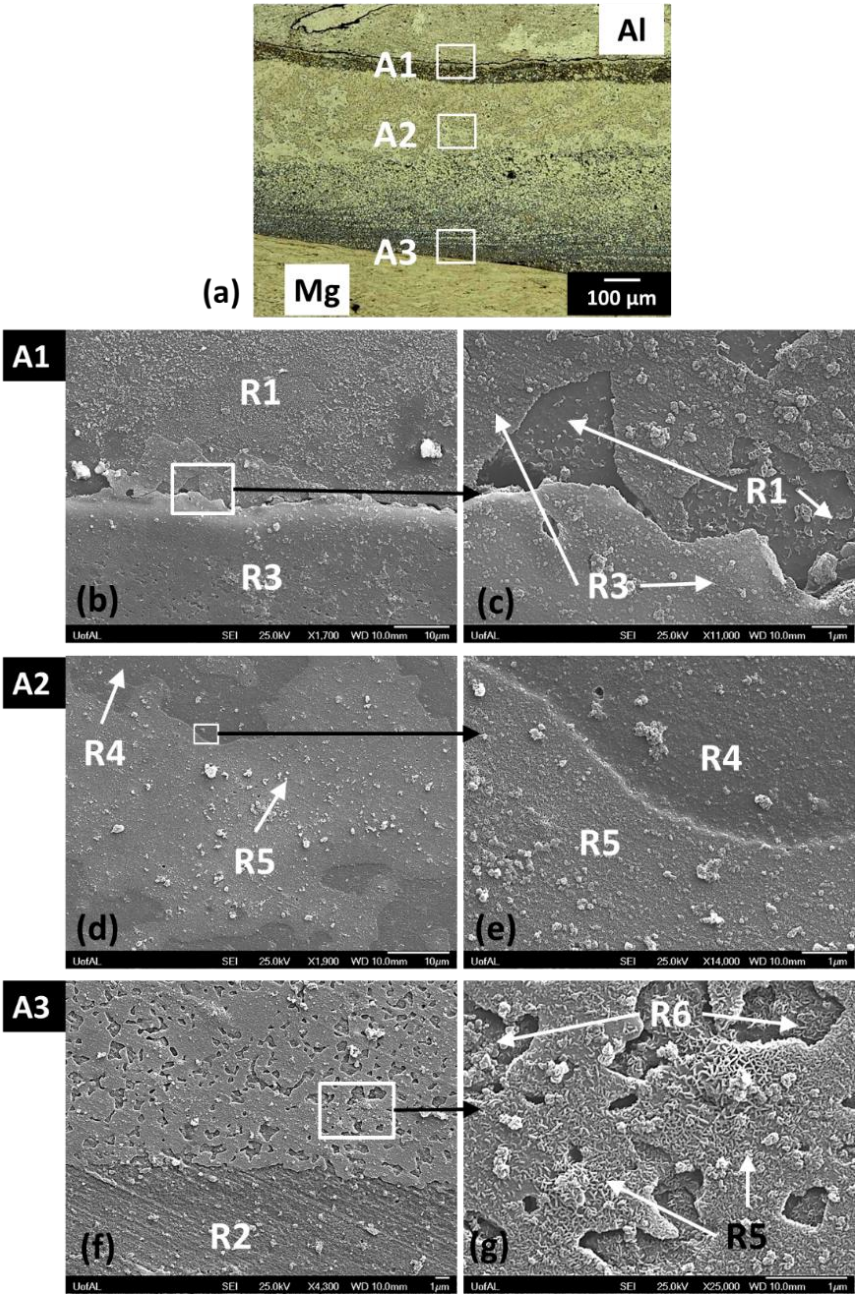

Figure 5-10: SEM images of the welds produced at 1500 rpm and 75 mm/min tool traverse speed (a) optical microscopic picture indicating the three different areas of which the chemical analysis were conducted (b) region A1 at the interface of the aluminum and IMC (c) magnified view of the region A1 (d) region A2 from the center of the IMC (e) magnified view of a small area in region A2 (f) region A3 at the base of the magnesium and IMC interface (g) magnified view of a small area in region A3.

Hence the Al3Mg2 is characterized by finer particles while the lower portion of the stir zone is characterized by what appears to be small strands of the Al12Mg17 in Mg rich phase. At the faying surface away from the stir zone in the weld nugget, a thin layer of IMCs were observed on RS and AS of the weld. During the welding stage, the two sheets are held down very firmly by a clamping fixture. Also there is the forging force applied by the weld tool shoulder. The high temperature right below the weld tool shoulder can favor the atoms of the Mg and Al to diffuse into each other which is evident in Fig. 5-11.

Four different regions, two on the RS (Z1, Z2) and two on the AS (Z3, Z4) (refer Fig. 5-11(a)) were observed under SEM to measure the dimensions and chemical compositions of these IMCs layers. The IMCs on the RS faying surface (Fig. 5-11(b), 11(c)) were much thinner compared to IMCs formed on the AS faying surface (Fig. 5-11(d), 5-11(e)). Previous studies have indicated, the temperature on the AS of the weld is much higher than at the RS of the welds [26,28] and higher temperatures facilitate the formation of the IMCs in dissimilar welding. The layer of IMCs were composed of Al2Mg3 on the Al rich of the faying surface and Al12Mg17 on the Mg rich side of the faying surface. Similar to what was observed in stir zone IMCs, there is no visible separation between the two IMCs but they appear to be partially bonded to top Al and bottom Mg sheet.

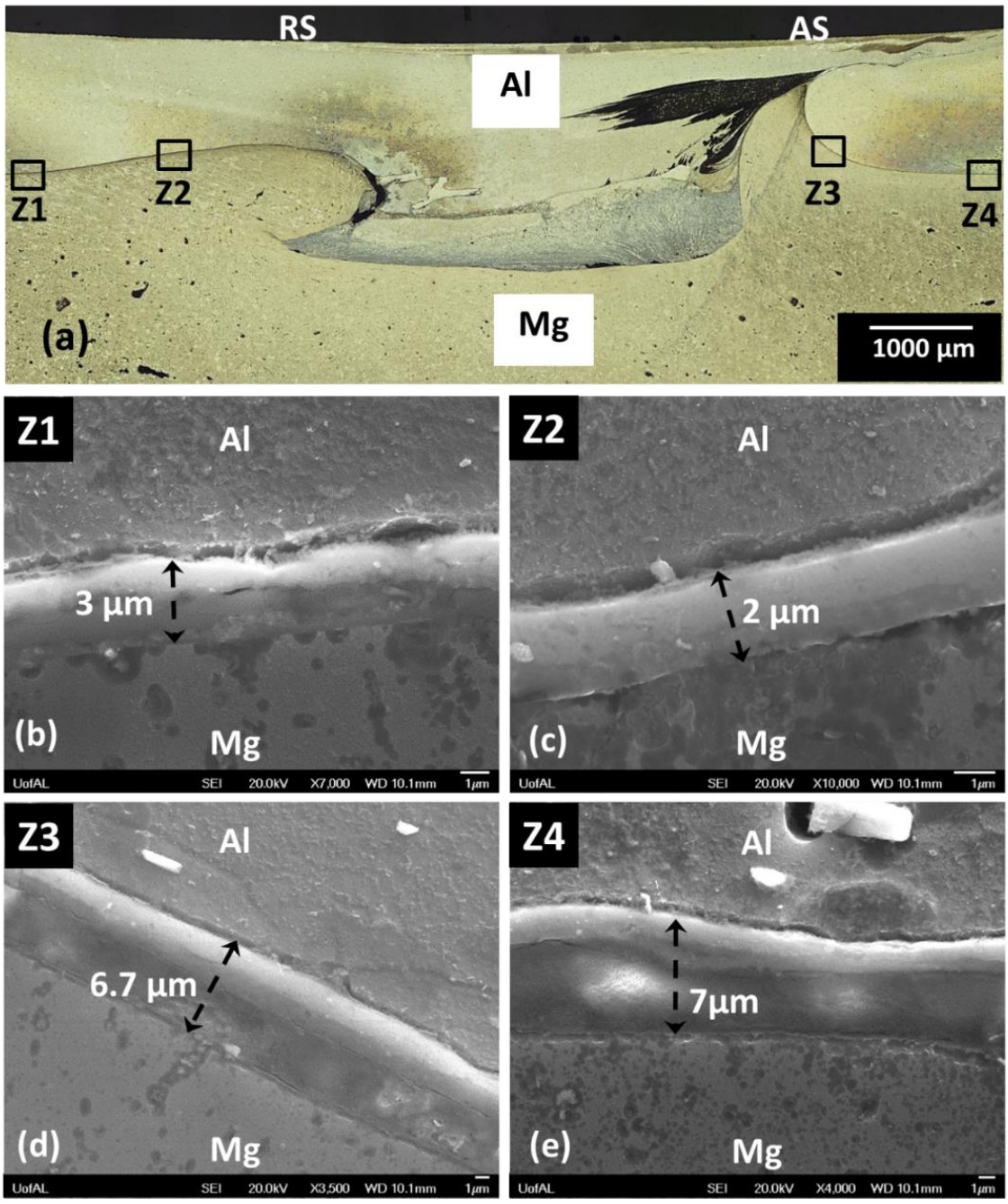

Figure 5-11: SEM images of the thin IMC layer at the faying surface (a) optical microscopic picture indicating the four different areas of interest (b) region Z1 on the RS fraying surface away from the weld nugget (c) region Z2 on the RS fraying surface close to the weld nugget (d) region Z3 on the AS fraying surface close to the weld nugget (e) region Z4 on the AS fraying surface away from the weld nugget.

5.3.2. Failure Mechanism

To understand the mechanism of failure in FSLW dissimilar alloys, the lap-shear test was video recorded. The failure modes in all the weld coupons in this current study were similar to each other, which was by nugget pullout. For a better understanding of the failure mechanism, it is divided into four different stages as shown in Fig. 5-12(a). The bold white arrows on the opposite ends of the weld coupons indicate the loading direction during the lap-shear test. Two kinds of crack were observed, a secondary crack (SC), which do not cause the failure and a dominant crack (DC) which cause the failure. In stage 1 during the early loading stage, the secondary crack (SC) propagates through the faying surface on the RS and terminates very close to the weld nugget. In stage 2, with the gradual increase of load, the dominant crack (DC) propagates though the faying surface on the AS and terminates at the base of the AS hook. It is clearly seen that the entire load is carried by the weld nugget. On further increase in load, the dominant crack propagates along the curved AS hook and through the weld nugget. The complete load is now carried by the small bonded region on the RS of the weld nugget as seen in stage 3. As the RS is the loading side of the weld coupon, further increase in load causes the weld nugget to fail completely due to shear overload as seen in stage 4. The analysis of the representative failed coupon shown in Fig. 5-12(b) indicates the DC grew on the AS faying surface along the thin IMC layer. A small chunk of IMC layer is still visibly adhered to the top of the Al sheet in Fig. 5-12(b). It appears that the DC traversed through the lower side of the weld nugget, at the interface between the Mg and IMC in the stir zone.

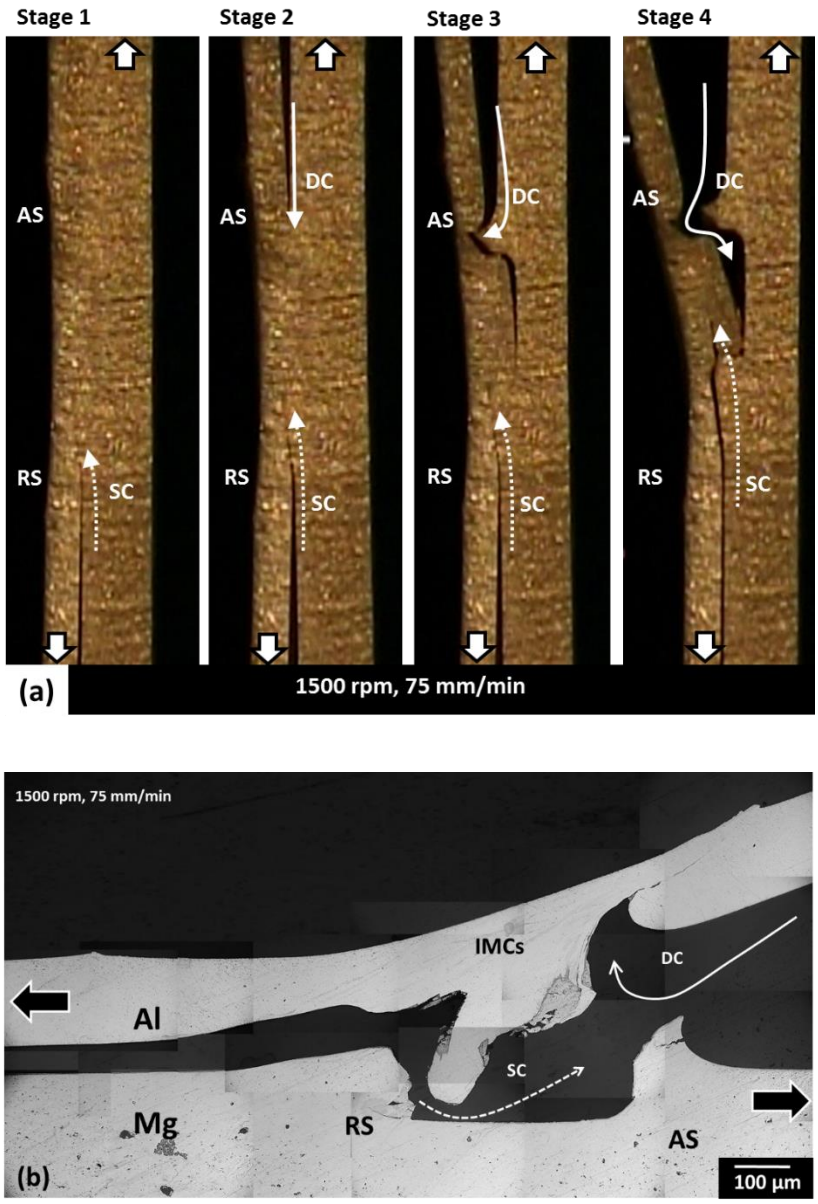

Figure 5-12: Failure analysis of the FSLW test coupon produced at 1500 rpm and 75 mm/min tool traverse speed (a) video grab of the lap-shear test of the dissimilar FSLW coupon indicating different stages of failure, the bold short arrows indicates the loading direction and the long thin arrows indicate the mode of crack propagation (b) cross section of a polished failed FSLW coupon.

The RS of the weld nugget in stage 3 and 4 appears to hold the two sheets together (Fig. 5-12(a)), where the DC faces resistance due to the suppressed RS cold lap feature. Once the load reached sufficiently large enough to break this bond, the DC grew along the cold lap feature and the top Al sheet pulled out of the weld nugget.

5.4. Conclusions

1. This study revealed that under the right tool rotation rate and tool travers speed, the dissimilar alloys of aluminum and magnesium can be joined effectively by friction stir linear welding.
2. The formation of IMCs $Al_{12}Mg_{17}$ and Al_2Mg_3 cannot be avoided in dissimilar welding. The frictional heat has a dominant role in formation of these IMCs in the stir zone of the weld nugget and along the faying surface.
3. The weld process condition has a significant effect on producing a sound and strong welds. Very low heat input either by low tool rotation rate or high tool traverse speed produces welds with poor performance. A very high tool rotation rate and slower traverse speed introduces a high frictional heat which produced channel defects and voids.
4. The thin layer of IMCs along the faying surface offers a partial bonding between the top aluminum and bottom magnesium sheet. But the major load bearing member of the weld is along the interface between the bottom magnesium sheet and the IMCs in the stir zone.
5. The dominant crack always grows from the ascending side of the weld and hence care must be taken to produce welds in a manner that the ascending side is not the loading side of the weld.

6. The retreating side of the weld, which has a suppressed cold lap feature, offers the maximum resistance to dominant crack. Hence welds should be produced in a manner the cold feature does not continue or terminate very close to ascending side hook in the weld.

5.5. Bibliography

[1] G.S. Cole, A.M. Sherman, Mater. Charact. (1995) 3.

[2] P. Thornton, A.R. Krause, R.G. Davies, Weld. J. 75 (1996) 101s.

[3] A. Gean, S.A. Westgate, J.C. Kucza, J.C. Ehrstrom, Weld. Journal- New York 78 (1999) 80s.

[4] W.Thomas, E.Nicholas, J. Needham, M.Murch, P. Templesmith, C.Dawes, Frcition Stir Butt Welding, G.B. Patent 9125978.8, 1991.

[5] C. Zhou, X. Yang, G. Luan, Scr. Mater. 53 (2005) 1187.

[6] M. Sutton, B. Yang, A.Reynolds, R. Taylor, Mater. Sci. Eng. A 323 (2002) 160.

[7] S.M. Chowdhury, D.L. Chen, S.D. Bhole, X. Cao, Mater. Sci. Eng. A 527 (2010) 6064.

[8] Q. Yang, X. Li, K. Chen, Y.J. Shi, Mater. Sci. Eng. A 528 (2011) 2463.

[9] W. Woo, H. Choo, M.B. Prime, Z. Feng, B. Clausen, Acta Mater. 56 (2008) 1701.

[10] N. Afrin, D.L.L. Chen, X. Cao, M. Jahazi, Mater. Sci. Eng. A 472 (2008) 179.

[11] L. Commin, M. Dumont, J.-E. Masse, L. Barrallier, Acta Mater. 57 (2009) 326.

[12] C.I. Chang, C.J. Lee, J.C. Huang, Scr. Mater. 51 (2004) 509.

[13] W. Xunhong, W. Kuaishe, Mater. Sci. Eng. A 431 (2006) 114.

[14] Y.C. Chen, K. Nakata, Scr. Mater. 58 (2008) 433.

[15] A. Kostka, R.. Coelho, J. dos Santos, A.. Pyzalla, Scr. Mater. 60 (2009) 953.

[16] N. Yamamoto, J. Liao, S. Watanabe, K. Nakata, Mater. Trans. 50 (2009) 2833.

[17] X.J. Cao, M. Jahazi, Mater. Sci. Forum 638-642 (2010) 3661.

[18] K. Kimapong, T. Watanabe, Mater. Trans. 46 (2005) 2211.

[19] Y.C. Chen, K. Nakata, Mater. Des. 30 (2009) 3913.

[20] S. Hirano, K. Okamoto, M. Doi, H. Okamura, M. Inagaki, Y. Aono, Q. J. Japan Weld. Soc. 21 (2003) 539.

[21] A. Gerlich, P. Su, T.H. North, G.J. Bendzsak, Mater. Forum, 2005, pp. 290–294.

[22] D.H. Choi, B.W. Ahn, C.Y. Lee, Y.M. Yeon, K. Song, S.-B. Jung, Intermetallics 19 (2011) 125.

[23] A. McLean, G.L.F. Powell, I.H. Brown, V.M. Linton, Sci. Technol. Weld. Join. 8 (2003) 462.

[24] Y.J. Kwon, I. Shigematsu, N. Saito, Mater. Lett. 62 (2008) 3827.

[25] V. Firouzdor, S. Kou, Metall. Mater. Trans. A 41 (2010) 3238.

[26] S. Kou, Weld. J. 88 (2009) 213.

[27] Y.S. Sato, S.H.C. Park, M. Michiuchi, H. Kokawa, Scr. Mater. 50 (2004) 1233.

[28] V. Firouzdor, S. Kou, Metall. Mater. Trans. A 41 (2010) 2914.

[29] T. DebRoy, H.K.D.H. Bhadeshia, Sci. Technol. Weld. Join. 15 (2010) 266.

[30] W. Yuan, B. Carlson, R. Verma, R. Szymanski, Sci. Technol. Weld. Join. 17 (2012) 375.

[31] M.K. Yadava, R.S. Mishra, Y.L. Chen, B. Carlson, G.J. Grant, Sci. Technol. Weld. Join. 15 (2010) 70.

[32] H.M.Rao, J.B.Jordon, M.E.Barkey, Y.B.Guo, X. Su, H. Badarinarayan, Mater. Sci. Eng. A 564 (2013) 369.

[33] W. Yuan, R.S. Mishra, S. Webb, Y.L. Chen, B. Carlson, D.R. Herling, G.J. Grant, J. Mater. Process. Technol. 211 (2011) 972.

[34] P. Su, A. Gerlich, T.H. North, G.J. Bendzsak, Sci. Technol. Weld. Join. 11 (2006) 163.

[35] H.S. Shin, Y.C. Jung, J.K. Lee, Met. Mater. Int. 18 (2012) 685.

[36] K.N. Solanki, J.B. Jordon, W. Whittington, H. Rao, C.R. Hubbard, Scr. Mater. 66 (2012) 797.

CHAPTER 6

FATIGUE TESTING AND FAILURE ANALYSIS OF FRICTION STIR LINEAR WELDING OF DISSIMILAR ALUMINUM 6022 TO MAGNESIUM AM60B

Abstract

The fatigue behavior and failure analysis of friction stir linear welded (FSLWed) aluminum 6022-T4 to cast magnesium AM60B in lap-shear configuration was examined. Two stitch welds were produced using a triangular tool pin profile at 1500 rpm tool rotation rate and 75 mm/min tool traverse speed. Next, two welded coupons one from each stitch welds were water jet cut for testing purposes. The two coupons cut from the respective stitch welds exhibited different weld structures. Three modes of failure were observed during the fatigue testing. In the first mode, mode A, the failure occurred when the dominant crack propagated through the bottom magnesium sheet. The second mode, mode B, failure was at the weld interface. In the last failure mode, mode C, the failure occurred when the dominant crack propagated through the top aluminum sheet. Fretting-like debris was found at the fatigue crack initiation sites for failure mode A and mode C. In failure mode B, the welds failed due to shear overload in the weld nugget which were marked by micro voids and channel defects. At higher applied fatigue loads, mode B was the dominant failure and at lower applied fatigue loads the failure modes were random with combinations of all three. Overall the fatigue data exhibited significant scatter in fatigue life and substantial relationship between the loading condition and failure modes were established.

6.1. Introduction

With ever increasing dependency on fossil fuels, escalating fuel prices and out of environmental concerns, efforts are being made to make the commercial cars/trucks more fuel efficient. Hence automotive industries around the globe are looking into lightweight materials for mass saving to improve the fuel efficiency of the cars, trucks and other automobiles. Light weight alloys based on magnesium and aluminum has found a favorable place to replace the existing heavy steel based alloys. Although, aluminum has been widely used, the use of magnesium in automotive industry is hindered by the fact that common welding techniques are not favorable for mass production methods [1–3]**.** Over the years, research studies have established the friction stir welding (FSW) technique as an efficient methodology to weld magnesium alloys. Most research on FSW has been relatively confined to joining of similar magnesium to magnesium alloys or aluminum to aluminum alloys. Previous studies have established the influence of welding process parameters on the micro and macro features of the weld and how these features effect the weld strength in a friction stir linear welded (FSLW) joint [4–14].

At times owing to design, geometric and economic constraints, two or more materials may be used in combination with each other. The major challenge in using the dissimilar materials in conjunction arises during the assembly and joining process. Applying heat and force during the welding process leads to the formation of brittle and structurally frail intermetallic compounds (IMCs). During the FSW of magnesium and aluminum alloys, constitutional liquation occurs in the weldment leading to formation of these IMCs ($Al_{12}Mg_{17}$, Al_3Mg_2) in the stir zone [15–24].

Most studies on FSW of dissimilar magnesium to aluminum have discussed the formation of IMCs and its effect on the static strength of the welds [16,18,21,22,25–28]. Typically, in-real world applications, these welded joints are subjected to fatigue loading and hence it's imperative to study the fatigue behavior of these dissimilar welded joints. In one of the few existing studies on the fatigue of dissimilar FSW joints, Chowdhury et al. [35] studied the fatigue life properties of friction stir spot welded (FSSW) dissimilar magnesium to aluminum. The fatigue life of FSSW dissimilar magnesium to aluminum was reported to be much lower compared to fatigue life of similar aluminum to aluminum and magnesium to magnesium. Two distinctive failure modes were observed in the dissimilar FSSW joints, nugget pull and keyhole failure. In FSSW of aluminum to magnesium with adhesive, the fatigue life of weld joints produced with magnesium stacked on top of aluminum was much higher compared to the fatigue life of welded joints produced with aluminum stacked on top of magnesium [36]. Very limited studies has been done on the fatigue behavior of dissimilar friction stir welded joints and are largely based on joining dissimilar aluminum to aluminum alloys [29–34]. However, to the best of the authors' knowledge, there are no other existing studies on the study of fatigue life properties of friction stir spot welded or friction stir linear welded on dissimilarly joined magnesium to aluminum alloys. Hence, an attempt has been made in this study to analyze the fatigue life properties of FSLW magnesium to aluminum alloy. As such, this is the first study to investigate the fatigue life properties and failure modes in FSLW of dissimilar Al 6022-T4 to Mg AM60B alloys. Factors and properties that directly influence the fatigue performance of FSLW lap-shear welds will be discussed in detail.

6.2. Materials and Experiment

A rolled AA6022-T4 aluminum alloy of 1.5 mm in thickness was FSLW to cast AM60B magnesium alloy of thickness 3.5 mm. The FSLW tool used to produce the lap-shear coupons for this study is shown in Fig. 6-1(a). The weld tool was made of standard tool steel (H13) and constituted a concave tool shoulder of a diameter 12 mm and a triangular pin with smooth surface with an equivalent triangle diameter of 5.4 mm and pin length of 2.4 mm. The aluminum sheet was stacked on top of the magnesium sheet in lap-shear configuration with an overlap area of 152.4 mm x 30 mm as shown in Fig. 6-1(b). Two stitch welds each measuring 65 mm in length were produced as shown in Fig. 6-1(b) and henceforth these welds will be addressed as weld #1 (W1) and weld #2 (W2) throughout this paper. The stitch welds were produced in one single step, that is, the tool after producing W1 would retract and traverse 15 mm in air and would plunge back into top aluminum sheet to produce W2. All the welds were produced at a tool rotation rate of 1500 rpm, tool traverse speed of 75 mm/min, tool shoulder plunge depth of 0.3 mm and the tool tilt angle was maintained at 2.5^0. The tool traversed from the right of the weld setup to the left as indicated by the bold arrows in Fig. 6-1(b), the dotted arrows around W1 and W2 indicate the tool rotation direction (counter clockwise). This was to ensure, the welds produced would have the advancing side (AS) at the free end of the coupon and retreating side (RS) was on the loading side of the coupon as shown in Fig. 6-1(b) and Fig. 6-1(c). Four weld test coupons, each measuring 30 mm in width were water-jet cut from W1 and W2 and only the lap-shear coupons without keyholes were studied in this research for fatigue properties.

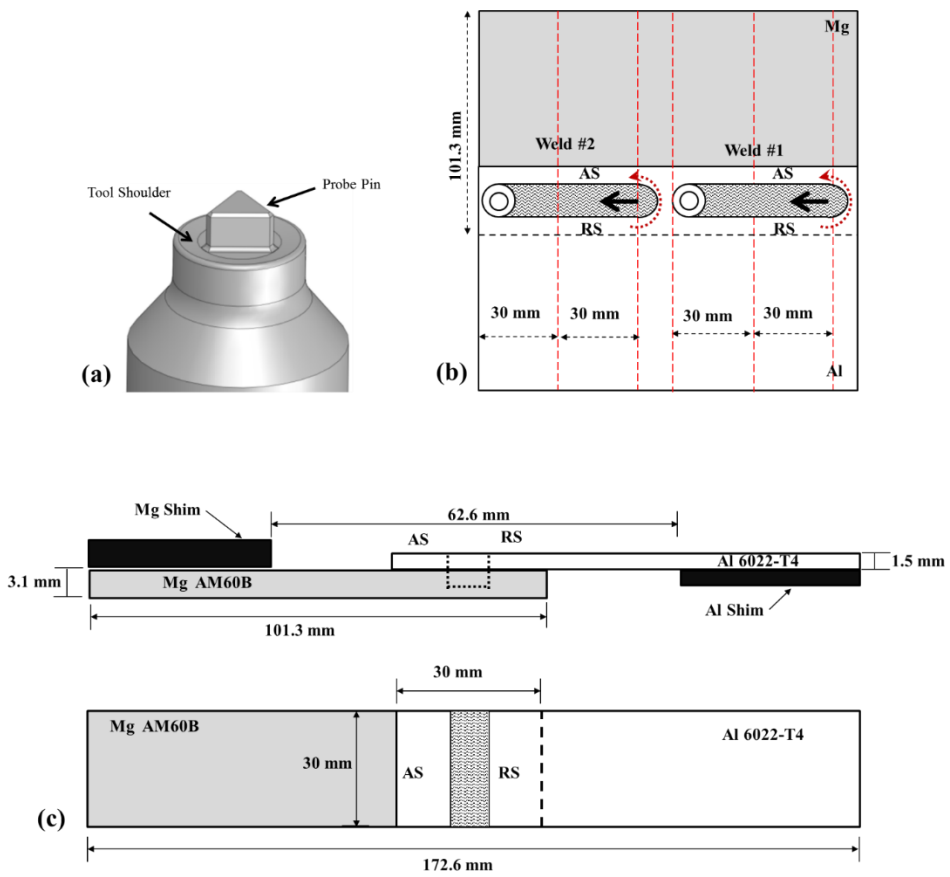

Figure 6-1: Representation of (a) FSLW tool profile (b) The FSLW methodology indicating the tool traverse direction, tool rotation direction and geometrical dimensions of the materials used (c) geometrical dimensions of the FSSW test coupon after water-jet cut.

The final dimensions of the lap-shear test coupons is shown in Fig. 6-1(c). Since these welds were to be a part of the shock tower assembly, which would be subjected to paint job and baking, the lap-shear test coupons were baked in a forced convection oven at 180^0 C for 30 minutes. For fatigue tests, the lap-shear were cyclically tested on a MTS 810 servo-hydraulic load frame under load control with a sinusoidal wave front. The lap-shear coupons were all tested at load ratio of 0.1 and below maximum tensile strength of the lap-shear coupons which is about 3500 N. The load range tested for both weld W1 and W2 was between a maximum of 3150 N

(90% of 3500 N) and minimum of 1155 N (33% of 3500 N). The fatigue tests were conducted at a frequency of 20Hz and magnesium and aluminum shims were employed on the lap-shear coupons during the testing (refer Fig. 1(c)) to avoid bending moments and additional loads. The grip to grip distance was maintained at 62.6 mm for each lap-shear coupon.

For weld characterization, samples were sectioned through the center of the nugget and parallel to loading direction. The samples were cold mounted in epoxy and were mechanically ground and fine polished using 0.05 µm aluminum oxide (alumina). Since two different materials were polished simultaneously, only de-ionized water was used through the polishing steps. In order to reveal the microstructure and IMCs, AM60B was etched using an acetic glycol solution (20 ml acetic acid, 1 ml HNO_3, 20 ml H2O, and 60ml ethylene glycol) and the AA6022-T4 was etched with 20% NaOH solution (caustic etching). The microstructures of welds were analyzed using Keyence VHX-1000 digital optical microscope. Typical optical micrographs of the stir zone, thermomechanically affected zone (TMAZ), heat-affected zone (HAZ) and base metal were obtained. Microhardness measurements of representative lap-shear coupons from W1 and W2 were performed on Wilson hardness testing machine. A load of 100 g and dwell time of 5 s were employed to measure the Vickers hardness (HV). Hardness measurements was recorded for top aluminum and bottom magnesium sheet starting from base metal on end and traversing towards to the base material on the other end. A total of 55 indents in each sheet was measured at a distance of approximately 0.5 mm from each other.

Representative fatigued lap-shear coupons from W1 and W2 were also observed under Keyence microscope to identify failure modes and fracture surface. In addition, fracture surface of fatigue tested lap-shear coupons were examined under Jeol 7000 scanning electron microscope

(SEM) to investigate the fracture surface, crack propagation and chemical analysis using energy-dispersive X-ray spectroscopy (EDX).

6.3. Results

6.3.1. Geometrical features of W1 & W2

The as welded lap-shear coupons were observed under digital optical microscope to study the key geometrical features of the weld. The faying surface in a FSW in the weld nugget normally forms a curve like geometric feature which appears like a 'hook'. For convenience, these hooks on retreating side (RS) will be addressed as RS hook and the hook on advancing side (AS) will be addressed as AS hook. Along with the RS and AS hook, weld bond width forms the key macro weld features in FSLW lap-shear coupons. These macro features affect the load bearing capacity of the weld and influence the crack initiation and propagation [5,37]. The cross section of the untested welds W1 and W2 revealed a considerable difference in the weld macro features. Table 6-1 provides a cross section view of the two welds W1 and W2 and summarizes geometrical dimensions of key macro weld features. The RS effective sheet thickness which is the distance between the apex of the RS hook to nearest free surface in top aluminum sheet, H1 was larger in W1 compared to W2. The AS effective sheet thickness or the distance between the apex of the AS hook to nearest free surface on top aluminum sheet, H2 was also much larger for W1 compared to W2. The weld bond width, the distance between the two hooks was much larger for W2. The RS and AS hook in W1 appeared to be more flat, while the RS and AS hook in W2 were more pronounced. The AS hook in W1 appears more flat and terminates in the weld nugget, while the AS hook in W2 has a distinct geometry, it is more curved and terminates away from the weld nugget pointing backwards away from the weld nugget and top free surface.

Table 6-1: Summary of geometrical dimension of FSLW features of W1 and W2

Weld Type	Dimensions (mm)		
	H1	**H2**	**BW**
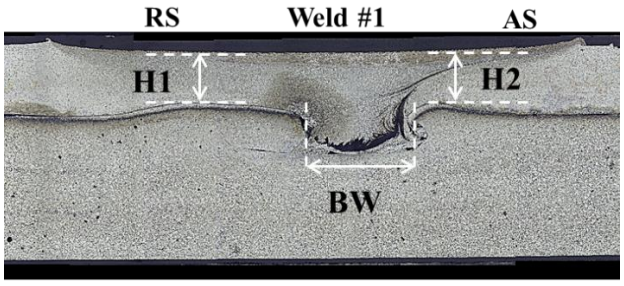	11.01	10.25	3.28
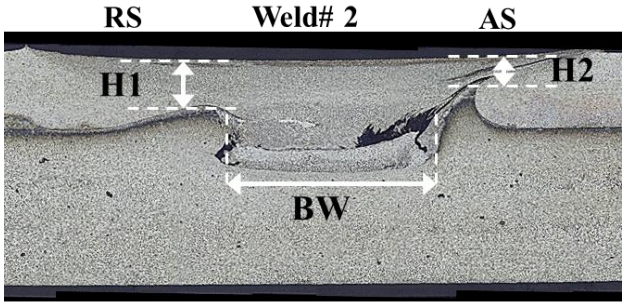	10.03	4.50	4.52

6.3.2. Microstructure and Microhardness profile

Regarding the microstructure zones, the stir zone (SZ), thermomechanically affected zone (TMAZ) and heat affected zone (HAZ) were identified in both W1 & W2. Both the top aluminum and the bottom magnesium sheets exhibited all the three microstructural zones. For brevity, only microstructure zones which are of importance with regards to this current study will be discussed. The microstructure features of the various regions of interest in the top aluminum and bottom magnesium sheet of W1 and W2 are shown in Fig. 6-2 and Fig. 6-3 respectively. The cross sections

of the untested W1 and W2 shown in Figure 6-2(d) and Fig. 6-3(d) has several rectangular boxes indicating different regions interest. In Fig. 6-2(a) and Fig. 6-3(a), the dotted line indicates the sharp transition of the SZ to TMAZ on the RS of the weld W1 and W2 respectively. A clear distinction between the fine grains of SZ and large recrystallized grains of TMAZ is clearly visible in both W1 and W2. The SZ is characterized by finer grains due to dynamically recrystallization as shown in Fig. 6-2(b) for W1 and Fig. 6-3(b) for W2. On the AS of the weld, the SZ transforms to TMAZ along the black dotted lines shown in Fig. 6-2(c) and Fig. 6-3(c) for W1 and W2 respectively. The bottom magnesium sheet had little change in microstructure. Since the tool plunge depth is 0.3 mm, only a small portion of the magnesium surface was under the weld tool resulting in a minor change in microstructure. Figure 6-2(e) and Fig. 6-3(e) shows the small microstructural regions of the magnesium in W1 and W2 respectively. Unlike in aluminum sheet, the magnesium has smaller SZ and TMAZ characterized by recrystallized grains.

The microhardness data recorded on W1 and W2 are plotted in Fig 6-4 for aluminum and magnesium sheets. Figure 6-4(a) shows the plot comparing the Vickers hardness of the top aluminum sheet in W1 and W2. Only a small amount of variation in hardness was observed, as this reflects the observations made in the microstructure analysis earlier which showed no significant difference in grain size.

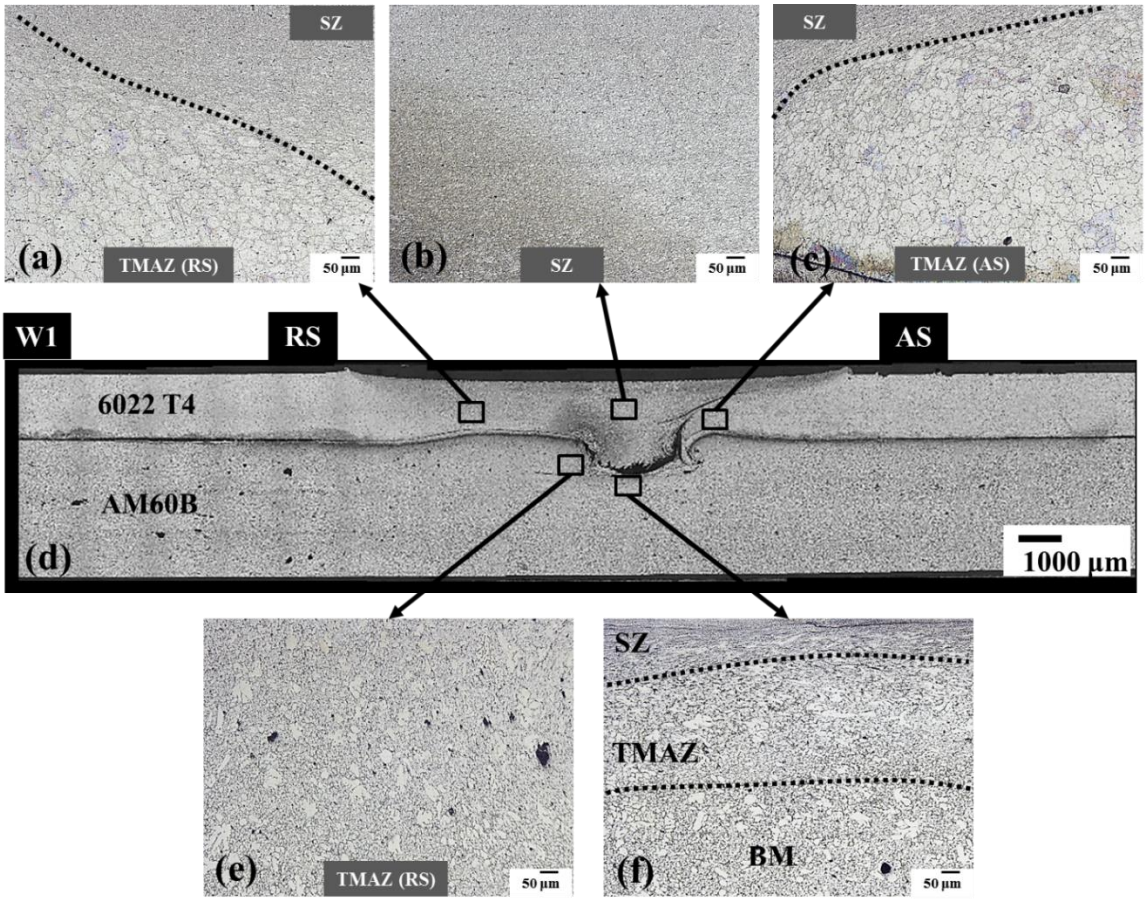

Figure 6-2: Microstructure of various regions in weld#1 (a) transition of SZ to TMAZ on RS of weld in aluminum sheet (b) SZ in the aluminum sheet (c) transition of SZ to TMAZ on AS of weld in aluminum sheet (d) cross section view of the untested weld#1 representative (e) TMAZ in the magnesium sheet (f) SZ, TMAZ and BM region in magnesium sheet.

It appears the only difference in W1 and W2 is the slightly larger SZ size of W2 compared to Z of W1. The SZ in the weld nugget which constituted fine recrystallized grains had a hardness value of about 80 HV in both W1 and W2. The TMAZ in aluminum sheet of W1 and W2 was the softest part of the weld with average hardness value ranging to about 60 HV. The hardness measurement comparison of bottom magnesium sheet in W1 and W2 is plotted in Fig. 6-4(b).

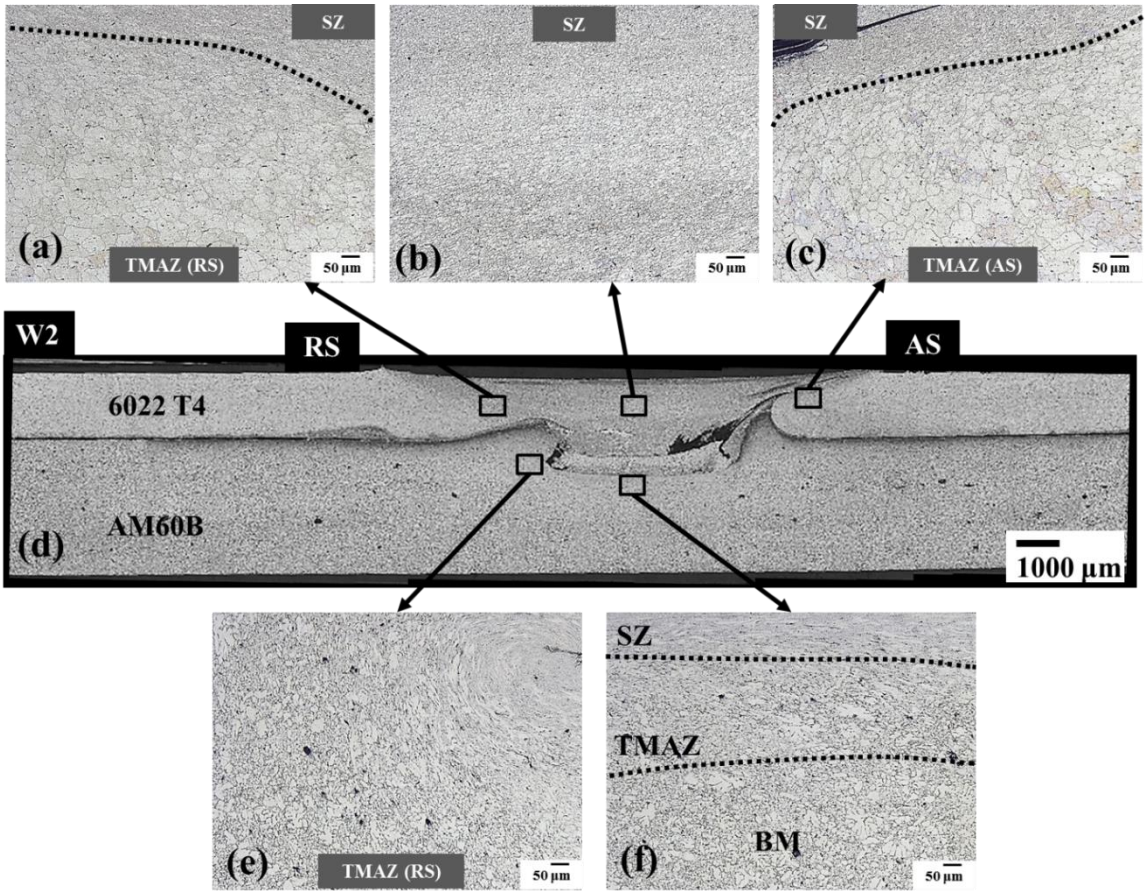

Figure 6-3: Microstructure of various regions in weld#2 (a) transition of SZ to TMAZ on RS of weld in aluminum sheet (b) SZ in the aluminum sheet (c) transition of SZ to TMAZ on AS of weld in aluminum sheet (d) cross section view of the untested weld#2 representative (e) TMAZ in the magnesium sheet (f) SZ, TMAZ and BM region in magnesium sheet.

The results indicate the SZ of W1 is marginally harder than the SZ of W2 at about 75 HV and 70 HV, respectively. The hardness value dropped to about 60HV in TMAZ for both W1 and W2 and leveled out at just above 65 HV in BM. The hardness gradient between the BM and SZ did not significantly varying indicating the bottom magnesium sheet experienced minimal thermal affect.

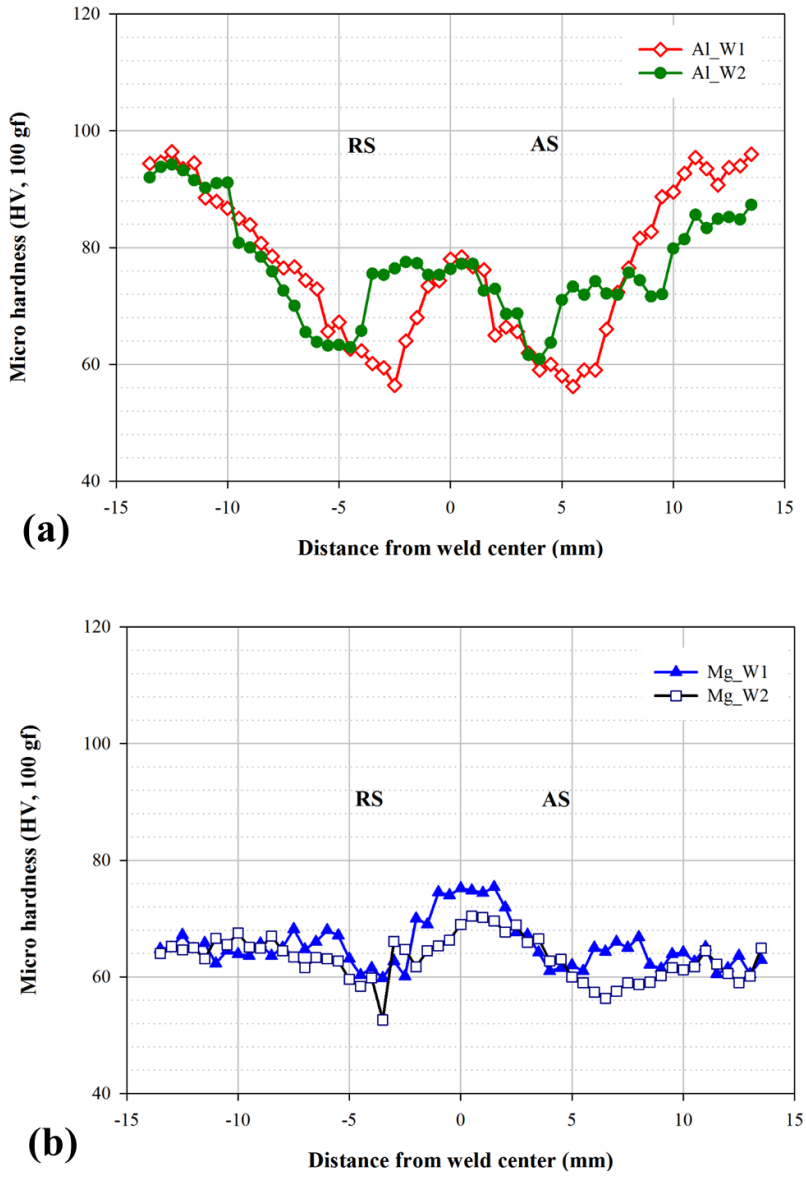

Figure 6-4: Microhardness profile across the friction stir welded specimens comparing hardness values of (a) top aluminum sheets of W1 and W2 (b) bottom magnesium sheets of W1 and W2.

6.3.3. Intermetallic compound (IMCs) on faying surface

Observation of the lap-shear weld coupons, W1 and W2 under scanning electron microscopy (SEM) revealed a thin layer of material formed in-between the top aluminum and

bottom magnesium sheet all along the faying surface. Shown in Fig. 6-5(a) is the cross section of the weld W1 and the square boxes indicate the regions R1, R2, R3 and R4, where chemical characterization using the energy-dispersive X-ray spectroscopy (EDS) was performed. For brevity sake, the exact weight % of each element will not be provided for this analysis. Chemical characterization of the material layer in region R1, R2, R3 and R4 using EDS indicated the material are composed of a sandwich layer of Al_3Mg_2 close to aluminum sheet and $Al_{12}Mg_{17}$ near to the magnesium sheet. Previous studies have indicated and explained the formation of inter metallic compounds (IMCs), Al_3Mg_2 and $Al_{12}Mg_{17}$ in dissimilar welding of aluminum and magnesium [16,24,25,36,38]. The IMCs layer in region R1 which is close to where the faying surface flattens out on RS of the W1 measured about 3 μm in thickness as seen in Fig. 6-5(b). Further moving towards the hook part on the RS of W1, region R2, the IMCs layer measured about 2 μm in thickness as seen in Fig.6-5(c). On the AS of the W1, in region R3, the IMCs layer measured about 5.2 μm in thickness as seen in Fig. 6-5(d) and in region R4, the thickness of IMCs layer measure about 5.5 μm as seen in Fig. 6-5(e). The weld W2 had a similar layer formed along the faying surface. Figure 6-6(a) shows the cross section of the untested W2 and the rectangular boxes indicating the regions S1, S2, S3 and S4 where the EDS was performed.

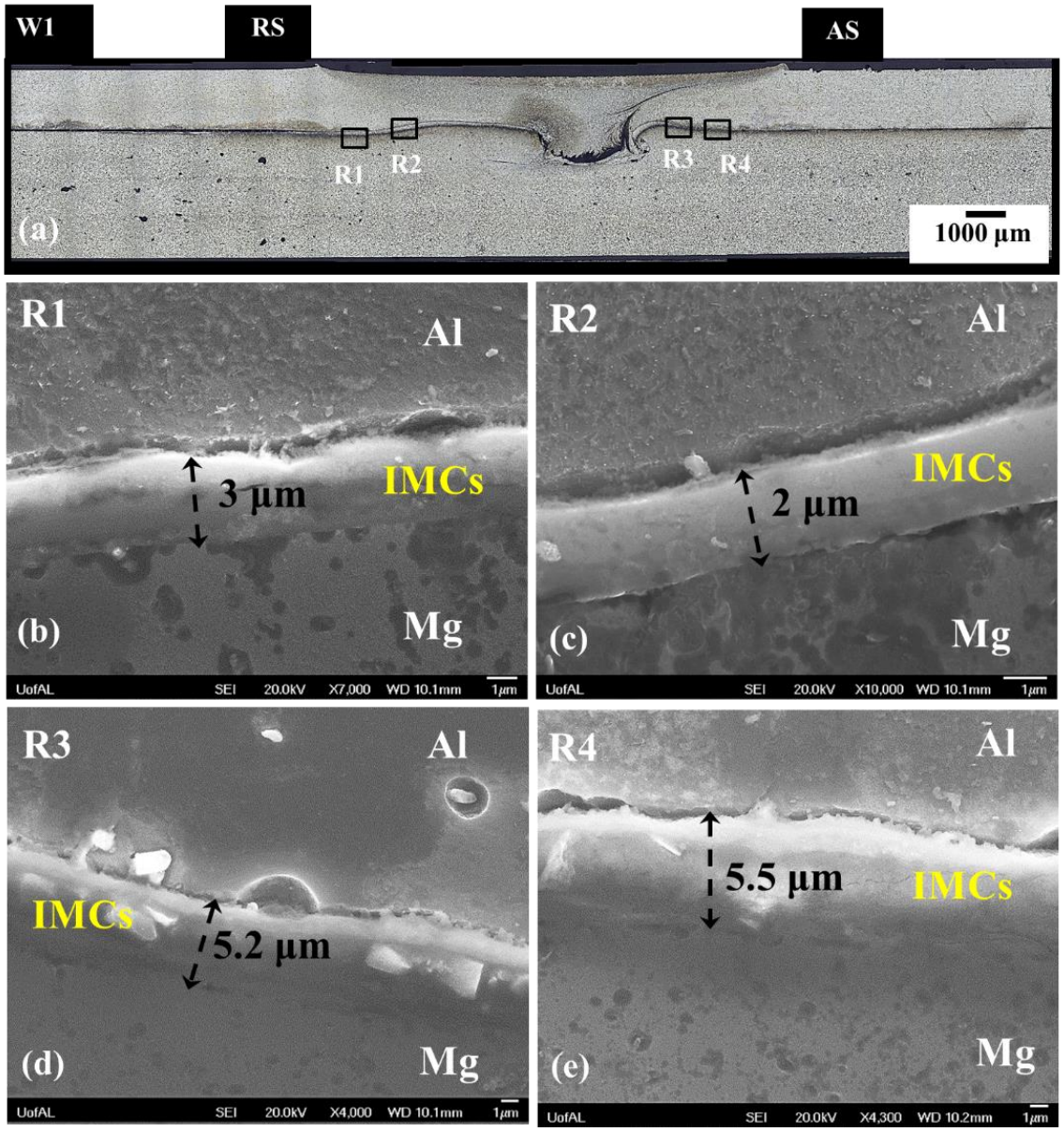

Figure 6-5: SEM images of the IMCs on the faying surface in W1 (a) representative cross section of untested W1 indicating regions of interest (b) region R1 on the RS (c) region R2 on the RS (d) region R3 on the AS and (e) region R4 on the AS of W1.

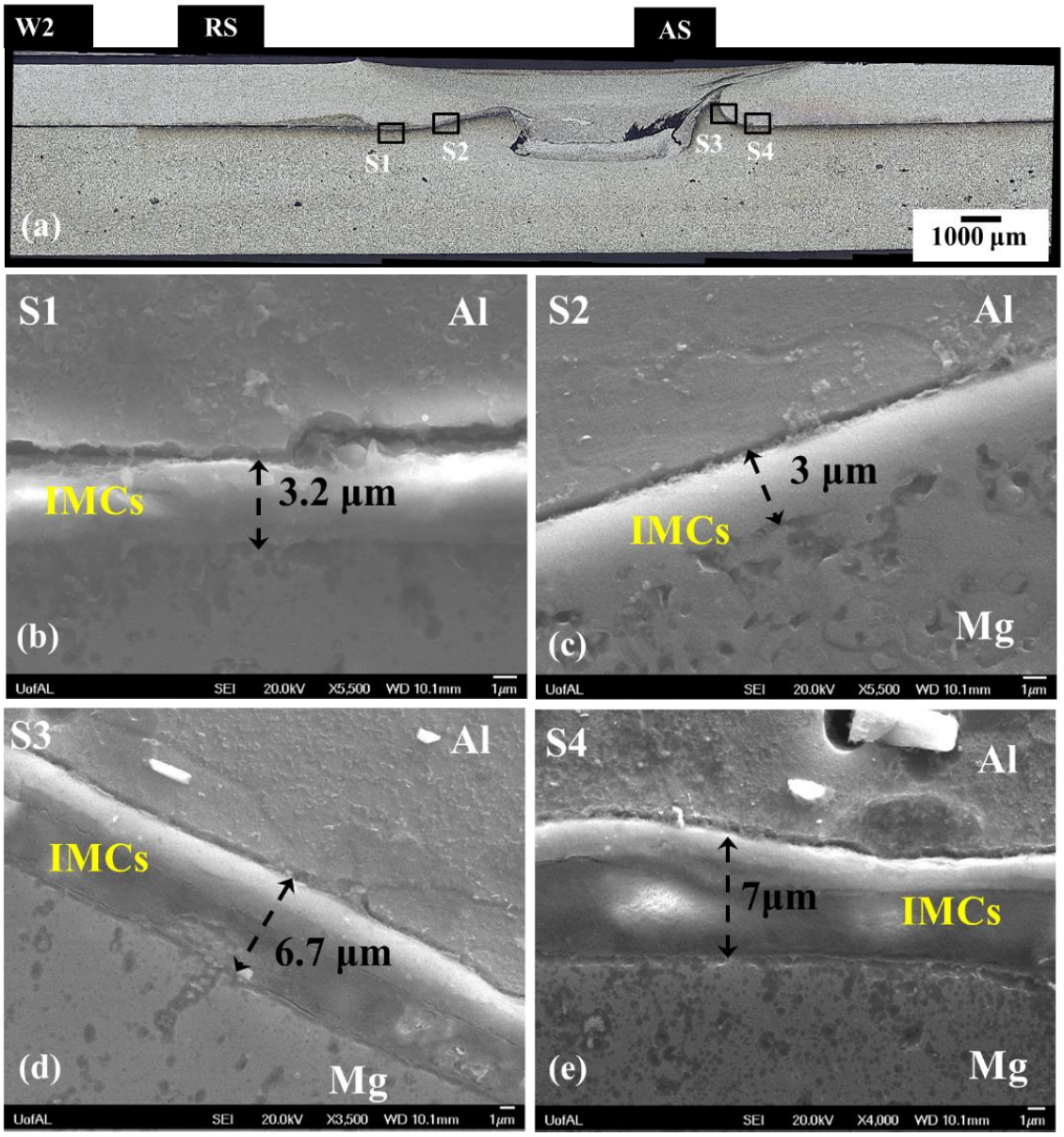

Figure 6-6: SEM images of the IMCs on the faying surface in W2 (a) representative cross section of untested W2 indicating regions of interest (b) region R1 on the RS (c) region R2 on the RS (d) region R3 on the AS and (e) region R4 on the AS of W2.

Region S1 on the RS of W2 in Fig. 6-6(b) shows the IMCs layer of about 3.2 µm in thickness. The thickness of the IMCs layer in region S2 on the RS of W2 measured about 3 µm in thickness as

seen in Fig. 6-6(c). The thickness of the IMCs layer on the AS of W2 in regions S3 and S4 respectively measured about 6.7 μm and 7 μm as seen in Fig. 6-6(d) and Fig. 6-6(e).

6.3.4. Fatigue testing

The fatigue results for lap-shear testing of weld W1 and W2 is shown in Fig. 6-7(a) and the Fig. 6-7(b) shows the various failure modes relative to the overall test results. In general, the results of the lap-shear fatigue tests indicate a wide scatter in fatigue life and no relationship between the fatigue life properties of welds W1 and W2 were obtained. Lap-shear welds tested below the load level of 1300 N exhibited good fatigue life properties and lap-shear weld tested beyond 2000 N showed a wide scatter in fatigue life. Comparison of fatigue life between the welds tested at same load level shows a huge disparity and is more apparent for welds tested at higher loads. At low applied fatigue loads, the lap-shear welds failed in all the three modes and at higher applied fatigue loads, mode B was the dominant failure mode. These results also provided no strong evidence as to which weld (W1 or W2) exhibited better fatigue life properties.

6.3.5. Failure modes

During the fatigue testing of the dissimilar FSLW of aluminum and magnesium, the lap-shear welds failed in three different modes. Table 6-2 summarizes the three different failure modes and a pictorial illustration for each failure mode is also provided. In mode A, the dominant crack initiated at the faying surface on the AS of the weld and propagated downwards through the magnesium sheet. In mode B, the dominant crack propagated through the weld nugget and the welds failed due to interfacial failure. In mode C, the dominant crack initiated at the faying surface on the RS of the weld and propagated through the top aluminum sheet.

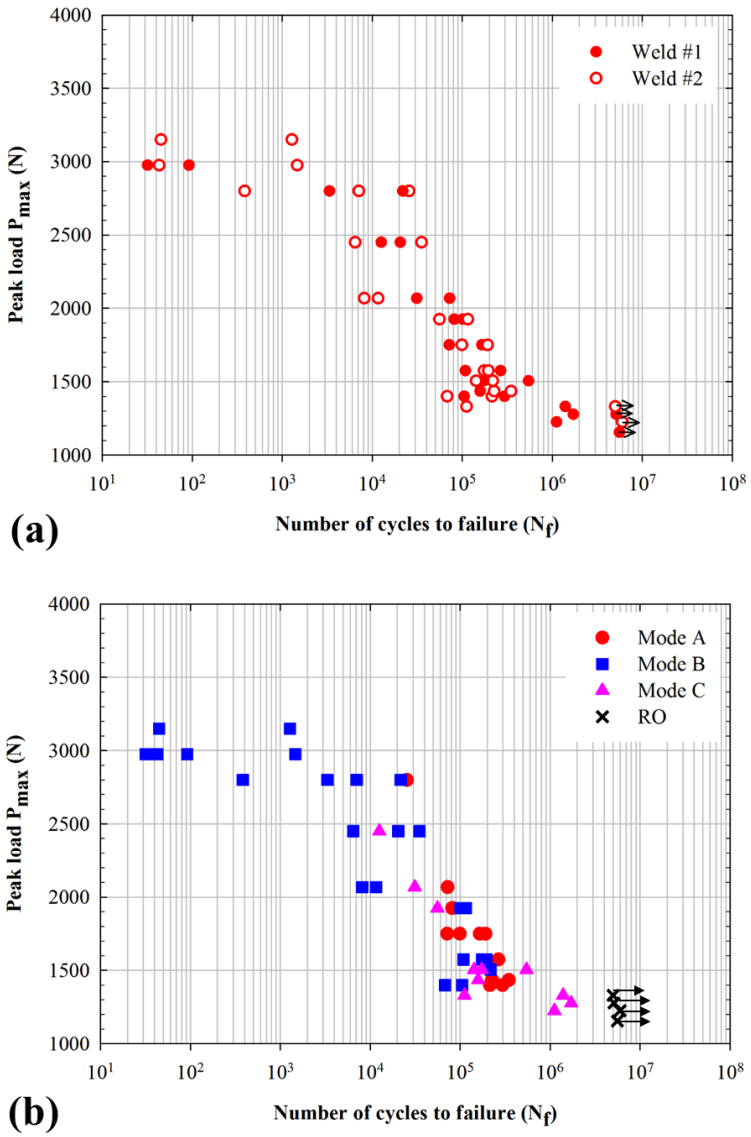

Figure 6-7: Experimental results of the fatigue test data (a) comparison of fatigue life of weld#1 and weld#2 (b) fatigue data plot indicating modes of failure.

Table 6-2 also provides information on the total number of welded coupons that failed under each mode and the breakdown of the type of weld. Of the 48 lap-shear welds tested in this study, 13 failed in mode A, 23 in mode B and 12 in mode C. The breakup also indicates in mode A, that

weld type W1 and W2 failed approximately in equal numbers and in mode B, weld type W2 failed in highest number and in mode C, weld type W1 failed in larger numbers.

Table 6-2: Summary of failure modes

Modes	Pictorial description	Weld type	No. of coupons that failed	Total
A	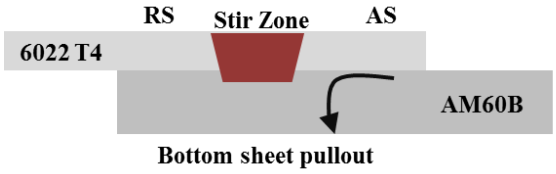	W1	7	13
		W2	6	
B	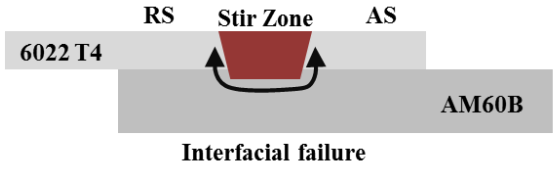	W1	8	23
		W2	15	
C	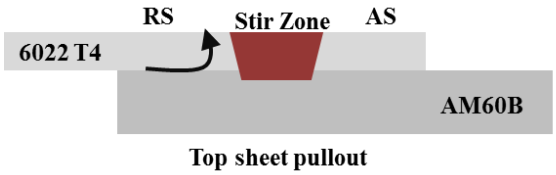	W1	9	12
		W2	3	

To further verify if there is any correlation between the weld structures of W1 and W2 to the failure modes, macrographs of the representative lap-shear welds subjected to fatigue tests from W1 and W2 were investigated. The cross-section view of the representative weld failed in mode A is shown in figure 6-8. The bold arrows on the top and bottom corners in Fig. 6-8(a) and Fig.6- 8(b) indicates

the loading direction. The dotted arrow indicates the direction of crack propagation in AS of weld through the magnesium sheet of W1 and W2. The rectangular dotted box around the crack indicates the region that has been magnified and shown in Fig. 6-8(c) and Fig. 6-8(d) for respective welds. From Fig. 6-8(a) and Fig. 6-8(b), it is clear, there are no secondary cracks in the weldment. The weld nugget is visibly intact and the only crack that is evident from the figures is the dominant crack in magnesium sheet. The etched macrographs of the region A1 in Fig. 6-8(c) indicate the dominant crack initiated and propagated away from the weld nugget in the TMAZ on the AS of W1. Similarly for W2, the crack propagated in the TMAZ on the AS of W2, away from the weld nugget. The magnified region A2 in Fig. 6-8(d) indicates the crack propagated just before the faying surface forms hook like geometry.

The failure in mode B was due to interfacial shear overload, the top aluminum sheet pulled out of the weld nugget as seen in Fig. 6-9(a) for W1 and in Fig. 6-9(b) for W2. The macrographs of W1 indicate a secondary crack which became non-dominant on the RS of the weld. In W2, there was no evidence of secondary cracks in the weldment. The magnified region B1 shown in Fig. 6-9(c) and region B2 shown in Fig. 6-9(d) indicates that the dominant crack propagated through the weld nugget. However, it is not clear if the crack propagated from RS of the weld to the AS of the weld or vice versa.

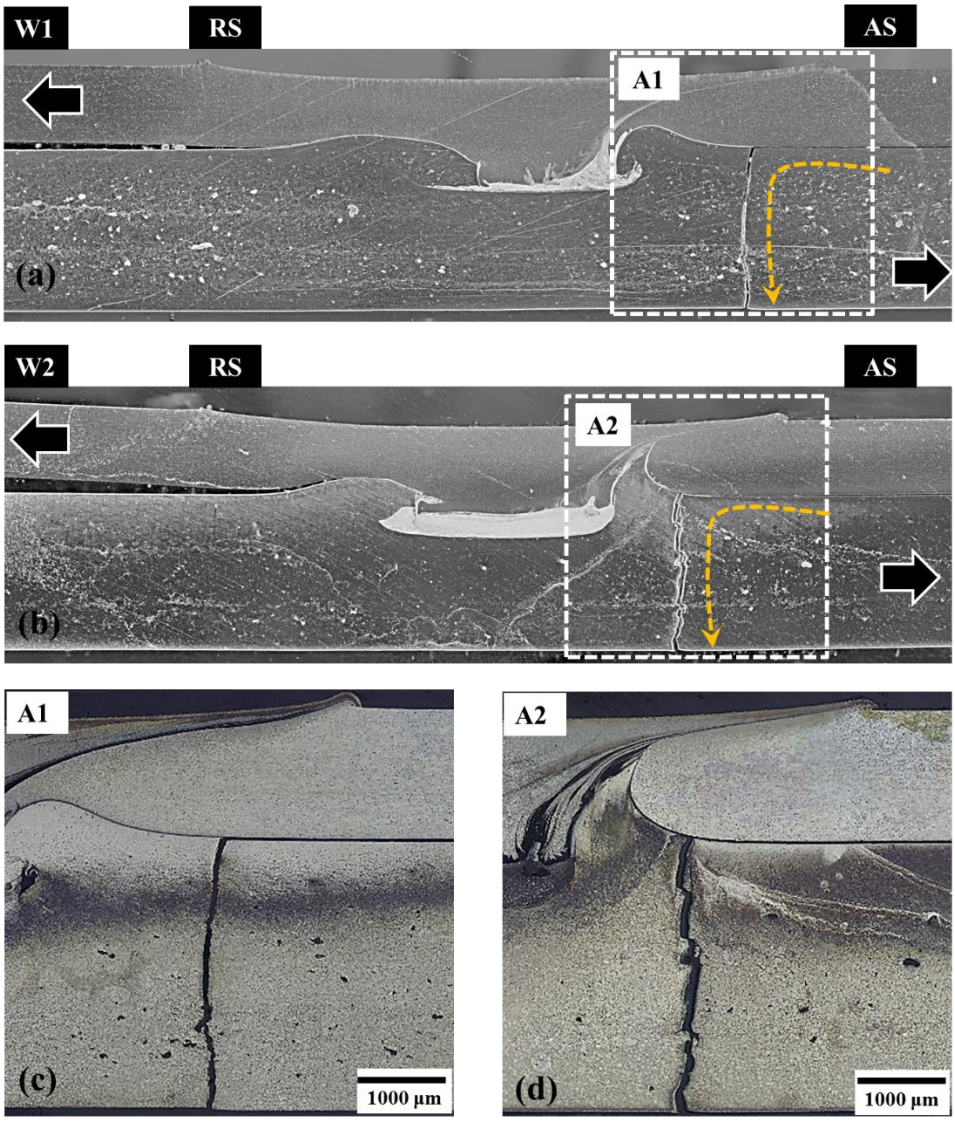

Figure 6-8: Failure mechanism in FSLW failed in mode A (a) overview of a representative W1 coupon indicating the region of crack propagation (b) overview of a representative W2 coupon indicating the region of crack propagation (c) magnified view of the region A1 indicating crack propagation region in W1 (d) magnified view of the region A2 indicating crack propagation region in W2. Bold arrows in (a) and (b) indicate the loading direction and dotted arrows in (a) and (b) indicate the crack propagation direction.

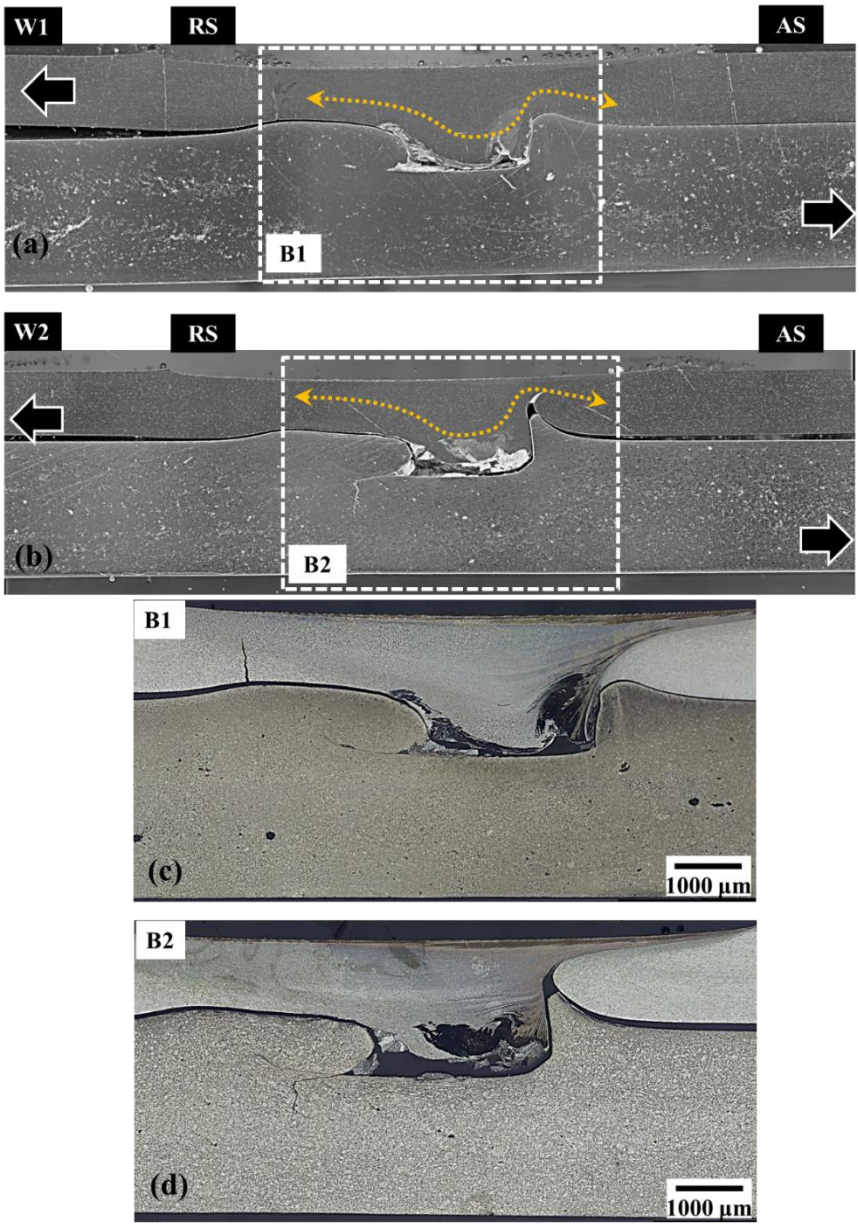

Figure 6-9: Failure mechanism in FSLW failed in mode B (a) overview of a representative W1 coupon indicating the region of failure (b) overview of a representative W2 coupon indicating the region of failure (c) magnified view of the region B1 indicating crack propagation region in W1 (d) magnified view of the region B2 indicating crack propagation region in W2. Bold arrows in (a) and (b) indicate the loading direction and dotted arrows in (a) and (b) indicate the crack propagation direction.

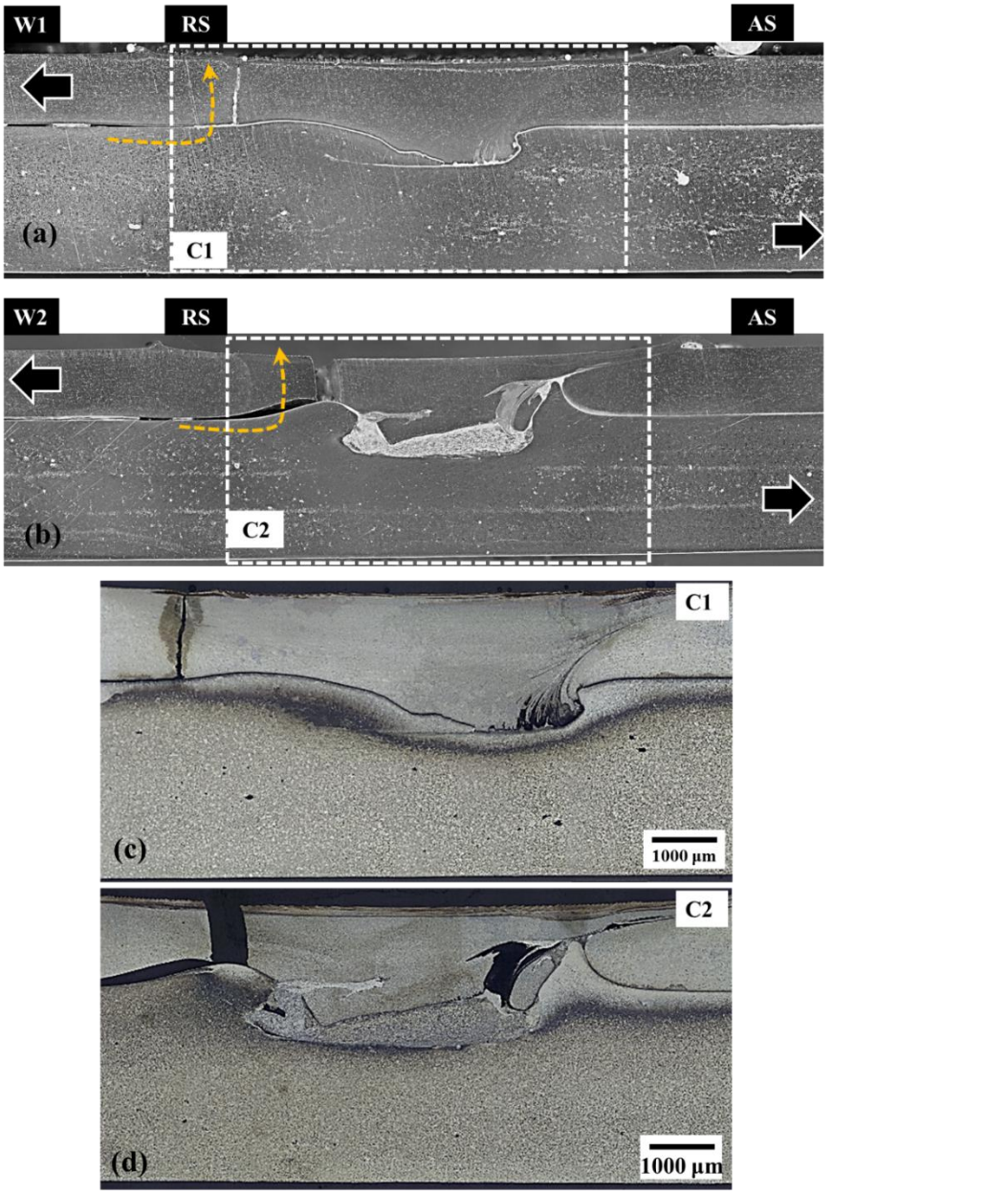

Figure 6-10: Failure mechanism in FSLW failed in mode C (a) overview of a representative W1 coupon indicating the region of crack propagation (b) overview of a representative W2 coupon indicating the region of crack propagation (c) magnified view of the region C1 indicating crack propagation region in W1 (d) magnified view of the region C2 indicating crack propagation region in W2. Bold arrows in (a) and (b) indicate the loading direction and dotted arrows in (a) and (b) indicate the crack propagation direction.

In mode C, the dominant crack initiated on the RS of the weld in both W1 and W2 as seen in Fig. 6-10(a) and Fig. 6-10(b). Further examination of the magnified region C1 in W1 indicates that the crack initiated in the TMAZ on the RS of the weld as seen in Fig. 6-10(c) and propagated upwards in the aluminum sheet. The crack propagation in W2 was similar to W1 and is evident from Fig. 6-10(d). In both welds W1 and W2, no secondary crack were visible and the weld nugget remained intact after the failure.

6.3.6. Fractography analysis

To acquire a better understanding of the failure modes and root cause of failure, representative lap-shear welds from each failure mode were investigated under SEM. Since the mode of failure in weld W1 and W2 were no different from each other, only one representative weld from each failure mode was analyzed. For mode A, the fracture surface on magnesium sheet that remained intact in the weld nugget after the failure was analyzed. For mode B, the fracture surface of the weld nugget on magnesium and aluminum sheet were analyzed. The fracture surface of the aluminum sheet in mode C, which remained intact to the weld nugget after failure was analyzed.

The macrograph in Fig. 6-11(a) shows the fracture surface on the bottom magnesium sheet. Fretting-like debris was observed at certain regions along the faying surface, where it appears that the fatigue crack propagated from these regions downwards to about half the thickness of the sheet. This resulted in a reduced loading baring area of the magnesium sheet and resulted in magnesium sheet peeling off from the remaining weldment. Closer observation of the fretting region in Fig. 6-11(b) indicates there different regions, region 1 which is near to the faying surface, region 2 in the cyclic loading region and region 3 in the fast fracture region. The magnified region 1 in Fig. 6-

11(c) shows the presence of crack initiation region which appears to be due to fretting of the faying surfaces. The region 2 in Fig. 6-11(d) shows the crack propagation region, where arrows point towards the fatigue striation indicating the crack growth direction. The magnesium AM60B sheet used in this study was cast and hence casting pore/voids were evident towards the bottom side of the magnesium sheet as seen in Fig. 6-11(e). The underside of the aluminum sheet facing the faying surface exhibited a large area of fretting-like debris intact as seen in Fig. 6-11(f). The EDS analysis of the regions R1 and R2 (Fig. 6-11(g)) which are on the thin layer of fretting debris indicated the presence of IMCs, Al_3Mg_2 + oxide and $Al_{12}Mg_{17}$. The chemical composition and weight % of the IMCs identified has been summarized in table 6-3.

Table 6-3: Composition (weight %) measured using EDS at various locations in the fretting region

Region	Phase	Mg (Wt. %)	Al (Wt. %)	O (Wt. %)	Total
R1	Al_3Mg_2 + oxide	29.5	57.0	13.5	100.0
R2	$Al_{12}Mg_{17}$	71.8	20.6	7.6	100.0
R3	$Al_{12}Mg_{17}$	54.0	43.6	2.3	100.0
R4	Al_3Mg_2 + oxide	37.4	40.1	22.5	100.0

The weld nugget region in the top aluminum and bottom magnesium sheet were observed for lap-shear welds that failed in mode B. Figure 6-12(a) shows the macro pictures of weld nugget on aluminum and magnesium sheet, the bold arrows around the weld nugget indicate the fretting areas.

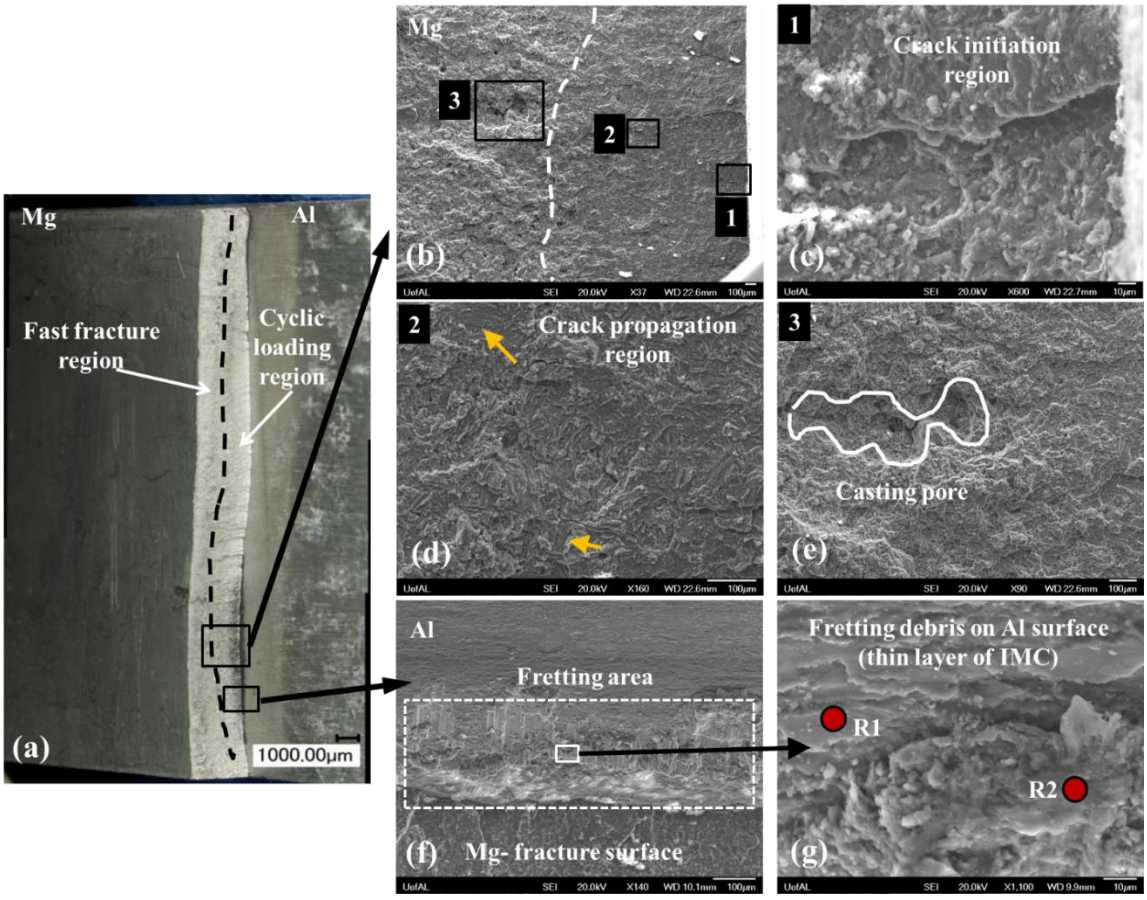

Figure 6-11: Fracture surface analysis of a representative weld failed in mode A (a) macro graph of the magnesium fracture surface (b) overview of a small region on fracture surface indicating regions 1, 2 and 3 which are of interest (c) magnified region 1 showing the crack initiation region close to faying surface (d) magnified region 2 on the fracture surface, arrows indicate the crack propagation region (e) magnified region 3 on the fast fracture region showing the casting pores in magnesium (f) overview of the fretting region on the aluminum surface close to crack initiation point (f) magnified view of the fretting debris on the aluminum surface and dotted R1 and R2 indicate the EDX analysis region.

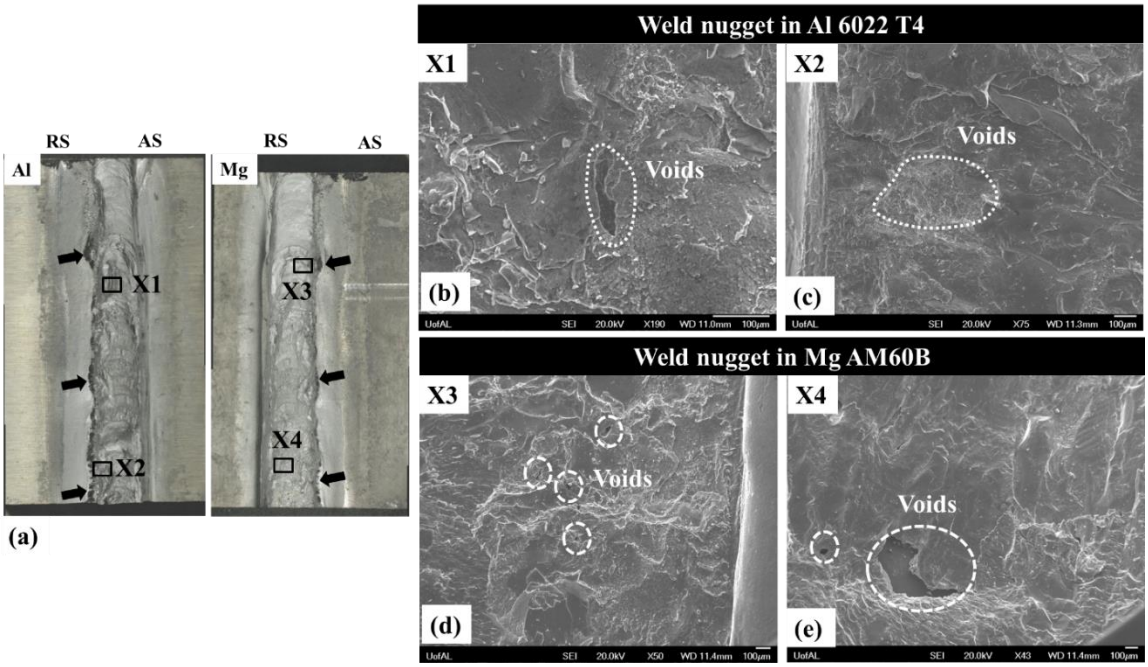

Figure 6-12: Fracture surface analysis of a representative weld failed in mode B (a) macro graph of the aluminum and magnesium fracture surface along the weld nugget (b) magnified view of the region X1 on the weld nugget of the aluminum showing the weld voids and brittle fracture surface (c) region X2 on the weld nugget of the aluminum showing the weld voids (d) region X3 on the weld nugget of magnesium showing numerous weld voids in the region and (e) region X4 on the weld nugget of magnesium showing the weld voids. Bold arrows in (a) indicate the fretting regions along the weld nuggets of aluminum and magnesium.

Yuan et al. [5] observed the failure load properties of FSLW in magnesium alloys was higher when the RS of the weld was on the loading side compared to when AS was the loading end. This supports the hypothesis that the fretting-like debris visible on the RS of the weld nugget indicates the entire load was carried by the RS of the weld. The rectangular boxes on the weld nuggets of the aluminum and magnesium sheets in Fig. 6-12(a) indicate the regions where further observations were done. A closer examination of regions X1 and X2 in the weld nugget of aluminum in Fig. 6-12(b) and Fig. 6-12(c) and X3 and X4 regions in the weld nugget of magnesium

shown in Fig. 6-12(c) and Fig. 6-12(d) showcase a brittle fracture surface. Weld pores/voids were visible at different areas of the weld nugget are also visible and are indicated by the dotted circles in Fig. 6-12(b)-(e).

The macrograph of the fracture surface of the weld representative failed in mode C is shown in Fig. 6-13(a). The bold arrows indicate the several different fretting-like regions and points of dominant crack initiation. One small area of the fretting region has been magnified under SEM and shown in Fig. 6-13(b). Three areas, Y1 which is away from the faying surface, Y2 which is on the faying surface and Y3 which is the fracture surface area close to faying surface on aluminum alloy were investigated. As shown in Fig. 6-13(c), the area Y1 is magnified and has clear markings of fatigue striation as indicated by the bold arrow. The direction of the arrow also indicates the crack propagation direction which is outwards from the fretting zone. As shown in Fig. 6-13(d), the area Y2 on the faying surface is magnified and revealed an uneven surface on the bottom magnesium sheet close to fretting region as well as bright materials at the fracture area near to faying surface. EDS was performed to confirm the bright materials were oxides and to analyze the chemical composition of the uneven surface on the magnesium sheet. Region R3 on magnesium surface in Fig. 6-13(d) indicated the presence of $Al_{12}Mg_{17}$ and bright material in region R4 in Fig. 6-13(e) was composed of Al_3Mg_2 + oxide. Further ahead from the fretting-like area in Fig. 6-13(e), the bold arrows indicate the crack propagation direction. This indicates that the crack initiated at the fretting-like region close to faying surface of the weld and grew outwards into the top surface of the aluminum sheet. The area Y3 on the fracture surface of the aluminum, away from the fretting region is shown in Fig. 6-13(f).

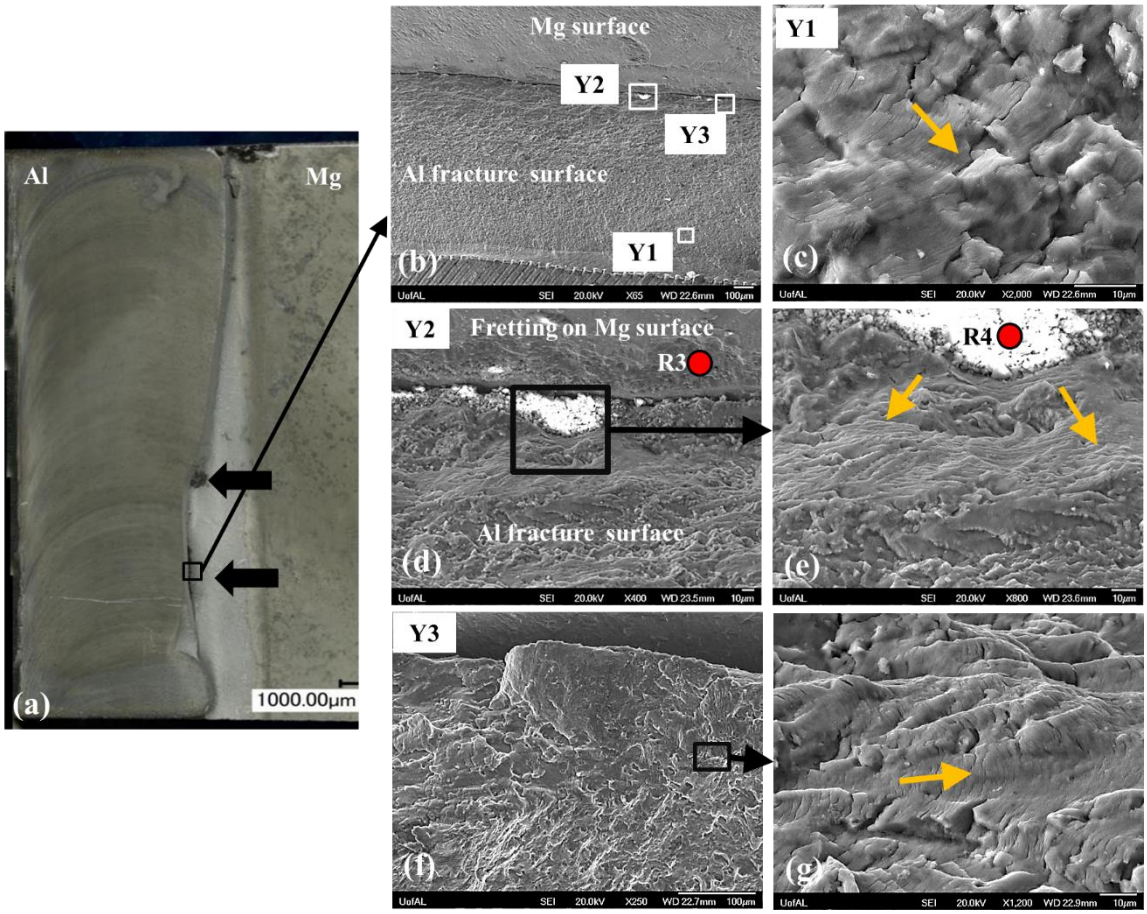

Figure 6-13: Fracture surface analysis of a representative weld failed in mode c (a) macro graph of the aluminum fracture surface (b) overview of a small region on fracture surface indicating regions Y1, Y2 and Y3 which are of interest (c) magnified region Y1 away from the faying surface showing the fatigue striation in the region, arrows point the crack propagation direction (d) magnified region Y2 on the fracture surface close to faying surface on the fractured aluminum surface (e) magnified region of Y2 very close to the faying surface where the dominant crack initiated, arrows indicate the crack propagation direction (f) region Y3 close to faying surface and away from the fretting region (f) magnified view of the region Y3 showing the presence of fatigue striation, arrows point the direction of crack propagation. Dotted regions R3 in (d) and R4 in (e) indicate the EDX analysis region.

The separation of the aluminum and magnesium alloy sheet is clearly visible at the top side of Figure 6-13. Further, a small region indicated by a rectangular box was magnified to show the surface morphology of the fracture surface. The surface was characterized by the presence of fatigue striations as shown in Fig. 6-13(g) and again the bold arrows in the figure indicate the direction of crack propagation.

6.4. Discussion

The fatigue test of FSLW dissimilar lap-shear welds indicate a wide scatter in fatigue life. Even for welds tested at same load level, the fatigue life varied between the welds, signifying that the strength of welds depends on the quality of the weld. The weld strength of a FSW lap-shear coupons depend on various macro and micro weld features such as the effective sheet thickness (EST), weld bond width and microstructure features like the grain size and grain refinement in the stir zone. In the present study, the difference in weld macro features between the weld type W1 and W2 which were produced on the same plate and under same weld process condition indicates the effect of pre-heating. The heat produced during the first stich weld W1, preheated the entire plate progressively and this resulted in W2 exhibiting a substantially different weld macro features. The Vickers hardness test shows no considerable change in microhardness value between the two weld types W1 and W2. This indicates, the unintentional pre-heating during the welding process had little impact on the microstructure but was sufficient to influence the change in macro features of the weld. Hence the difference in macro features of the FSLA lap-shear welds may be the cause for the scatter in the fatigue life. Yuan eta al. [5] reported, the weld strength in FSLW of magnesium alloys was higher for welds with significantly larger EST on RS of the weld and or if the RS hook terminated away from the AS hook. For weld type W1, the EST on the RS was slightly

larger than the EST on RS of weld W2. The weld bond width in W1 is smaller than the weld bond width of the W2. This necessarily should favor the W1 to exhibit a better fatigue life in terms of EST and W2 to exhibit a better fatigue life in term of weld bond width. But it has to be noted that the lap-shear joints in this current study involved dissimilar alloys and hence the influence of IMCs on the failure life needs to be further analyzed.

The number of lap-shear welds that failed in mode A and mode C is almost similar in numbers. And the number of lap-shear welds that failed in mode B is almost double of the combined the number of lap-shear welds that failed in mode A and mode C. In a lap-shear weld, the weld nugget bears the entire tensile, compression load, and the bending moment that is introduced during the fatigue loading condition. The fatigue data indicates the dominant failure mode at high loading conditions were in mode B (Fig. 7(c)). This is reasonable as the brittle IMCs which constitute the weld nugget failed and resulted in nugget pullout, a commonly observed failure mode during lap-shear tensile testing. For lap-shear welds that failure in mode B at low loading conditions, fractography analysis of provided some indication of cause-and-affect. If the weld nugget has presence of weld voids/pores or channel defects, it reduces the load bearing area of the weld nugget and hence affects the fatigue life of the lap-shear welds. The weld pores/voids and channel defects may also act as crack initiation sites and result in multiple crack growth across the weld nugget. In this current study, the analysis of the failed lap-shear weld in mode B (Fig. 12) exhibited the presence of several weld voids/pores along different areas of the weld nugget. The absence of any secondary cracks along the weldment (Fig. 9) also strengthens the argument that the drop in loading bearing area of the weld nugget due to weld pores/voids resulted in overload of the weld nugget and ultimately failed due to shear overload along the interface. The FSW of dissimilar materials throws a lot of challenge as to how to control the formation of IMCs in the stir

zone. The lap-shear welds produced for this current study otherwise indicate the controlled formation of IMCs in stir zone did provide a good weld strength except for the presence of weld defects in a few joints.

The failure mode A and mode C appears to be dominant in lap-shear welds tested at low loads. The analysis of the fatigue tested welds in mode A (Fig. 8) and in mode C (Fig. 10) shows no secondary cracks in the weldment. It also appears that the faying surface on the AS of the weld in case of mode A and faying surface on RS of the weld in case of mode C were intact. Previous studies have indicated the AS hook and RS hook played a dominant role in failures of the FSLW similar alloys [4,11]. This indicates, the weld bond in selected lap-shear welds that failed in mode A and mode C possessed weld nuggets with minimal flaws. In a lap-shear weld, the area close to weld nugget on the bottom sheet in the AS and on the top sheet in the RS of the weld experience high stress concentration. Depending on the microstructural and macro features of the weld, the crack may grow in the bottom sheet or in the top sheet [39]. In both the failure modes A and C, fretting likely initiated the dominant fatigue crack and resulted in failure either by top sheet pullout or the bottom sheet pullout. Chemical characterization of the fretting debris in the welds that failed in mode A and mode C indicated the debris were composed of IMCs Al_3Mg_2 and $Al_{12}Mg_{17}$. Previous studies have indicated, if the two faying surface are held close to each other and under high temperature, the atoms from one material will diffuse to other and vice-versa forming the IMCs [15,24]. In this study to produce the lap-shear FSLW coupons, the top aluminum was stacked on bottom magnesium sheet and were firmly clamped. The downward force of the tool shoulder and high temperature that is produced around the weld nugget clarifies the formation of thin layer of IMCS along the faying surface on either side of the weld nugget.

Close observation of welds that failed in mode A (Fig. 8(c) and Fig. 8(d)) indicate presence of visibly large casting pores in magnesium sheet close to where the crack propagated. It is possible that the casting pores reduced the strength of the magnesium sheet around the region and introduced bending moments which faintly opened the faying surface on the AS of the weld. The IMCs on these faying surface formed the fretting debris which initiated crack in the bottom magnesium sheet. As discussed earlier, the high stress concentration in the magnesium sheet may have favored the crack to propagate through the magnesium sheet.

For the welds tested at very load levels, mode C was the dominant failure mode. Closer observation of the welds that failed in mode C indicate the crack initiated in the TMAZ of the top aluminum sheet and propagated to the nearest free surface. The top aluminum sheet is half the thickness of the bottom magnesium sheet and unlike magnesium sheet, the aluminum sheets were rolled. Examination of the fatigue tested lap-shear welds that failed in mode C (Fig. 10(c) and Fig. 10(d)) indicates the absence of visually large casting pores in magnesium on the AS of the weld. The RS of the weld nugget experience a very high stress concentration as this is on the loading side of the lap-shear weld. During high cycle fatigue, the faying surface fret against each other and the IMCs on these faying surface forms the fretting debris which initiated the fatigue crack. The combination of high stress concentration and bending moment resulted in the dominant crack to propagate through the TMAZ of the top aluminum sheet.

6.5. Conclusions

The fatigue life results and the failure modes of the FSLW dissimilar aluminum to magnesium alloy was studied. The following conclusions are made.

1. The FSLW of dissimilar lap-shear shows a wide scatter in the fatigue life.
2. The formation of IMCs along the faying surface affected the fatigue life. For welds that failed in mode A and mode C, fretting was the main crack initiation factor. The presence of IMCs accelerated the effect of fretting on the faying surface and initiated cracks which resulted in failure of the lap-shear welds.
3. The presence of weld voids or channel defects in the stir zone reduces the structural-integrity of the weld and resulted in failure due to shear overload along the weld nugget.
4. At higher applied loads, lap-shear welds failed by interfacial welding and at lower load close to run out, crack propagation into the aluminum sheet was the prominent failure mode.

6.6. Bibliography

[1] G.S. Cole, A.M. Sherman, Mater. Charact. (1995) 3.

[2] P.Thornton, A.R. Krause, R.G. Davies, Weld. J. 75 (1996) 101s.

[3] A. Gean, S.A. Westgate, J.C. Kucza, J.C. Ehrstrom, Weld. Journal- New York 78 (1999) 80s.

[4] W. Thomas, E. Nicholas, J. Needham, M.. Murch, P. Templesmith, C.. Dawes, Frcition Stir Butt Welding, G.B. Patent 9125978.8, 1991.

[5] C. Zhou, X. Yang, G. Luan, Scr. Mater. 53 (2005) 1187.

[6] M. Sutton, B. Yang, A.. Reynolds, R. Taylor, Mater. Sci. Eng. A 323 (2002) 160.

[7] S.M. Chowdhury, D.L. Chen, S.D. Bhole, X. Cao, Mater. Sci. Eng. A 527 (2010) 6064.

[8] Q. Yang, X. Li, K. Chen, Y.J. Shi, Mater. Sci. Eng. A 528 (2011) 2463.

[9] W. Woo, H. Choo, M.B. Prime, Z. Feng, B. Clausen, Acta Mater. 56 (2008) 1701.

[10] N. Afrin, D.L.L. Chen, X. Cao, M. Jahazi, Mater. Sci. Eng. A 472 (2008) 179.

[11] L. Commin, M. Dumont, J. E. Masse, L. Barrallier, Acta Mater. 57 (2009) 326.

[12] C.I. Chang, C.J. Lee, J.C. Huang, Scr. Mater. 51 (2004) 509.

[13] W. Xunhong, W. Kuaishe, Mater. Sci. Eng. A 431 (2006) 114.

[14] D. H. Choi, B. W. Ahn, C.-Y. Lee, Y. M. Yeon, K. Song, S. B. Jung, Intermetallics 19 (2011) 125.

[15] N. Yamamoto, J. Liao, S. Watanabe, K. Nakata, Mater. Trans. 50 (2009) 2833.

[16] A. McLean, G.L.F. Powell, I.H. Brown, V.M. Linton, Sci. Technol. Weld. Join. 8 (2003) 462.

[17] Y.C. Chen, K. Nakata, Scr. Mater. 58 (2008) 433.

[18] Y.J. Kwon, I. Shigematsu, N. Saito, Mater. Lett. 62 (2008) 3827.

[19] V. Firouzdor, S. Kou, Metall. Mater. Trans. A 41 (2010) 3238.

[20] S. Hirano, K. Okamoto, M. Doi, H. Okamura, M. Inagaki, Y. Aono, Q. J. Japan Weld. Soc. 21 (2003) 539.

[21] A. Gerlich, P. Su, T.H. North, G.J. Bendzsak, in:, Mater. Forum, 2005, pp. 290–294.

[22] S. Kou, Weld. J. 88 (2009) 213.

[23] Y.S. Sato, S.H.C. Park, M. Michiuchi, H. Kokawa, Scr. Mater. 50 (2004) 1233.

[24] V. Firouzdor, S. Kou, Metall. Mater. Trans. A 41 (2010) 2914.

[25] A. Kostka, R.. Coelho, J. dos Santos, A.. Pyzalla, Scr. Mater. 60 (2009) 953.

[26] X.J. Cao, M. Jahazi, Mater. Sci. Forum 638-642 (2010) 3661.

[27] K. Kimapong, T. Watanabe, Mater. Trans. 46 (2005) 2211.

[28] Y.C. Chen, K. Nakata, Mater. Des. 30 (2009) 3913.

[29] T. DebRoy, H.K.D.H. Bhadeshia, Sci. Technol. Weld. Join. 15 (2010) 266.

[30] D. Fersini, a. Pirondi, Eng. Fract. Mech. 74 (2007) 468.

[31] A.M.S. Malafaia, M.T. Milan, M.F. Oliveira, D. Spinelli, Procedia Eng. 2 (2010) 1815.

[32] P. Lin, J. Pan, T. Pan, Int. J. Fatigue 30 (2008) 74.

[33] D. A. Wang, C.H. Chen, J. Mater. Process. Technol. 209 (2009) 367.

[34] V. Tran, J. Pan, T. Pan, Int. J. Fatigue 30 (2008) 2175.

[35] K.N. Solanki, J.B. Jordon, W. Whittington, H. Rao, C.R. Hubbard, Scr. Mater. 66 (2012) 797.

[36] H.Rao, J.Jordon, M.. Barkey, Y. Guo, X. Su, H. Badarinarayan, Mater. Sci. Eng. A 564 (2013) 369.

[37] J.B. Jordon, M.F. Horstemeyer, S.R. Daniewicz, H. Badarinarayan, J. Grantham, J. Eng. Mater. Technol. 132 (2010) 041008.

[38] S.H. Chowdhury, D.L. Chen, S.D. Bhole, X. Cao, P. Wanjara, Mater. Sci. Eng. A 562 (2013) 53.

[39] S.H. Chowdhury, D.L. Chen, S.D. Bhole, X. Cao, P. Wanjara, Mater. Sci. Eng. A 556 (2012) 500.

[40] C. Y. Lee, W.-B. Lee, J. W. Kim, D.-H. Choi, Y. M. Yeon, S.-B. Jung, J. Mater. Sci. 43 (2008) 3296.

[41] W. Yuan, B. Carlson, R. Verma, R. Szymanski, Sci. Technol. Weld. Join. 17 (2012) 375.

[42] A. Gerlich, P. Su, T.H. North, Sci. Technol. Weld. Join. 10 (2005) 647.

[43] M.K. Yadava, R.S. Mishra, Y.L. Chen, B. Carlson, G.J. Grant, Sci. Technol. Weld. Join. 15 (2010) 70.

CHAPTER 7

CONCLUSIONS AND FUTURE WORK

With growing demand and federal mandates for fuel efficient cars and trucks, the automotive industry is exploring weight reduction through the use of lightweight metals. Magnesium alloys is the lightest structural metal and is a potential replacement for steels in some automotive applications due to its good physical and mechanical properties. However, similar to aluminum alloys, magnesium is difficult to join using conventional welding technique such as the resistance spot welding. In this research study, efforts were made to understand the factors that influence structural-integrity in friction stir welding of similar magnesium-to-magnesium and dissimilar magnesium-to-aluminum joints. The main conclusions in this study are as follows:

- This study demonstrated that friction stir spot welding (FSSW) is a viable technique to join rare-earth element containing magnesium ZEK100 alloy. As in FSSWed of non-rare earth element containing magnesium alloys, the static weld strength of FSSWed ZEK100 magnesium alloys were highly influenced welding conditions, where factors influencing static strength are rank ordered as follow: effective sheet thickness > hook height > weld bond width. In particular, welds with large effective sheet thickness displayed superior static weld strength compared to welds with smaller effective sheet thickness. Interfacial shear failure was observed in welds with smaller weld bond width compared to welds with large weld bond

width that failed due to top sheet pullout. These geometrical features were highly influenced by welding process conditions, where the effective sheet thickness decreased with an increase in tool rotation rate. Hence, welding process conditions should be chosen such that, the welds produced would have a larger effective sheet thickness and larger weld bond width.

- The fatigue life of FSSWed magnesium AZ31 alloy was highly influenced by the macro and micro features of the weld. For the welds produced under two different process conditions, the FSSW joints containing a larger effective sheet thickness exhibited better fatigue performance. In fact, the effective sheet thickness is significance because it was observed the fatigue cracks initiated along the faying surface and then propagated through the interfacial hooks. At high cycle fatigue, in lap-shear welds produced using a triangular tool pin, the fatigue crack propagated through the bottom sheet rather than the top sheet as observed in lap-shear welds produced using a cylindrical tool pin profile. Since the interfacial hooks were formed in the thermomechanically affected zone (TMAZ) which are characterized by large recrystallized grains, the fatigue cracks propagated at much higher rate in welds produced using a cylindrical tool pin. This suggests, that in lap-shear FSSWed magnesium AZ31 alloy, the fatigue performance and structural-integrity are highly influenced by effective sheet thickness.
- In the development FSSW of dissimilar magnesium-to-aluminum alloys, the formation of intermetallic compounds (IMCs) played a prominent role. Welds with discontinues formation of IMCs in the stir zone exhibited better static weld strength compared to welds having continues formation of IMCs in the stir zone. Also, welds with large weld bond width and interfacial hooks, which terminated away from key-hole, exhibited better static weld strength. And unlike in FSSW of similar magnesium alloys, effective sheet thickness had no significant

impact on the static weld strength. Hence, it is suggested that welds should be produced such that the IMCs in the stir zone is discontinues, has a large bond width, and the interfacial hook terminated away from the key hole. This may be accomplished by choosing weld conditions which produces sufficient frictional heat to plastically deform the material and good material mixture. However, too much fractional heat results in insufficient material mixture and formation of IMCs.

- In friction stir linear welding (FSLW) of dissimilar aluminum-to-magnesium, the lap-shear welds with good material mixture in the stir zone and retreating side hook which terminated away from the advancing side hook exhibited the best static weld strength. To produce lap-shear FSLW joints with optimum static weld strength, the welding process should be such that welds are produced with good material mixture in the stir zone, has minimum voids or channel defects and discontinues hooking. In the current study, a tool rotation rate of 1500 rpm and 75 mm/min tool traverse speed produced FSLW lap-shear welds with the best static performance.
- Regarding fatigue performance of dissimilar aluminum-to-magnesium FSLWed joints, experimental testing resulted in a wide scatter. This scatter in test results is largely tied to the failure mode, where the FSLWed joints exhibited either interfacial failure or top or bottom sheet failure. For lap-shear welds which failed in either the top sheet or bottom sheet, fractography analysis suggested that fatigue cracks initiated at fretting like debris. The formation of a thin layer of IMCs along the faying surface created fretting-like debride and likely lead to accelerated fatigue crack initiation. Large channel defects and weld voids in the stir zone resulted in weaker welds and lead to resulted in interfacial weld separation. Thus, from the results of this study, it is suggested that the FSLW lap-shear welds can be produced

in a way such that there is minimum weld voids or channel defects, the scatter in the fatigue behavior would decrease considerably.

Future Work

While this study investigated the structural-integrity of FSLW and FSSW of similar and dissimilar joining of magnesium alloys, much more research is needed to fully realize this welding method as a viable joining technique. First and foremost, welds should be manufactured and tested to analyze the performance of the magnesium-to-magnesium and magnesium-to-aluminum in configurations other than lap-shear. In this study, all welds were tested in the lap-shear loading conditions, but other coupon configuration like coach-peel or cross-tension, and T-tension will provide additional insight into the fatigue performance of welds.

Another area of research that should be studied is related to impact of thermal interaction among the tool, tool holder, clamping device and base plate in a laboratory setup versus a production environment. The test coupons for this study were produced in a lab setting, where the heat dissipated during welding via the weld tool, clamps and backing plate. However, the current study did not investigate the impact of thermal interaction in a production environment and hence it is important to analyze the effect of different environments for welding. It is imperative to understand, while transferring this welding technology from a lab setting to production environment, how heat dissipated during FSW impacts the structural integrity of the joint. Specifically, studies, should focus on cooling techniques such as use of heat sinks, forced air cooling, etc.

The current method of producing FSW in laboratory setting is laborious and time consuming which is predominantly due to the initial weld setup and by use of manual clamping during the welding. Hence it is important to understanding the effect of cycle time on structural integrity for producing welds in a laboratory and a production environment. For a particular FSW process to be effectively implemented in a production environment, a study should be conducted on the determining the most appropriate clamping devices and jigs in order to reduce cycle time.

In addition, a real time monitoring system or method should also be investigated into where the operator would have in-situ feedback during welding in order to make necessary corrections to the weld process to maintain optimal welding characteristics. This type of real-time monitoring could also involve non-destructive techniques. Furthermore, specific non-destructive techniques (NDT) for FSW should be identified and documented for more standardized use. Potential use of NDT techniques such as the X-ray, ultrasonic mapping could be used to verify the structural integrity of the weld and could save time and material wastage.

Lastly, one of the major factors that should be studied and understood is the issue of corrosion on structural-integrity and fatigue performance of FSW. In particular, galvanic corrosion in dissimilar magnesium-to-aluminum FSWed joints is a significant issue that needs be fully examined. In addition, several specific environmental effects such as the moisture, ultra violet light, low temperatures, and salt water on the FSWed similar and dissimilar welds should be examined.

APPENDIX

Information on the journal publications of the chapters in this report.

Chapter 2

H.M. Rao, R.I. Rodriguez, J.B. Jordon, M.E. Barkey, Y.B. Guo, H. Badarinarayan, W. Yuan, "*Friction stir spot welding of rare-earth containing ZEK100 magnesium alloy sheets*," Materials and Design, 750-754; (2014)

Chapter 3

H.M. Rao, J.B. Jordon, M.E. Barkey, Y.B. Guo, Xuming Su, H. Badarinarayan. "*Influence of Structural Integrity on Fatigue Behavior of Friction Stir Spot Welded AZ31 Magnesium Alloy*," Material Science and Engineering A (564), 369–380; (2013)

Chapter 4

H.M. Rao, W. Yuan, H. Badarinarayan, "*Effect of Process Parameters on Mechanical Properties of Friction Stir Spot Welded Dissimilar Alloys*," Materials Science and Engineering A (In preparation)

Chapter 5

H.M. Rao, W. Yuan, H. Badarinarayan, "*Feasibility Study and Mechanical Properties of Friction Stir Linear Welding Dissimilar Alloys*," Materials and Design (In preparation)

Chapter 6

H.M. Rao, J.B. Jordon, M.E. Barkey, Xuming Su, "*Fatigue Testing and Failure Analysis of Friction Stir Linear Welded Dissimilar Aluminum 6022-T4 to Magnesium AM60B*," International Journal of Fatigue (In preparation)

-End-